Master Thesis of Science

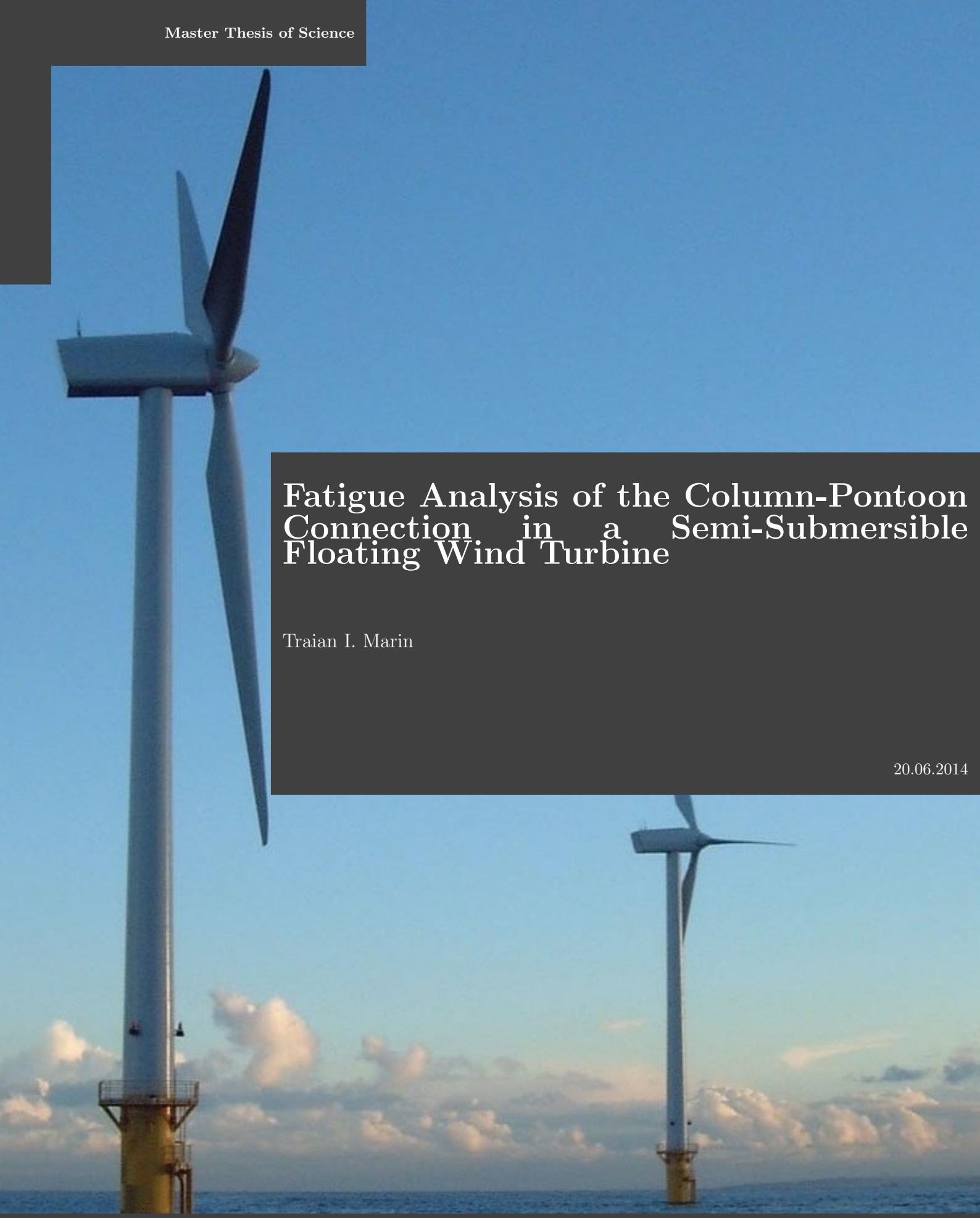

Fatigue Analysis of the Column-Pontoon Connection in a Semi-Submersible Floating Wind Turbine

Traian I. Marin

20.06.2014

European Wind Energy Master - EWEM- Offshore Track

Fatigue Analysis of the Column-Pontoon Connection in a Semi-Submersible Floating Wind Turbine

Master of Science Thesis

For obtaining the degree of Master of Science in Offshore Engineering at Delft University of Technology and in Technology-Wind Energy at Norwegian University of Science and Technology.

Traian I. Marin

20.06.2014

European Wind Energy Master - EWEM
DUWIND - Delft University of Technology
Norwegian University of Science and Technology - NTNU

Copyright © Traian I. Marin
All rights reserved.

European Wind Energy Master - EWEM
Of
Offshore Track

The undersigned hereby certify that they have read and recommend to the European Wind Energy Master - EWEM for acceptance a thesis entitled **"Fatigue Analysis of the Column-Pontoon Connection in a Semi-Submersible Floating Wind Turbine"** by **Traian I. Marin** in partial fulfillment of the requirements for the degree of **Master of Science**.

Dated: 20.06.2014

Supervisor: _____
Prof.Dr.Ir. Mirek Kaminski of TU Delft

Supervisor: _____
Prof.Dr.Ir. Torgeir Moan of NTNU

Reader: _____
Dr.Ir.Zhen Gao of NTNU

Thesis outline

MSC THESIS IN MARINE TECHNOLOGY

SPRING 2014

FOR

STUD.TECHN. Traian I. Marin

Fatigue Analysis of the Column-Pontoon Connection in a Semi-Submersible Floating Wind Turbine

Background:

Semi-submersible floating wind turbines have been proposed for deep water offshore wind energy application. A conventional semi-submersible consists of three or four columns interconnected by braces. A novel pontoon-type semi-submersible floating wind turbine has been developed at CeSOS, NTNU. It consists of four cylindrical columns with one central column supporting the 5MW NREL wind turbine. Each side column is spaced at a 120-degree interval and connected at the bottom to the central column by a rectangular pontoon.

The column-pontoon connection presents a challenge for fatigue design when the floating wind turbine is subjected to combined wind and wave loads. A smooth structural transition from cylindrical column to rectangular pontoon should be designed to avoid sharp corners and to reduce stress concentration. Internal stiffeners, girders and bulkheads should be considered for both columns and pontoons. The central column, which supports the wind turbine, is directly subjected to the wind turbine aerodynamic loads

and the wave loads. The joint between the central column and the pontoons needs to be strengthened considering both wind and wave loads, while the fatigue loads in the other three side columns are mainly induced by wave loads and rigid-body motions (i.e. inertial load effects).

The thesis work will be a continuation of the project work, in which the structural design (with two alternatives) of the side column-pontoon connections in this novel semi-submersible floating wind turbine and the corresponding linear stress analysis have been carried out.
In the thesis work, the MSc student should carry out a detailed FE analysis of one design to determine the stress distribution at various hot-spots under different cross-sectional loading conditions, estimate the uni-axial fatigue damage, assess the multi-axial effects on the structure and propose a method for including these effects in the fatigue calculation.

The global response analysis results for representative wind and wave conditions will be provided by the PhD candidate Chenyu Luan.

Assignment:

The following tasks should be addressed in the project work:

1. Literature review on structural design of joints or connections in semi-submersible floaters and design of local structural details for improvement of fatigue performance, finite element analysis to determine the stress concentration factor, the S-N curve approach for fatigue analysis, and multi-axial fatigue criteria.

2. Use the developed FE model in GeniE to identify the area with high stress concentration and improve the design of local structural parts with respect to fatigue. Refine the mesh in these areas and perform a FE analysis using the sub-modeling technique to determine the stress distribution under various cross-sectional loading conditions.

3. Assume a linear structural behavior and estimate the stress distribution due to actual combined loading conditions. Important cross-sectional loads, such as vertical bending moment, axial force, as well as torsional moment for different wind and wave directions should be considered.

4. Estimate fatigue damage for selected environmental conditions and make a long-term uni-axial fatigue prediction.

5. Study the theory of multi-axial fatigue criteria and formulate it for time-domain fatigue analysis.

6. Conclude the work and give recommendations for future work.

7. Write the MSc thesis report.

In the thesis the candidate shall present his personal contribution to the resolution of problem within the scope of the thesis work.

Theories and conclusions should be based on mathematical derivations and/or logic reasoning identifying the various steps in the deduction.

The candidate should utilize the existing possibilities for obtaining relevant literature.

The thesis should be organized in a rational manner to give a clear exposition of results, assessments, and conclusions. The text should be brief and to the point, with a clear language. Telegraphic language should be avoided.

The thesis shall contain the following elements: A text defining the scope, preface, list of contents, summary, main body of thesis, conclusions with recommendations for further work, list of symbols and acronyms, reference and (optional) appendices. All figures, tables and equations shall be numerated.

The supervisor may require that the candidate, in an early stage of the work, present a written plan for the completion of the work. The plan should include a budget for the use of computer and laboratory resources that will be charged to the department. Overruns shall be reported to the supervisor.

The original contribution of the candidate and material taken from other sources shall be clearly defined. Work from other sources shall be properly referenced using an acknowledged referencing system.

The thesis report shall be submitted in two copies as well as an electronic copy on a CD:

- Signed by the candidate
- The text defining the scope included
- In bound volume(s)
- Drawings and/or computer prints which cannot be bound should be organized in a separate folder.

Supervisors:
Professor Torgeir Moan
Professor Mirek Kaminski
Zhen Gao

Deadline: 20.06.2014

Preface

This report presents the work done by Traian Ionut Marin for the Master Thesis, in order to obtain the double degree, MSc Offshore Engineering from Delft University of Technology (TU Delft) and MSc Technology-Wind Energy from Norwegian University of Science and Technology (NTNU). The work was carried out during spring 2014, in Trondheim, Norway.

The main scope of the present thesis is to carry out a fatigue assessment of the side joint connection in the novel semi-submersible floater 5-MW-CeSOS. First, a proper geometrical model of the column-pontoon connection was developed in GeniE, aiming for an improved local structural response. The hot spot stresses were then calculated and combined with the dynamic response analysis to obtain the stress time series. Then, a long term fatigue calculation was performed, considering only uni-axial effects, and a method for multi-axial fatigue calculation was proposed.

The dynamic response analysis of the structure was performed by PhD candidate Chenyu Luan, in order to provide information needed for the investigation of local fatigue under different sea states.

In fall 2013, I worked on the design and stress analysis of the same joint connection, for the Thesis Pre-Project at NTNU. The present paper is a continuation of the work done in the Pre-Project; the knowledge gained working on that report was very valuable and helped in understanding the main challenges in structural analysis of marine structures. It was very rewarding to have the chance to continue working with the same structure, but with a more challenging goal.

Summary

The geometry design of a column-pontoon joint connection in the 5-MW-CeSoS semi-submersible floating offshore wind turbine, followed by a stress analysis and a detailed fatigue investigation is presented in this paper.

The geometry was proposed by the author, based on logic, mathematical derivations, as well as information from the literature. The SESAM package provided by DNV was used for this thesis, including GeniE, Sestra, Submod, SESAM Manager and Xtract. The geometry was developed in the FEM software GeniE, which uses Sestra as solver, while the rest of the tools were utilized for the sub-modeling technique.

Two different geometries of the column-pontoon connection were designed and their performances under different loads were analyzed and compared. The model which appeared to be more reliable regarding fatigue was further investigated and optimized in order to reduce the SCF, which are of great importance for fatigue predictions. One crucial hot spot underwent a detailed stress analysis, using the sub-modeling technique, i.e. cutting the structure at a specified location and refining the mesh.

The stress assessment at the location of interest was performed in Xtract, and for further extrapolation of the stress results in order to compute the hot spot stresses and the SCFs, an Excel spreadsheet was used. Using the load time series from the dynamic analysis of the global model, and combining them with the hot spot stresses, the stress time series were output for a certain sea state.

The actual fatigue calculations were performed in Matlab, using the freely available WAFO package. First, the well established uni-axial fatigue case was performed, utilizing the rainflow counting method, a proper S-N curve and the Miner's rule. A number of 13 sea states with 10 seeds each, with aligned wind and wave were considered. The fatigue assessment was performed for four different sea headings with respect to the pontoon's direction, i.e. 0, 30, 60 and 90 degrees. Next, an approach for considering multi-axial effects in fatigue analysis was proposed, combining two recently developed methods, *Equilibrium Equivalent Structural Stress* and the *Path-Dependent Maximum Range*. Considerations

on the importance of multi-axial effects on the analyzed structure were further made, followed by conclusions and recommendations for future work.

Acknowledgements

I would like to thank my supervisors, Professor Torgeir Moan from NTNU and Professor Mirek Kaminski from TU Delft for their unconditioned support and dedication in helping me achieve this goal.

Also, I would like to acknowledge the contributions of Zhen Gao and Chenyu Luan to this thesis, and thank them for the continuous guidance and eagerness to always help me find the best answers. The regular meetings with them were key points in overcoming obstacles and proceeding further with the best solution.

I would like to mention my EWEM fellows for the academic collaboration and for the great time we had together in the past two years, Bas, Jinchao, Marijn, Marius, Niels, Oliver, Qiang, Simon, Tim and Ying.

Last, but not least, I would like to give very special thanks to my family.

Trondheim, Norway
20.06.2014

Traian I. Marin

Contents

List of Figures

List of Tables

Nomenclature

Latin Symbols

A	Section area	$[m^2]$
a	Constant value in the S-N curve	[-]
D	Accumulated fatigue damage	[-]
d	Fatigue damage per second	[1/s]
D_f	Fatigue damage in a constant amplitude test	[-]
D_i	Fatigue damage from one short term sea states in one hour period	[-]
D_{tot}	Total fatigue damage from all the sea states in one hour period	[-]
f	Maximum stress value during one fatigue cycle	$[N/mm^2]$
$F(\delta)$	Dimensionless parameter as a function of out-of-phase angle δ	[-]
F_i	Load component (force or moment)	$[kN]$ or $[kNm]$
$f_{y'}$	Line force in the y' direction	$[N/m]$
$f_{z'}$	Line force in the z' direction	$[N/m]$
k	Material constant	[-]
k	Number of stress blocks	[-]
L_c	Calculated fatigue life	[days]
L_d	Design fatigue life	[days]
$log\bar{a}$	Intercept of log N-axis by S-N curve $loga - 2S_{logN}$	[-]
log	Logarithmic function with base 10	[-]
$loga$	Intercept of mean S-N curve with the log N-axis	[-]
m	negative inverse slope of the S-N curve	[-]
$m_{x'}$	Line moment about the x' direction	$[N/m]$

$m_{y'}$	Line moment about the y' direction	$[N/m]$
N	Number of cycles	[-]
N_i	Number of cycles to failure at constant stress range $\Delta\sigma_i$	[-]
n_i	Number of stress cycles in stress block i	[-]
N_x	Axial force	[N]
$P1\ to\ P5$	Fatigue points	[-]
p_i	Probability of occurence of a certain sea state	[%]
T	Fatigue lifetime	[days]
t	Plate thickness	[mm]
t	time	[s]
t_f	Time to failure	[s]
T_{ts}	Length of time-series	[s]
W_y	Section modulus about the y-axis	$[m^3]$

Greek Symbols

β	Material constant	[-]
δ	Out of phase angle between $\Delta\sigma_s$ and $\Delta\tau_s$	[rad]
$\Delta\sigma$	Stress range	$[N/mm^2]$
$\Delta\sigma_1, \Delta\sigma_2$	Principal stress ranges	$[N/mm^2]$
$\Delta\sigma_e$	Reference stress range in the PDMR method	$[N/mm^2]$
$\Delta\sigma_{\parallel}$	Stress range parallel to the weld	$[N/mm^2]$
$\Delta\sigma_{\perp}$	Stress range perpendicular to the weld	$[N/mm^2]$
$\Delta\sigma_{Eff}$	The effective hot spot stress range	$[N/mm^2]$
ΔS_e	Effective stress range in the PDMR method	$[N/mm^2]$
ΔS_e	Fatigue limit under pure $\Delta\sigma_s$	$[N/mm^2]$
η	usage factor	[-]
ω	Angular frequency	$[rad/s]$
ϕ	Angle of the critical plane	[-]
σ_b	Bending stress component of the structural stress	$[N/mm^2]$
σ_m	Membrane stress component of the structural stress	$[N/mm^2]$
σ_s	Structural stress	$[N/mm^2]$
$\sigma_{hotspot}$	Hot spot stress	$[N/mm^2]$
σ_{hss_i}	Derived normal hot spot stress for one load component	$[N/mm^2]$
$\sigma_{nominal}$	Nominal stress	$[N/mm^2]$
σ_{total}	Total normal stress, obtained by superposition	$[N/mm^2]$
σ_{xx}	The stress in the direction of x-axis	$[N/mm^2]$
σ_{yy}	The stress in the direction of y-axis	$[N/mm^2]$

τ_z	Transverse shear stress component	$[N/mm^2]$
τ_{hss_i}	Derived shear hot spot stress for one load component	$[N/mm^2]$
τ_{total}	Total shear stress, obtained by superposition	$[N/mm^2]$
τ_{xy}	Shear stress	$[N/mm^2]$

Abbreviations

ALS	Accidental Limit State
API	American Petroleum Institute
$ASME$	American Society of Mechanical Engineers
$ASTM$	American Society for Testing and Materials
BV	Bureau Veritas
DFF	Design Fatigue Factor
DNV	Det Norske Veritas
DOF	Degree of Freedom
$EWEM$	European Wind Energy Master
FEM	Finite Element Method
FLS	Fatigue Limit State
LC	Load Case
MW	Mega-Watt
$NREL$	National Renewable Energy Laboratory
$NTNU$	Norwegian University of Science and Technology
$PDMR$	Path-Dependent Maximum Range
ROP	Read-out-Points
SCF	Stress Concentration Factor
SLS	Serviceability Limit State
TLP	Tension Leg Platform
ULS	Ultimate Limit State
$WAFO$	Wave Analysis for Fatigue and Oceanography

Chapter 1

Introduction

1.1 Motivation and background

The offshore wind energy industry is a relatively young industry, but with huge potential for exponential growth in the coming years. According to the European Environment Agency (EEA), Europe's offshore wind potential is able to meet seven times over its demand [4]. The wide open-sea space, the great interest in reducing the CO2 emissions and the technology advancement are decisive factors in developing new offshore wind farms and reaching new targets.

A series of great challenges are accompanied by the emerging status of the offshore wind industry, including development of new concepts, design criteria and specific standards, manufacturing, installation, operation and maintenance, decommissioning, reliability and serviceability. All these challenges must be overcome in a cost-effective way to guarantee the affordability and the competitiveness of the offshore wind industry.

The current capacity of the offshore wind farms in Europe is around 6.6 GW, with most of the turbines installed in relative shallow waters, up to 50 meters water depth, mounted on bottom fixed support structures (monopiles, jackets, gravity-based, tripods and tripiles). These structures present limitations when it comes to going into deeper waters, becoming economically unreasonable. Therefore, new types of structures need to be designed in order to cope with deeper waters and still be cost-effective.

Floating offshore wind turbines represent an option and might become a viable solution for future offshore wind farms. A turbine mounted on a floater has the big advantage that it can be towed out and installed far away from land, at large water depths, becoming invisible from the shore, thus not impacting the aesthetics of the landscape. But the challenges that come with developing such a structure that can withstand a rough environment and remain economically profitable in the long term are very demanding and a huge amount of research effort must be made to achieve it. So far, only three floating turbines have been installed and are operating, while many other concepts are being

investigated around the world. The figures below illustrate the first three prototypes of floating turbines that are currently operating in open seas.

Figure 1.1: *Hywind prototype*

Figure 1.2: *WindFloat prototype*

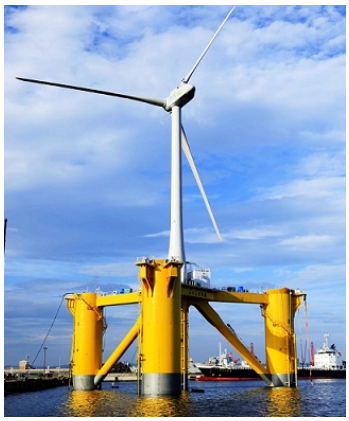

Figure 1.3: *Fukushima Mirai prototype*

Several other concepts of floaters are being researched and tested, different configurations of semi-submersibles, barges, tension-leg platforms (TLP) and spars. The support structure is of crucial importance, and it should be designed to withstand the environmental conditions over the envisaged lifetime, without affecting the performance of the turbine. Thoroughly investigating different concepts leads to a deep understanding of the requirements, capabilities, advantages and limitations of these structures and it ensures the enhancement of new and valuable knowledge towards the practical execution of new floating offshore wind models.

One of the most challenging problems with designing new floater prototypes is represented by the fatigue lifetime. This very sensitive issue affects all the offshore and marine structures, requiring special attention and deep understanding of the phenomenon and of the methods available in the industry. Each case represents a different problem and it needs to be tackled using the right approach, provided the necessary skills and understanding.

Motivated by the exciting potential of the new floating offshore wind concepts, this thesis aims to analyze the fatigue behavior of a novel semi-submersible floating offshore wind turbine, developed at CeSOS, NTNU, which consists of four cylindrical columns with one central column supporting the 5 MW NREL wind turbine [31].

1.2 Objectives

This thesis's main goal is to investigate the fatigue behavior of the floater concept analyzed, performing long-term uni-axial fatigue analysis, and proposing a method for the multi-axial fatigue problem.

Fatigue calculations on semi-submersibles are well documented, especially from the oil and gas industry, that has a long history with this king of structures. However, to transfer that knowledge to the offshore wind sector is not completely straight-forward, given the great differences in requirements, operability, environmental loads and so on. Therefore, the methods need to be adapted, and taken to a new level, and each case to be judged on its own. For this particular concept, the following objectives were fulfilled:

1. Preliminary design of two different geometries for the column-pontoon connection;
2. Analysis of the stress patterns in the two concepts:
    - Apply forces and moments at the pontoon's cut in order to observe the distribution of the stress for each load case;
    - Carry out a linear stress analysis using the finite element method software GeniE;
    - Identify the possible hot spots and optimize the design in order to reduce the stress concentration factors (SCF);
    - Compare the behavior of the two concepts and choose the right model to continue the investigation;
    - Perform a detailed analysis of the stress variation using the sub-modeling technique;
    - Extrapolate the stresses at the hot spot and use them together with the global response of the structure, in order to compute the stress time-series of the hot spot.
3. Fatigue calculation:
    - Perform the uni-axial fatigue analysis using the established hot spot method, count the cycles using the rainflow counting, combine the results with the S-N curve and Miner's rule and estimate the fatigue lifetime;
    - Propose an approach for analyzing multi-axial fatigue damage and lifetime estimation ;
4. Conclude the results and make recommendations for future work.

1.3 Method

For the present master thesis, several software programs were used, either directly by the author, or by PhD candidate Chenyu Luan, who provided the dynamic response analysis used for the fatigue lifetime prediction.

A number of 13 sea states, each with 10 seeds were used in order to make a long term approximation considering both uni-axial and multi-axial fatigue.

The work sequence and the software used can be summarized as follows:

- Finite element modeling (GeniE, Xtract, Submod, SESAM Manager)
- Dynamic response analysis (SESAM package, TDHMill)
- Analysis of the hot spot stress (Xtract, Excel)
- Fatigue damage calculation (Matlab - WAFO package)
- Pre- and post-processing (Matlab)

Only the fatigue limit state (FLS) was considered in this thesis, the Ultimate-, Serviceability- and Accidental limit states (ULS, SLS, ALS) were disregarded.

1.4 Thesis overview

The second chapter presents the relevant theory for the design and fatigue analysis of a structural joint connection, describing both the uni-axial and multi-axial fatigue approaches. Chapter 3 presents the FE modeling of the two designs and the comparison between them. In the 4th chapter, the hot spot stress procedure and analysis are shown, together with the results for the SCFs. Chapter 5 contains the uni-axial fatigue analysis, comprising the long term fatigue life predictions. Chapter 6 describes an approach for multi-axial fatigue for the investigated structure, while Chapter 7 presents conclusions and recommendations for future work.

Chapter 2

Theory

The local connection analyzed in the present paper is part of a concept prototype, and it was designed based on logical and engineering assumptions. The floating wind energy sector is quite immature, and at this stage consistent researched is being carried out in order to develop methods, test small scale models and gain experience in order to develop reliable standards for the industry.

The oil and gas industry could be used as a reference, given the wide experience with floating structures. There are both similarities and differences between the requirements of the two industries. Therefore, the design criteria need to be carefully considered when developing a new floater for offshore wind.

DNV provides the most consistent set of standards for the design of offshore structures and fatigue analysis ([11], [13], [8], [9], [10]). Of importance for the present thesis are the requirements for the geometry with respect to fatigue analysis, and the method for life prediction.

2.1 Design of the joint connection

2.1.1 Geometrical features

A global structural model shall represent the global stiffness and should be represented by a large volume, thin-walled three dimensional finite element model. A thin-walled model should be modeled with shell or membrane elements, sometimes in combination with beam elements. The structural connections in the model shall be modeled with adequate stiffness in order to represent the actual stiffness in such a way that the resulting responses are appropriate to the model being analyzed. The global model usually comprises [8]:

- pontoon shell, longitudinal and transverse bulkheads;

- column shell, bulkheads and trunk walls;
- bracing, transverse and longitudinal stiffeners.

The main goal of the local analysis of the structure is to identify the hot spots and reduce the SCFs. These factors are very sensitive to the geometry of the structure and therefore, it is very important to make a valuable judgment based on mathematical calculations and logical reasoning when designing the geometry.

It is in generally recommended to avoid sharp corners and to make the transition between different parts of the structure as smooth as possible. The use of girders, brackets, bulkheads and stiffeners is required in order to transfer the loads inside the structure without or with low stress concentrations. An option which gives good results is to precast the critical parts of the structure. This solution avoids the welds in the hot spots, which is a great advantage, given the generally weak strength of the weld.

The pontoons should be divided into compartments in order to avoid the flooding of the entire pontoon in case of water going in, while the walls of the compartments need to have watertight doors.

2.1.2 Modeling requirements

When creating the FE model, in order to investigate the stress distribution in the structure, some rules, assumptions and simplifications shall be applied. Even though the standards in this direction are not very detailed, some recommendations as a result of practical experience exist, and need to be implemented to achieve good results.

Some of the recommendations from DNV are presented below:

For the **Global model**:

- All the load effects from global and local loads are to be included;
- All the stress components are combined using the correct phase angle;
- The global model is modeled with relative uniform and coarse mesh;
- The stiffeners are typically modeled as beam elements;
- Doors and large openings are fitted to mesh size;
- A typical maximum size of the mesh cells of 2x2 meters is used for the global model;
- The mesh size is often smaller due to shifts in plate thickness and due to the internal configuration of the structure, consisting of bulkheads, frames, geometric details etc.
- The quadratic elements used for the mesh should have a length to breadth ratio of less than 1:5;

- Where stiffeners are lumped, the element edges should follow the actual stiffener direction as close as possible in order to avoid spurious hot spots;
- Typically 8 elements around the brace are used for smaller diameter braces (D∼2 meter) and 16 for larger diameters (D∼4 meter);
- For a circular brace with a transition cone and a quadratic connection to the columns, four-five 8-node elements in each quarter will normally be sufficient for the modeling of the transition;
- The bilge radius of a pontoon can normally be modeled with two or three 8-node elements;
- Primary girders modeled with shell elements shall normally have 2 (or more) elements over the height of webs in order to represent the bending and shear stiffness properly;
- To avoid rigid body motion of a global structural model, at least 6 degrees of freedom have to be fixed.

For the **Local model**:

- The boundaries of the sub-model should coincide with those elements in the global model from which the sub-model boundary conditions are extracted;
- The boundaries of the sub-model shall coincide with areas of the parent model where the displacements are well defined. The boundaries of the sub-model should not be midway between two frames if the mesh size of the parent model is such that the displacements in this area cannot be accurately determined;
- If differences in stiffness between local and global model exist, stresses will not be consistent. Therefore, the main difference from a global to a local model should be the mesh size (refined mesh) at the hot spot region(s);
- The sub-model shall be sufficiently large so that boundary effects, due to inaccurately specified boundary deformations, do not influence the stress response in areas of interest;
- Transfer of beam element displacements and rotations from the parent model to the sub-model should be especially considered;
- Element size in the order of plate thickness (t x t) is preferred in the hot spot region with 8/6-noded shell elements
- Eccentricities, cut-outs, rat holes, penetrations should be included;
- 8 node elements are recommended in areas of steep stress gradients;
- 4 node elements with improved in-plane bending represent an alternative;

- 6-node triangular elements can be used occasionally in areas where a mesh of 8-noded shell elements is difficult to fit. The triangular elements are stiffer and should therefore normally be avoided;
- Element size in the range of 0.5t x 0.5t to 2t x 2t may be used if the elements have additional degrees of freedom for improved in-plane behavior;
- The displacements at boundaries are set as 'prescribed' ;
- Element-to-node transfer is often used;
- The welds are not modeled;
- Boundaries should be located towards stiff parts, e.g. bulkheads, girders, stringers, web frames;
- Reasonable distance between hot spot and boundaries should be ensured in order to avoid distortions;
- Stiffness relation in global and local model must be equal.

Note: The *global model* referred to above represents the pontoon-column assembly that is analyzed in this thesis. The *local model* refers to a specific part of interest from the global model, that underwent a detailed stress analysis through the sub-modeling technique. The two models will be presented in the next chapter.

2.2 Fatigue

Fatigue is the tendency of a material to fracture by means of progressive brittle cracking under repeated alternating or cyclic stresses of an intensity considerably below the material's strength. Fatigue occurs when a material is subjected to repeated loading and unloading. If the load ranges are above a certain threshold, a micro-crack will begin to form at the hot spot. Eventually the crack will reach a critical size and it will propagate suddenly, resulting in fracturing of the structure (see Figure 2.1).

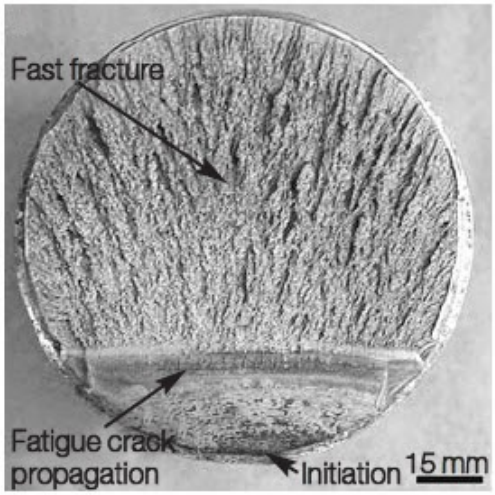

Figure 2.1: *Fatigue fracture surface [1]*

The geometry of the structure critically affects the fatigue life. Sharp corners, square holes and intersections of complex geometries will increase the stress concentration, while smooth transitions and round holes are preferred to improve the fatigue strength.

2.2.1 Fracture modes

Fracture mechanics is the field of mechanics concerned with the study of the propagation of cracks in materials. A fracture is a separation of an object or material into two or more pieces under the action of stress. The fracture of a solid almost always occurs due to the development of certain displacement discontinuity surfaces within the solid. If a displacement develops perpendicular to the surface of displacement, it is called a normal tensile crack or simply a crack; if it develops tangentially to the surface of displacement, it is called shear crack, slip band or dislocation. There are three ways of applying a force to enable a crack to propagate (Figure 2.2):

- Mode I fracture - Opening mode (a tensile stress normal to the plane of the crack);
- Mode II fracture - Sliding mode (a shear stress acting parallel to the plane of the crack and perpendicular to the crack front);
- Mode III fracture - Tearing mode (a shear stress acting parallel to the plane of the crack and parallel to the crack front).

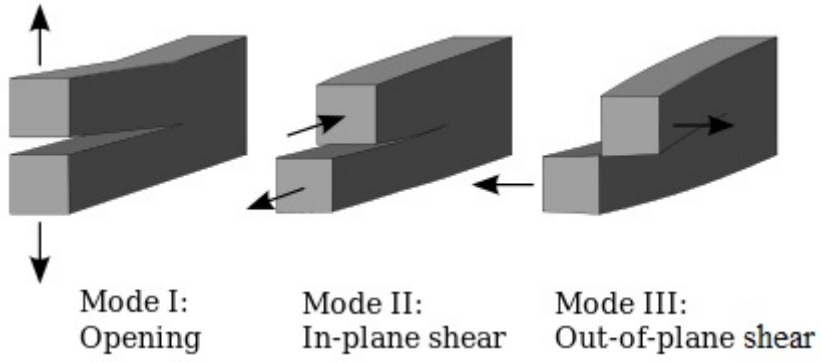

Figure 2.2: *Fracture modes [2]*

2.2.2 Hot spots

A **hot spot** can be defined as a point in a structure where a fatigue crack may initiate due to the combined effect of structural stress fluctuation and the weld geometry or a similar notch [9]. For FLS, these points represent the areas of interest that are vulnerable in the long term due to cyclic loading. For documented joints, e.g. tubular joints, the position of the hot spot is usually known, and the procedure is straight forward. For complex geometries, like the joint analyzed in the current thesis, the positions of the hot spots must be accurately determined and the stress patterns in those regions investigated in detail.

Hot spot stresses are calculated assuming linear material behavior and using an idealized structural model with no fabrication-related misalignment. The extent of the local model has to be chosen such that effects due to the boundaries on the structural detail considered are sufficiently small and reasonable boundary conditions can be formulated [9].
In plate structures, three types of hot spots at weld toes can be identified, as exemplified in Figure 2.2:

1. at the weld toe on the plate surface of an ending attachment;

2. at the weld toe around the plate edge of an ending attachment;

3. along the weld of an attached plate (weld toes on both the plate and attachment surface).

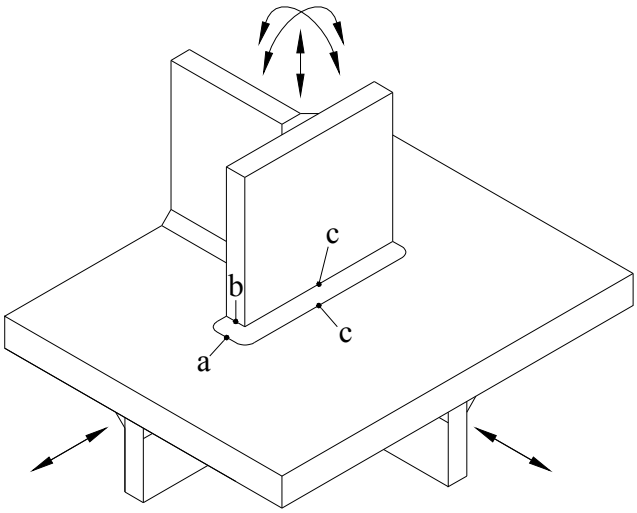

Figure 2.3: *Different hot spot positions [9]*

2.2.3 Stress concentration factor

The stress concentration factor (SCF) can be defined as the dimensionless ratio between the hot spot stress and the nominal stress, with regard to a certain weld:

$$SCF = \frac{\sigma_{hotspot}}{\sigma_{nominal}} \tag{2.1}$$

The SCFs are the most sensitive factors in estimating the fatigue lifetime. Therefore, special attention needs to be given in trying to lower their values. For complicated geometries, when the SCFs are not known, specific methods should be used for determining the nominal and the hot spot stresses. The nominal stress can be derived from the beam theory, or it can be chosen as the stress value far enough from the weld, where it is not influenced by the weld. For deriving the hot spot stress, a detailed analysis of the weld region is required, which involves extrapolation of the stresses, as it will be shown in Chapter 4 [9].

2.2.4 Hot spot stress method

The hot spot approach is usually used when the nominal stress is difficult to estimate from the FE model. Therefore, a simplified numerical procedure can be used to calculate the SCFs, together with an appropriate S-N curve:

- The stress concentration due to the weld itself is included in the chosen S-N curve, the D-curve;
- The stress concentration due to the geometry of the detail is calculated by means of a finite mesh model, through extrapolation.

When applying this method, the hot spot stress can be used directly with the S-N curve, without the need for calculating the nominal stress. Even though the nominal stress is not used directly in the fatigue calculations, an estimation of it is recommended in order to have an idea of the magnitude of the SCF.

2.2.5 S-N curves

An S-N curve, also know as Wöhler curve, is a graphical representation of the dependence of fatigue life in cycles (N) on fatigue strength (S). The S-N curves are derived from tests on samples of the material to be characterized, where a constant amplitude load, e.g. $F(t) = \sigma sin(\omega t)$, is applied by a testing machine, which also counts the numbers of cycles to failure. A relation between the number of cycles and the stress ranges can then be derived:

$$N = a(\Delta\sigma)^{-m} \tag{2.2}$$

where a is a constant and m is the negative inverse slope of the S-N curve [9]. Presented on a log-log scale, equation (2.2) becomes a straight line and is described by the formula:

$$logN = loga - mlog\Delta\sigma \tag{2.3}$$

The design S-N curve is more conservative and is obtained by subtracting two standard deviations, in order to account for uncertainties in the experimental S-N curves. Thus, $log\bar{a}$ is used instead of $loga$, where $log\bar{a} = loga - 2S_{logN}$, and S_{logN} is the standard deviation of $logN$. The basic design S-N curve is therefore given as:

$$logN = log\bar{a} - mlog\Delta\sigma \tag{2.4}$$

The thickness of the joining plates is also important for the fatigue strength. In order to take this into account, equation (2.4) was modified to:

$$logN = log\bar{a} - mlog(\Delta\sigma(\frac{t}{t_{ref}})^k) \tag{2.5}$$

where t_{ref} is 25 mm for welded connections other than tubular joints.

For joints in seawater, the S-N curve has two different slopes, with the changing slope at $N = 10^6$ cycles. A design curve with two slopes was used for this thesis.
All the values needed for the construction of the proper S-V curve are given in [9], for different types of joints, load conditions, weld types etc.

2.2.6 Palmgren-Miner rule

Fatigue design of welded structures is usually based on constant amplitude S-N data. An offshore structure, however, will experience a load history of a stochastic nature. The development of fatigue damage under stochastic or random loading is generally termed

cumulative damage. Numerous theories for calculating cumulative damage from S-N data may be found in the literature. However, the Miner summation has proven to be an efficient and accurate method, and simple at the same time. This method was proposed for the first time by A. Palmgren in 1924 and it was popularized by M.A. Miner in 1945.

The basic assumption in the Miner summation method is that the damage on the structure per load cycle is constant at a given stress range and equal to:

$$D = \frac{1}{N} \tag{2.6}$$

where N is the constant amplitude endurance at the given stress range. In a constant amplitude test, this leads to the following criterion [14]:

$$D_f \ \geq 1 \tag{2.7}$$

In a stress history of several stress ranges $S_{r,i}$, each with a number of cycles n_i, the damage sum follows from:

$$D = \sum_{i=1}^{k} \frac{n_i}{N_i} = \frac{1}{\bar{a}} \sum_{i=1}^{k} n_i \cdot (\Delta\sigma_i)^m \leq \eta \tag{2.8}$$

where,

D accumulated fatigue damage
$\bar{a}$ intercept of the design S-N curve with the log N axis
m negative inverse slope of the S-N curve
k number of stress blocks
n_i number of stress cycles in stress block i
N_i number of cycles to failure at constant stress range $\Delta\sigma_i$
η usage factor, equals to 1 [11]

In order to calculate the fatigue damage at a certain time t, assuming that the *i'th* cycle of a load has stress range $\Delta\sigma_k$ and it causes a damage equal to $1/N(\Delta\sigma_k)$, the following formula can be used:

$$D(t) = \sum_{t_i \leq t} \frac{1}{N(\Delta\sigma_k)} = \frac{1}{\bar{a}} \sum_{t_i \leq t} (\Delta\sigma)^m = \frac{1}{\bar{a}} D_m \tag{2.9}$$

where the sum contains all the cycles up to time t. The structure will fail if t equals t_f, which is the time when D(t)>1 for the first time.

In order to calculate the fatigue lifetime, certain sea states of a few hours are usually used, and the damage is calculate per second. If the length of the sea state is known, say T_{sea}, then the damage per second, d can be estimated as:

$$d = \frac{D(t)}{t} = \frac{D(T_{sea})}{T_{sea}} [1/s] \tag{2.10}$$

Then, the time to failure t_f corresponds to D(t)=1, and can be expressed as [37] :

$$t_f = \frac{1}{d}[s] \tag{2.11}$$

Equation (2.8) shows that the stress range $\Delta\sigma$ has the power of m, which means that for $m = 3$, an increase by a factor of 2, would result in an increase by a factor of 8 of the stress range. This illustrates how sensitive the SCFs are, and how important they are for the fatigue life prediction, as was also discussed in section 2.2.2.

2.2.7 Rainflow counting

For cumulative damage analysis, the stress time-series is broken down into individual cycles which are summed up to a distribution of stress ranges. A number of counting methods have been developed in order to extract the ranges from a variable amplitude stress time-series. Some of the most important are, *level crossing counting*, *peak counting*, *simple range counting* and *rainflow counting*.

The *rainflow counting* method is well documented and is the most widely used in the industry for fatigue assessment. The algorithm was developed in 1968 by T. Endo and M. Matsuishi and is designed to count reversals in accordance with a material's stress-strain response [16]. The idea of this algorithm is to not let the small oscillations (small cycles) stop the flow of large amplitudes. Figure 2.3 shows the basic principle of the rainflow counting method.

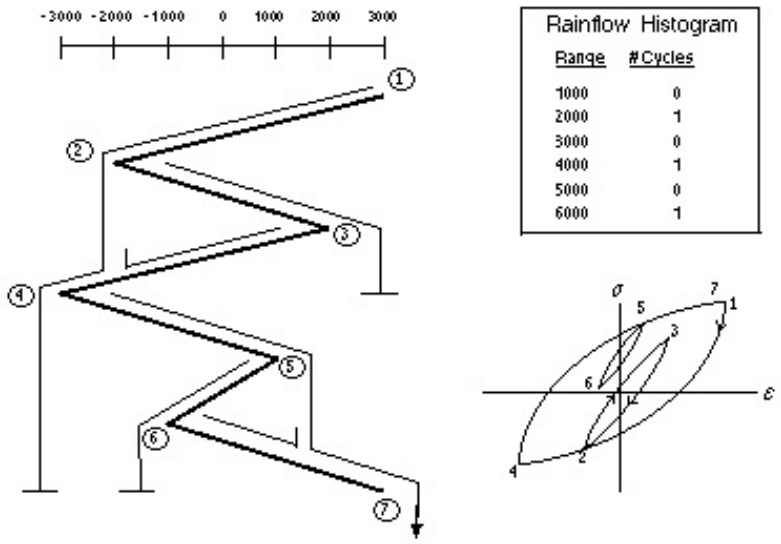

Figure 2.4: *Rainflow counting principle. Note the three complete hysteresis loops that are undisturbed by the smaller cycles [3]*

2.2.8 Uni-axial fatigue

The uni-axial fatigue problem is well documented in the literature and it has been applied on offshore structures since the mid 20th century. Uni-axial loading implies that the load is cyclically applied in only one direction and it would result in only one stress component in the structure, e.g. σ_{xx}. The load can either be with constant or variable amplitude. A schematic representation of uni-axial fatigue test is presented in Figure 2.4.

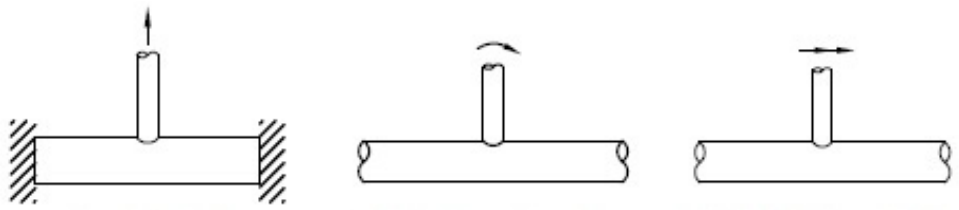

Figure 2.5: *Uni-axial fatigue loads: axial load, in-plane bending and out-of plane bending [9]*

For fatigue test experiments, in order to obtain the experimental S-N data, simple set-ups are used, the specimen is usually clamped and a constant or variable load is applied until it breaks [14].

The most used methods for assessing uni-axial fatigue are the nominal stress method and the hot spot method (see section 2.2.3). The procedures are straight-forward and it involves calculating the SCFs, obtaining the stress time-series, applying the rainflow counting and combining the resulted ranges with a proper design S-N curve and Miner's rule, to finally estimate the fatigue life span of the structure.

2.2.9 Multi-axial fatigue

In practice, the fatigue problem is usually much complicated than the uni-axial case, especially for the offshore industry. Random loads of different amplitudes and phase angles produce complex stress distributions in time at a certain hot spot (Figure 2.5). These load combinations create the premise for a multi-axial fatigue assessment.

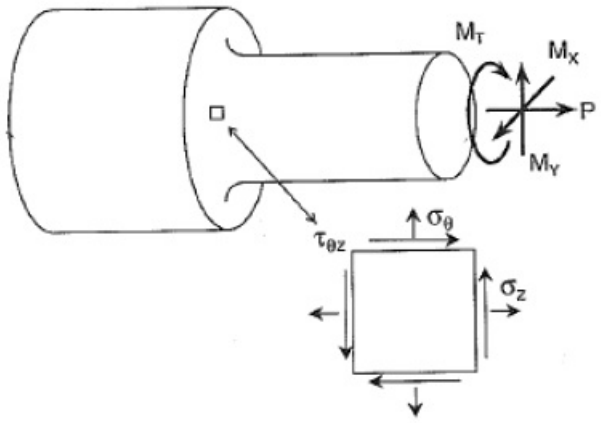

Figure 2.6: *Specimen under multi-axial loading [26]*

The main challenge for assessing multi-axial effects is to combine the time-histories of σ and τ in an effective way, which allows an accurate fatigue life prediction. Several types of methods have been developed to deal with the multi-axial fatigue problem and can be divided in 5 main categories [33]:

- Stress-based methods
- Strain-based methods
- Energy-based methods
- Fracture mechanics methods
- Methods for welded components

All calculation methods focus on fatigue life prediction. There are also different models included in each main category. Depending on the way the loads are applied on the structure, the following three categories can be distinguished:

1. Multi-axial loading with constant amplitude and in-phase loads
2. Multi-axial loading with constant amplitude and out-of-phase loads
3. Multi axial loading with variable amplitude and out-of-phase loads

Well known methods are used for assessing the first two cases of multi-axial fatigue. Some of them are shortly presented in the following.

Critical plane stress models

Models based on the critical plane stress have been developed from observations of fatigue cracking behavior on specimens which show that cracks initiate and propagate in preferential orientations [15]. The determination of the critical plane is dependent on the ratio

between the shear stress and the maximum normal stress. For each load history, suitable co-ordinate transformation relations can be used to find the angle ϕ, using the largest combination of f during one cycle or, for more complex histories, during one repetition of the load history:

$$f = \Delta\tau/2 + k\sigma_n^{max} \tag{2.12}$$

where k is a material constant

Different angles ϕ will be calculated depending on the ratio between σ and τ, and the fatigue life is then computed for the plane of maximum damage. There are many different models with different approaches of the critical plane definition, but the methodology is the same. The critical plane method has limitations when the shear stress approaches zero, and also for high ratios of σ/τ.

Nominal stress approach

The general design rules in Eurocode 3 recommend the use of nominal stress range combined with detail categories when calculating fatigue lifetime. The stress concentration effects shall be excluded. For spectrum loading, it is not practical to read the allowable stress ranges directly from curves in logarithmic scale. Because of this, an equivalent stress range is used, instead of the true stress spectrum. The equivalent stress range is normalized with N_{ref} stress cycles using the following formulas [32]:

$$\Delta\sigma_{eq} = \sqrt[m]{\frac{\sum_{i=1}^{n}(\Delta\sigma_{nom,i}^{m} \cdot n_i)}{N_{ref}}} \tag{2.13}$$

$$\Delta\tau_{eq} = \sqrt[m_\tau]{\frac{\sum_{i=1}^{n}(\Delta\tau_{nom,i}^{m_\tau} \cdot n_i)}{N_{ref}}} \tag{2.14}$$

For non-proportional loading conditions, the utilization factor of every stress component is checked separately, and their interaction is calculated as follows [6]:

$$\frac{\Delta\sigma_{eq,norm}}{\Delta\sigma_C} \leq 1 \tag{2.15}$$

$$\frac{\Delta\tau_{eq,norm}}{\Delta\tau_C} \leq 1 \tag{2.16}$$

Then, using the equivalent stress ranges for normal and shear stresses, the interaction between them is taken into account:

$$\left(\frac{\Delta\sigma_{eq,norm}}{\Delta\sigma_C}\right)^2 \left(\frac{\Delta\tau_{eq,norm}}{\Delta\tau_C}\right)^2 \leq 1.23 \tag{2.17}$$

Eurocode 3 recommends a different criterion when assessing the interaction between shear and normal stresses [5]:

$$\left(\frac{\Delta\sigma_{eq,norm}}{\Delta\sigma_C}\right)^3 \left(\frac{\Delta\tau_{eq,norm}}{\Delta\tau_C}\right)^5 \leq 1 \tag{2.18}$$

Hot spot stress approach

This method is well established among designers using the DNV standards and it is extensively described in [9]. The procedure involves using an FE model with a very fine mesh, usually recommended *txt*, and linearly extrapolating the stresses to the weld toe from the read out points at 0.5t and 1.5t away from the weld. Then, the effective hot spot stress ranges to be used with the proper hot spot S-N curve is derived as:

$$\Delta\sigma_{Eff} = max \begin{cases} \sqrt{\Delta\sigma_{\perp}^2} + 0.81\Delta\tau_{\parallel}^2 \\ \alpha\Delta\sigma_1 \\ \alpha|\Delta\sigma_2| \end{cases} \tag{2.19}$$

where α has a constant value, depending on the joint classification; the first principal stress is calculated as:

$$\Delta\sigma_1 = \frac{\Delta\sigma_{\perp} + \Delta\sigma_{\parallel}}{2} + \frac{1}{2}\sqrt{(\Delta\sigma_{\perp} - \Delta\sigma_{\parallel})^2 + 4\Delta\tau_{\parallel}^2} \tag{2.20}$$

and

$$\Delta\sigma_2 = \frac{\Delta\sigma_{\perp} + \Delta\sigma_{\parallel}}{2} - \frac{1}{2}\sqrt{(\Delta\sigma_{\perp} - \Delta\sigma_{\parallel})^2 + 4\Delta\tau_{\parallel}^2} \tag{2.21}$$

It is recommended that the derived hot spot stresses be used together with the D-curve [9].

This method is difficult to apply in cases of variable amplitude and out-of-phase loads because of the definition of the hot spot stress range that can not be consistent for such a case.

Equilibrium Equivalent Structural Stress Method (EESS

Another method for solving the multi-axial fatigue problem was developed more recently by P. Dong and J.K. Hong ([23], [19], [17]) and it is called the *Equilibrium Equivalent Structural Stress Method*. This method is based on the idea that the balanced nodal forces and moments always satisfy the equilibrium conditions at every nodal position. Stresses, however do not have to satisfy this condition at nodes or across element boundaries, especially at the welds. Therefore, the structural stress in the form of membrane and bending stress can be derived from the nodal forces and moments at the location of interest from an FE model, instead of using directly the stresses [20].
The great advantage of this method is the mesh insensitivity, in contrast to the hot spot approach, where the stresses increase as the mesh size becomes finer.

Based on elementary definitions from structural mechanics theory, the structural stress definition can be explained with the following considerations [17]:

- At a given location throughout the thickness of the plate, the stress state can be described with a simple distribution, as illustrated in Figure 2.6, as having a membrane and a bending component. The stress distribution in Figure 2.6(a) is equilibrium-equivalent to the local stress distribution in Figure 2.6(b).
- The structural stress distribution must satisfy the equilibrium conditions imposed by structural mechanics theory at both the hypothetical crack plane, e.g. at the weld toe, and a nearby reference plane, where the local distribution of the stresses are know from the FE analysis. This can be argued by considering the fact that the compatibility conditions of the corresponding finite element solutions are maintained at this location in such a calculation.
- Using the equilibrium condition in the context of elementary structural mechanics, should lead to the elimination of minimization of the mesh-sensitivity in the structural stress calculations. This is due to the fact that the local stress concentration close to a notch is dominated by self-equilibrating stress distribution.

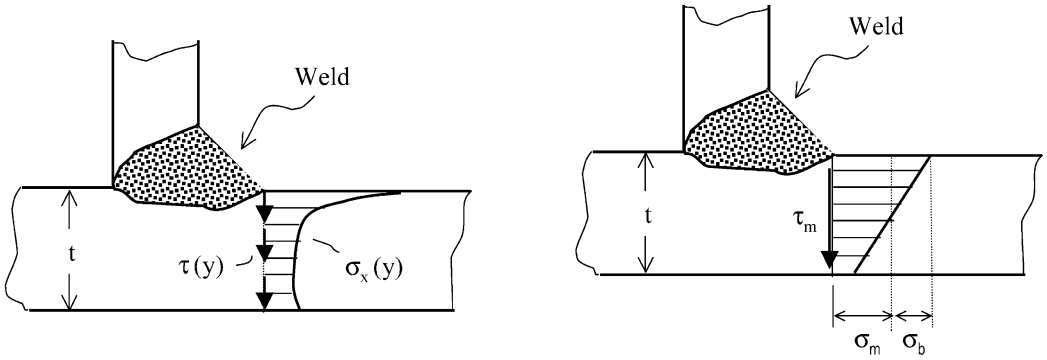

a) Local through-thickness normal and shear stress at weld toe

b) Structural stress definition at weld toe

Figure 2.7: *Structural stress definition for through-thickness fatigue crack [17]*

The structural stress components at each node along the weld can be calculated as:

$$\sigma_s = \sigma_m + \sigma_b = \frac{f_{y'}}{t} - \frac{6m_{x'}}{t^2} \tag{2.22}$$

$$\tau_s = \tau_m + \tau_b = \frac{f_{x'}}{t} - \frac{6m_{y'}}{t^2} \tag{2.23}$$

where $f_{y'}$ and $f_{x'}$ represent the line forces in y' and x' directions respectively, while $m_{x'}$ and $m_{y'}$ are the line moments about the corresponding axes in the local coordinate system as shown in Figure 2.7.

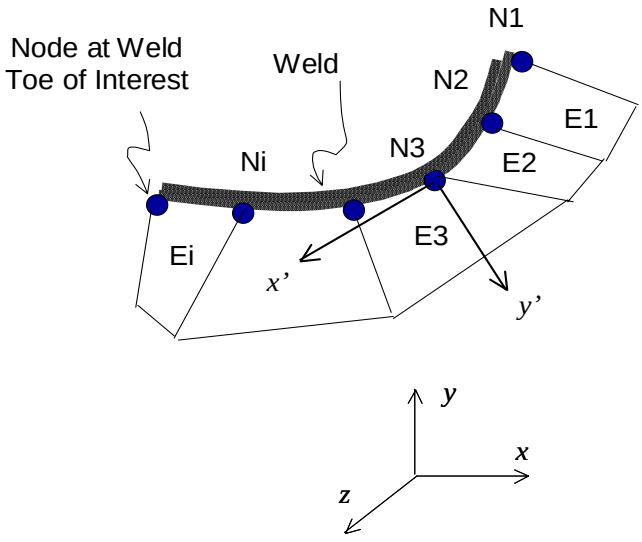

Figure 2.8: *Structural stress calculation procedure for an arbitrary curved weld [18]*

For in-phase and constant amplitude loading, the Von Mises, Tresca or Maximum Principle formulas can be applied directly [21]. For the out-of-phase loading case, a modified

Gough's ellipse describes the correlation between the normal and the shear stresses:

$$\left(\frac{\Delta\sigma_s}{\Delta S_e}\right)^2 + \left(\frac{\Delta\tau_s}{\Delta T_e}\right)^2 = [F(\delta)]^2 \tag{2.24}$$

where,

$\Delta\sigma_s$ and $\Delta\tau_s$	normal and shear stress components defined by eq. 2.22.
ΔS_e and ΔT_e	fatigue limits under pure $\Delta\sigma_s$ and $\Delta\tau_s$ respectively
$F(\delta)$	dimensionless parameter as a function of out-of-phase angle δ, with the minimum value of $1/\sqrt{2}$ [21]

The EESS method uses a single *Master S-N curve* that has been proven to be effective in consolidating a large amount of weld S-N data obtained from drastically different joint geometries, plate thicknesses and loading modes [20].

Path Dependent Maximum Range Method (PDMR

The PDMR method is a cycle counting method recently developed by researchers at Battelle to deal with complex multi-axial problems ([25], [38], [39]). Unlike any other method described before, it has been successfully applied to fatigue analysis of engineering components under variable amplitude, non-proportional, multi-axial fatigue loading histories. The PDMR begins by seeking the maximum possible distance (or range) between any two points in the equivalent stress/strain space over a given fatigue loading history, while also identifying the associated loading path-length. The process continues recursively until each loading path has been counted. The method then collects the cycles calculated and the associated path-lengths for subsequent calculations of the fatigue damage. The effectiveness of the PDMR method has been validated by its ability to correlate a large amount of fatigue data [24]. Under uni-axial loading conditions, the PDMR recovers exactly the same rainflow counting results.

After the stress time-series of the load history for the normal and shear stress are calculated, the corresponding points at each time step are plotted in a 2D graph. PDMR is just a counting method, i.e. it only takes care of calculating the stress ranges and the cycles from the stress time-series. Therefore, the time-series can be calculated with any other known method.

If a simple load path segment is considered, the counting procedure can be illustrated in Figure 2.8. The position R in the figure is referred to as a turning point. The distance from position R to the reference position P is a local maximum in distance traversed along the loading path. The position R* is a projected turning point on the actual loading path which is obtained by intersecting the loading path with the radius measured from P to R with respect to the reference position P. In the case of uni-axial fatigue, the virtual path R-R* becomes zero, since the corresponding time history in $\sigma_s - \sqrt{\beta}\tau_s$ is a straight line. Here, $\sqrt{\beta}$ is a constant representing a linear transformation with respect to $\sigma - \tau$ coordinate system. The method is applicable for both 2D and 3D stress or strain state with time-varying histories. A detailed description of the PDMR procedure can be found

in [25].

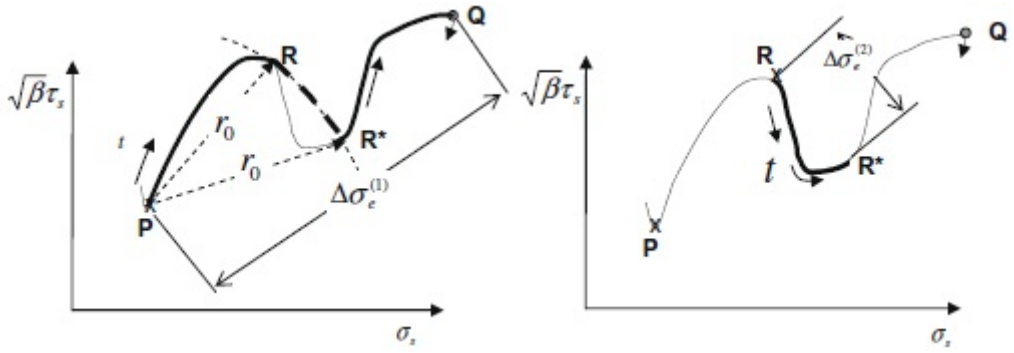

Figure 2.9: *Illustration of the PDMR cycle counting procedure [25]*

In the figure above, $\Delta\sigma_e$ is the *reference stress range*, and it represents the maximum distance between points P and Q or R and R*. The *effective stress range* ΔS_e (or the loading path) consists of the sum of all the segments comprised in a given path. The number of cycles and the corresponding stress ranges for the example in Figure 2.8 are summarized below.

Cycle counted	Range	Path length
0.5	P - Q	PR + RR* + R*Q
0.5	R - R*	RR*

Table 2.1: *PDMR cycle counting results for Fig. 2.8*

There are many algorithms that have been developed for this counting procedure. During the counting process, most of the CPU time is spent searching for the maximum range. A *brute force algorithm* is the easiest to implement and it would always provide a solution if it exists, but it has the drawback that the computational time is high, increasing with $O(n^2)$, where n is the number of spectrum data points. In order to speed up the execution of the PDMR method, more complex algorithm have been proposed, e.g. Graham Scan, Convex Hull algorithms (see Figure 2.9), Jarvis' March, "divide-and-conquer", "Marriage-before-conquest" and Chan's algorithm.

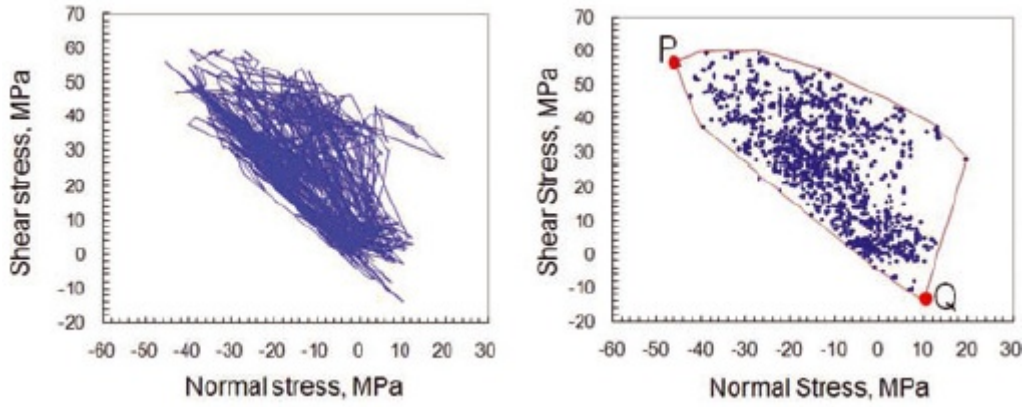

Figure 2.10: *Convex hull for a given loading path and data points [24]*

The standard procedure for the fatigue life assessment using the PDMR method comprises the following steps:

- Load the stress time histories $\sigma(t)$ and $\tau(t)$
- Apply a specific algorithm on the loading path, e.g. convex hull
- Apply a brute-force searching procedure to find the maximum range pair from the convex hull
- Count the number of cycles and the stress ranges

The PDMR procedure is briefly illustrated in Figure 2.10.

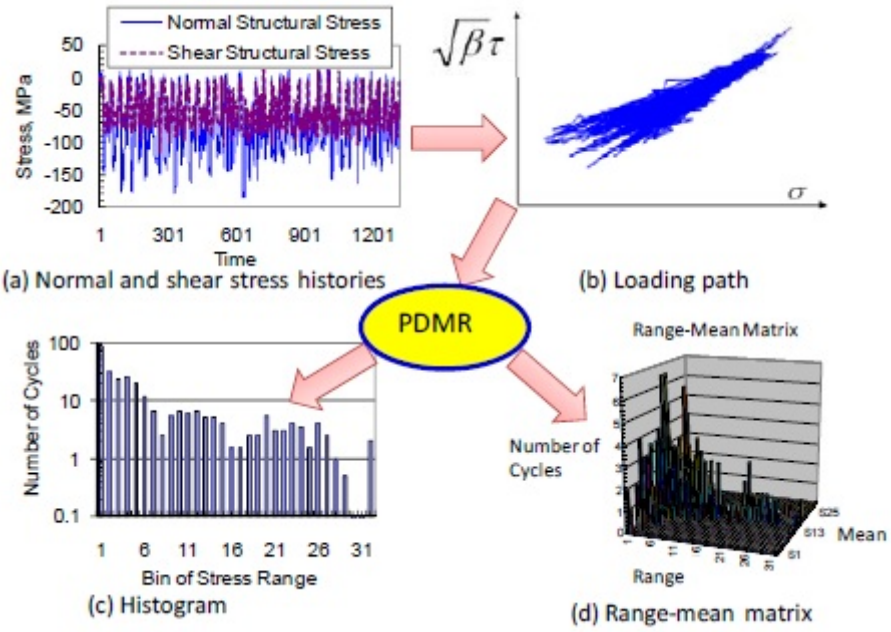

Figure 2.11: *Procedure of PDMR multi-axial cycle counting and fatigue life assessment [24]*

Based on experiments conducted so far [25], the application of Miner's rule with D=1 remains to be valid for non-proportional multi-axial fatigue.
Due to the innovative concept, correlation with classical methods and its ability to deal with complex multi-axial conditions under non-proportional loading histories, the PDMR method is proposed as a solution to cope with the multi-axial effects on the investigated structure.

Chapter 3

Finite Element Modeling

3.1 Software

The fatigue analysis was performed using a number of commercial software programs, each being used for certain steps in the work. The following programs were used by the author in order to obtain the fatigue damage results:

1. GeniE
2. Xtract
3. Matlab

The **GeniE** software is fully owned, supported and maintained by DNV. It is a software tool for designing and analyzing offshore and maritime structures made of beam and plates. Modeling, analysis and results are performed in the same graphical user interface [34] . SESAM GeniE is well suited for stability, loading and strength analysis, being able to export/import files to/from other software from the SESAM package.
The model is created by defining the structure's properties, e.g. cross section, material, boundary conditions. These can be pre-defined or user-defined. The mesh can be either generated automatically, or manually. The panel model and the finite element model can be saved as separate files. The software is able to perform linear static analysis, hydrodynamic analysis and pile/soil analysis, using **SESTRA** [35] as solver.

The **Xtract** software is a post processing tool, used to visualize the 3D model in detail, with or without analysis results. Its user friendly interface allows users to easily zooming, rotate and make graphs or animations for different load cases and different results attributes (displacements, stresses, reactions etc.) [36].

For the sub-modeling technique, **Sesam Manager** and **Submod** tools were used in order to export files from GeniE to Xtract.

Matlab is a high-level numerical computing program with its own scrip language based on C. For the present report it was used to process the results from the stress analysis, together with the load time-series and to calculate the fatigue life using the free and commercially available toolbox WAFO (Wave Analysis for Fatigue and Oceanography) [37]. A Microsoft Excel spreadsheet was used to extrapolate the stresses at the weld toe, which were further read and processed in Matlab.

Besides the above described software, some additional programs were used to obtain the force/moment time-series. This analysis was performed by PhD candidate Chenyu Luan utilizing the following software:

1. GeniE
2. HydroD
3. SIMO
4. RIFLEX
5. TDHMill

SIMO and RIFLEX tools are included in the "DeepC" application, which, together with GeniE and HydroD, are part of the DNV's SESAM package. This is a complete hydrodynamic and strength assessment system tool for the engineering of ships and offshore structures. TDHMill is a tool for calculating the wind thrust on a turbine.

3.1.1 Modeling procedure

The flowchart of the modeling procedure is presented in Figure 3.1. The blue boxes on the left hand side represent the dynamic response analysis, while the rest of the flowchart represents the work performed by the author.

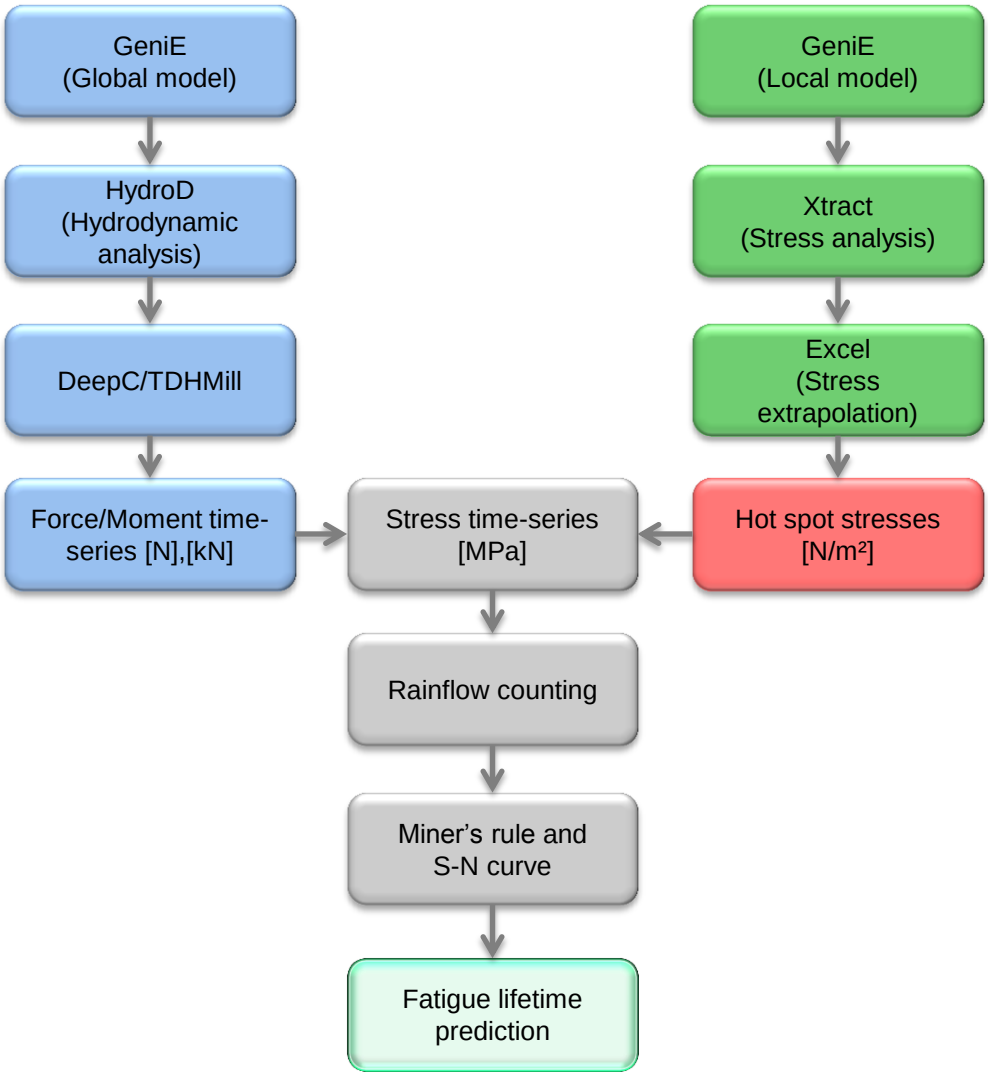

Figure 3.1: *Modeling procedure flowchart*

3.2 Global geometry of the floater

The semi-submersible offshore wind turbine prototype analyzed in this thesis was developed at CeSOS, NTNU and it consists of four columns, three on the sides, and one central column, supporting the 5MW NREL wind turbine [31]. The three pontoons connecting the side column to the central column are submerged and spaced at 120 degrees interval. The whole structure is made of steel, characterized by the Young's modulus of 210 GPa, the yield strength of 235 MPa, and the Poisson's ratio of 0.3

The dimensions of the global model were provided by PhD student Chenyu Luan [28]. A 3D model of the semi-submersible is shown in Figure 3.2. Note that the change in color in the column indicates the mean water level. The geometrical features of the floater are summarized below:

- length of the pontoons: 43 m
- dimension of the pontoon's section: 6x9 m
- diameter of the columns: 6.5 m
- freeboard: 20 m
- draft: 30 m
- displaced volume: 10550 m^3
- steel weight (hull): 1804 tons
- plate thickness: 30 mm.

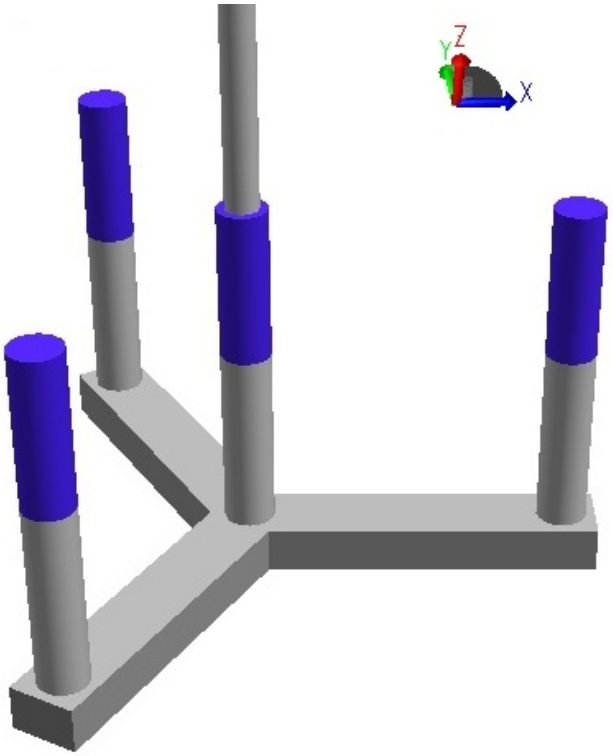

Figure 3.2: *3D model of the semi-submersible prototype*

Figure 3.3 illustrates the main dimension of the global model and the dimensions of the pontoon's section.

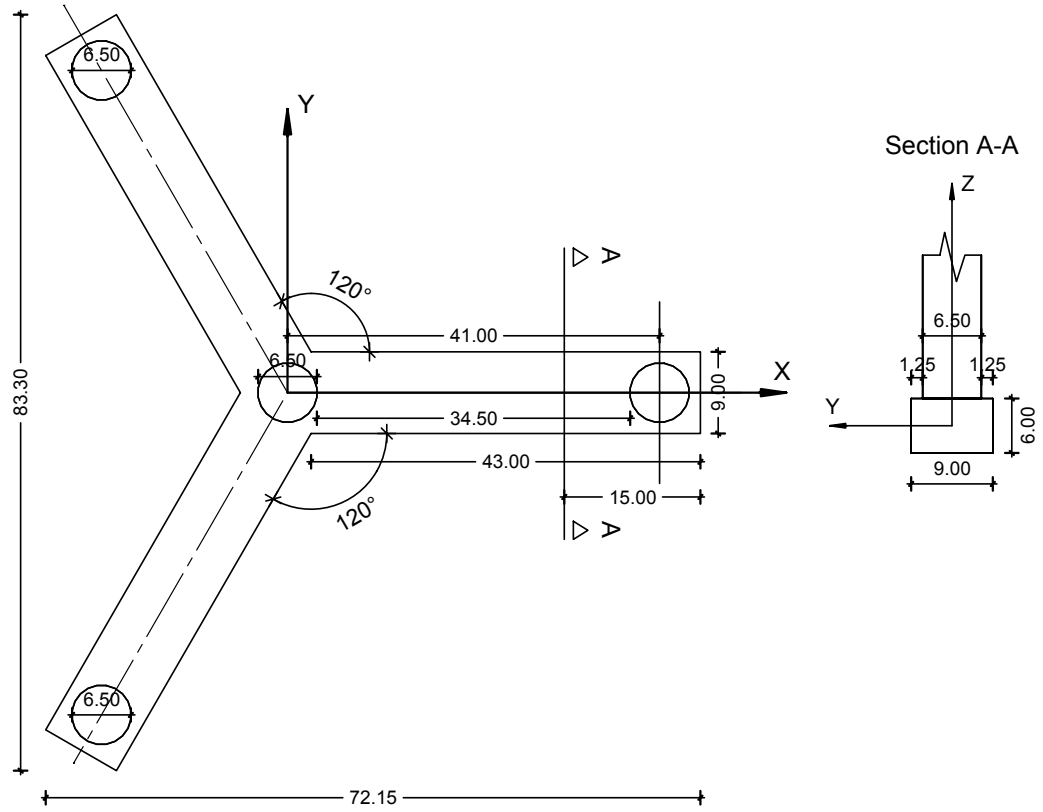

Figure 3.3: *Dimensions of the floater: view from upside and section*

3.3 Design of the joint connection

3.3.1 Coordinate system

The local coordinate system is a right hand coordinate system with the x-axis along the pontoon, pointing towards the side column. The z-axis always points upwards, and the y-axis is found using the right hand rule (Figure 3.4).

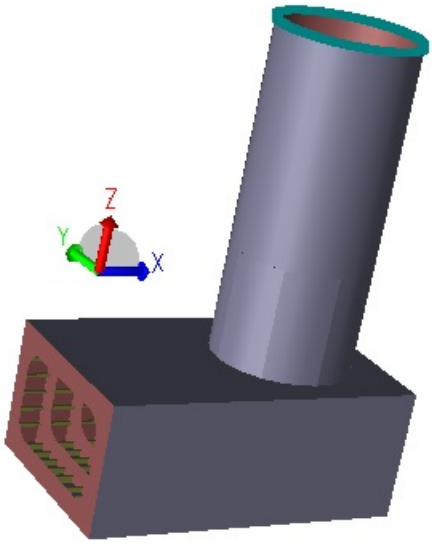

Figure 3.4: *Local coordinate system*

3.3.2 Geometry of the joint

The offset joint connection represents the local part of the structure where a pontoon intersects a side column. This region is critical for fatigue due to the sudden change in geometry, therefore, it should be treated with special consideration. Understanding the stress distribution in the structure is essential for designing the joint, strengthening critical areas using bulkheads, stiffeners and brackets, and limiting the magnitude of the stresses.

The global geometry of the floater provided for this analysis is simplified, considering only the exterior walls of the columns and the pontoons. This simplified model is adequate for a hydrodynamic and stability analysis, but for a detailed fatigue investigation is not appropriate. Thus, the joint connection had to go through a very consistent analysis, to redesign the geometry, in order to make the transition as smooth as possible. The pontoon was cut at 15 m away from its edge, and 7.25 m away from the column, in a region where the stresses are considered to be linear, unaffected by the hot spots, expected to occur at the base of the column. The column was cut 15 m above the top side of the pontoon, so there is enough space inside for vertical bulkheads and stiffeners, and the overall behavior of the assembly is captured.

Two different geometries were proposed and compared, in order to make a good assessment and to proceed further with the best solution. The detailed configurations and analysis results of the two geometries can be found in [29], while in the present paper only the main features and the most important results of each model are presented.

Model 1

The first model proposed was based on the idea that the change in geometry in the

column-pontoon area needs to be as smooth as possible. Therefore, the solution was to create a transition zone with a circular section at the top and a rectangular section at the bottom. The lowest part of the column is hence a square, which fits perfectly on the whole width of the pontoon, resting on its vertical walls.

Along the walls of the pontoon, horizontal T-section beam stiffeners were placed, spaced at 0.8 m between each other. In order to maintain the steel weight and the moment of inertia of the section in the same range as before the redesign, the plate thickness in the whole sub-structure was reduced to 25 mm. In the pontoon, vertical web frames and stiffeners were also designed. Inside the connection cage, the beams create grids attached to the walls, which give extra stiffness to the structure. These geometrical features can be observed in Figure 3.5.

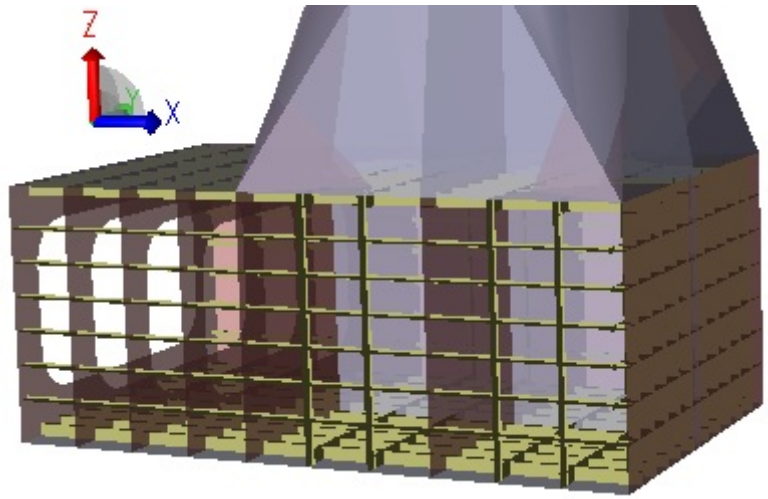

Figure 3.5: *Web frames and stiffeners in Model 1*

The pontoon and the column are connected through the transition piece described above, and through two rigid vertical bulkheads, perpendicular to each other. These elements go all the way from the bottom of the pontoon, up to 13 m in the column and end with a ring stiffener which provides extra rigidity. Another ring stiffener is placed at the top of the transition piece, 5 cm into the cylindrical part of the column, outside the area where a significant bending moment would appear.

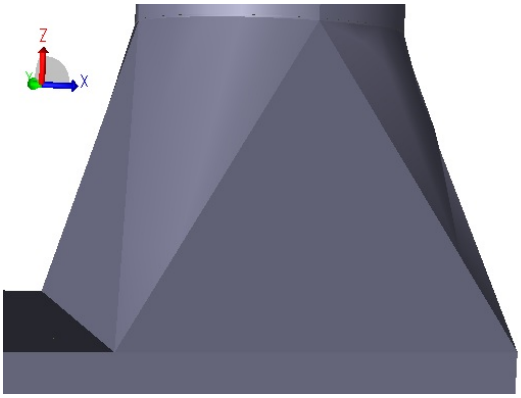

Figure 3.6: *Transition element in Model 1*

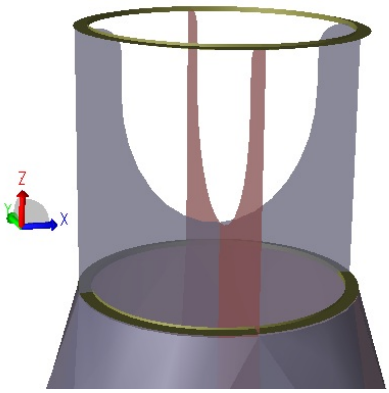

Figure 3.7: *Vertical bulkheads in Model 1*

An important improvement brought to this structure is the extra plates that consolidate the four corners at the bottom of the column (see Figure 3.8). The strengthening of the corners was obvious as the stresses in the region after this change in configuration dropped significantly [29].

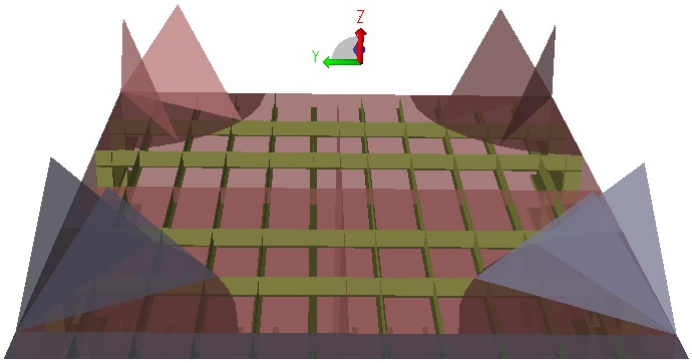

Figure 3.8: *Extra plates for improving Model 1*

The total mass of this model is 298.5 tons. It is expected that the critical parts for fatigue analysis will occur at the lower part of the cylinder because of the intersection of many elements with different shapes, and also at the bottom of the column, where the pontoon is intersected. The next two figures show the overall design of the first model proposed.

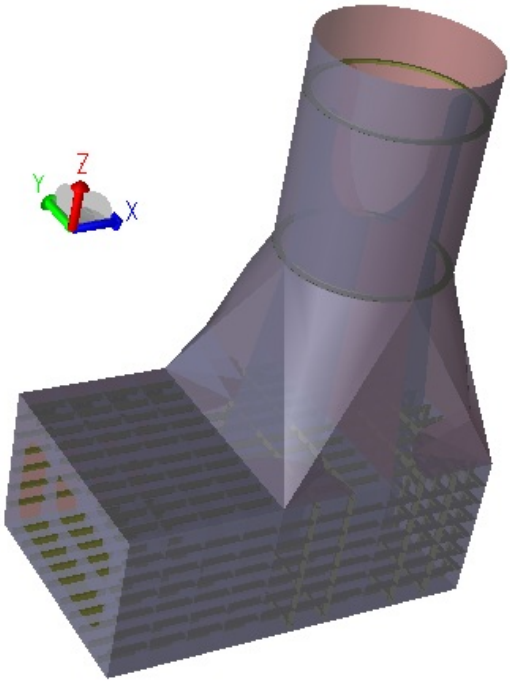

Figure 3.9: *Model 1 - view from above*

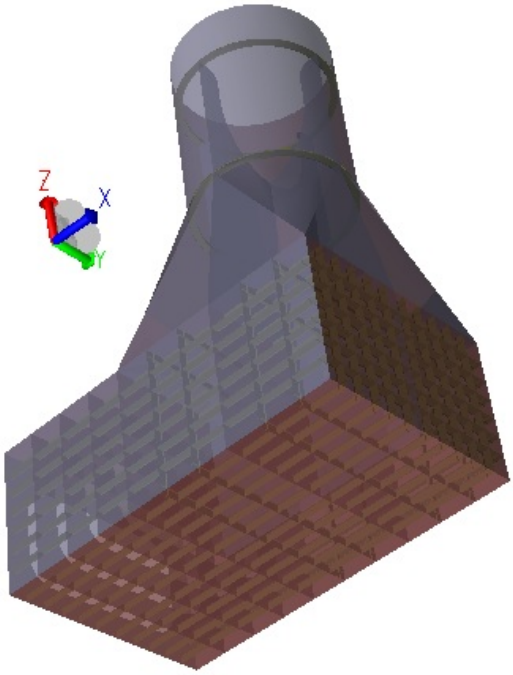

Figure 3.10: *Model 1 - view from below*

Model 2

The second model proposed for this joint connection was based on the idea that the column needs to go all the way through the pontoon, keeping its circular shape. Vertical bulkheads inside the structure make the whole assembly stiff and able to take and dissipate loads fairly uniformly.

The web frames and the beam stiffeners placed in the pontoon are arranged the same way as described in the first model. The only difference regarding this aspect is that the stiffeners attached to the top and bottom walls of the pontoon are stopped before intersecting the connection cage in order to avoid complex interactions with the vertical bulkheads.

A vertical watertight wall is placed 9 m away from the edge of the pontoon. This wall forms a cuboid shape cage with the external walls, inside which three other vertical bulkheads are placed at 45 degrees angles between each other. These elements go 5 m up into the column with a rounded geometry close to the top. A ring stiffener is again placed at the top to distribute the stresses and maintain the shape of the cylinder. All these characteristics are illustrated in the next two figures.

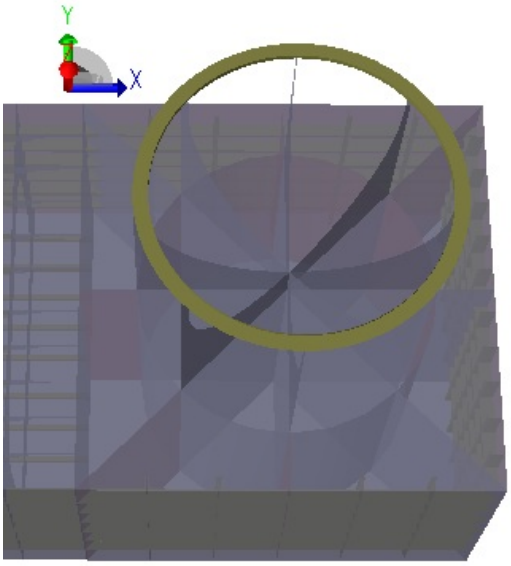

Figure 3.11: *Connection cage Model 2 - view from above*

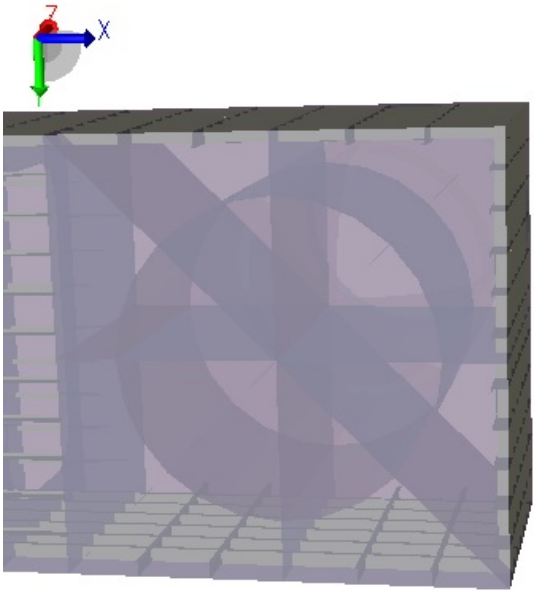

Figure 3.12: *Connection cage Model 2 - view from below*

This design can be characterized by a very stiff column-pontoon connection, but on the other side, there is a sudden change in geometry from the circular shape of the column, to the rectangular shape of the pontoon, where hot spots can develop. Also, at the top of the vertical bulkheads, stress concentrations might appear due to the direct transfer of the loads in those points. The total mass of this model is 306.8 tons, higher than in the first case. Two isometric views of the second design are presented below.

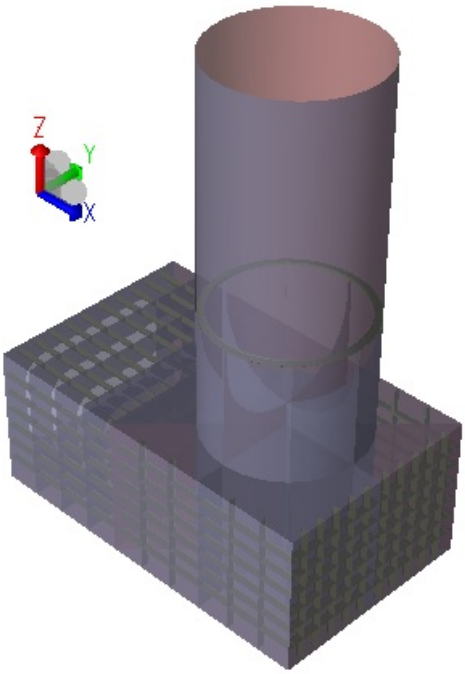

Figure 3.13: *Model 2 - view from above*

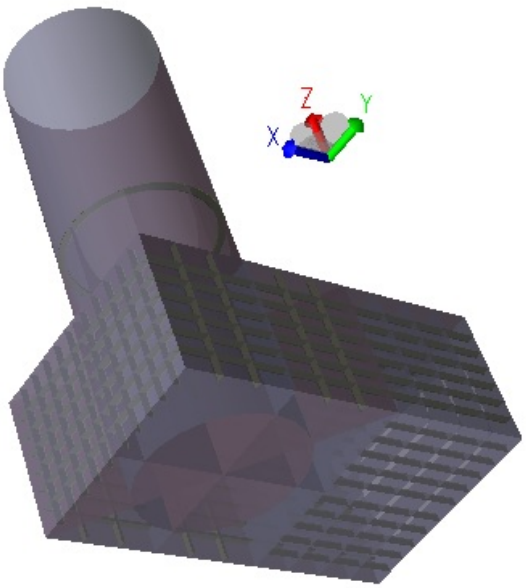

Figure 3.14: *Model 2 - view from below*

Comparison between the two models
Advantages of Model 1:

- 3% less steel consumption than the second model
- smooth transition between the column and the pontoon
- loads transmitted directly to the walls of the pontoon

Disadvantages of Model 1:

- very complex geometry, difficult to manufacture;
- large area exposed to waves and currents;
- transition element might be subjected to large stress concentration due to its complicated shape;

Advantages of Model 2:

- relative simple geometry, easy to manufacture;
- very rigid connection cage;
- the column is made in one piece;

Disadvantages of Model 2:

- large material consumption due to the 3 vertical bulkheads that make the connection;
- sharp corners due to the sudden change in geometry, where hot spots could occur.

Note: Usually the ridges of the pontoon are rounded for a better stress transfer, but for this thesis they were considered sharp corners, at 90 degrees, for the sake of simplicity.

More screen shots illustrating the geometries of the two models are show in Appendix A.

3.4 FEM analysis

The FE models for the two structures were created in the GeniE software. The steps in performing a finite element analysis in this software are:

1. Define the material properties and the elements' sections;
2. Create the geometry of the structure;
3. Create the boundary conditions;

4. Define the loads;
5. Mesh the structure;
6. Run the analysis;
7. View the results.

3.5 Boundary conditions

In order to analyze the joint connection, the global structure had to be cut by a plane in two locations. The boundary conditions then need to be defined at the column‘s cut. The loads were applied at the pontoon's cut.
It is very difficult to model the real behavior of the substructure because the whole assembly is free to move in reality. By limiting certain degrees of freedom, unrealistic reactions appear in the structure, hence extra stresses. A solution of compromise shall be established, based on assumptions.

3.5.1 Sensitivity study on boundary conditions

The second model was used to study the effects of the BC on the stress distribution. Four different conditions, all applied at the column's cut end were considered.

1. All 6 DOF were constrained. This is the most conservative approach, since large stresses will occur close to the boundary (Figure 3.15).

2. All 3 translations were constrained, while the rotations were set as ‘free’, thereby creating a hinge (Figure 3.16).

3. The third boundary condition is like the second one, but with 4 additional points on the boundary, with all 6 DOF restrained (Figure 3.17).

4. The last option considered was with all the rotations, plus the translations in -x and -y directions restrained, the translation in -z free, and 3 additional points with all 6 DOF fixed. In this way, the structure is partially allowed to translate in the xy plane, simulating the real behavior.

The results presented in the figures above represent the Von Misses stresses at the upper surface $[N/m^2]$, corresponding to an axial force F_x applied at the pontoon's cut. In all the cases, high stress concentrations occur close to the boundaries, as expected, and then the values decrease moving downwards on the column.

In the first three cases, the stress patterns are almost the same, with the remark that in the first case the hot spot is slightly more spread. For the second and the third boundary conditions, the results are identical, which means that the extra 4 fixed points do not significantly affect the stress distribution. In the last case, a small and intense hot spot can be noticed around the three fixed points. Because of the free translations in the xy plane, the reactions in the fixed points are very high, while going away from the hot spot, the stresses reduce rapidly to very low values. Therefore, this boundary condition does not capture properly the areas of interest.

The boundary condition that will be further used is the first case (clamp). This is the

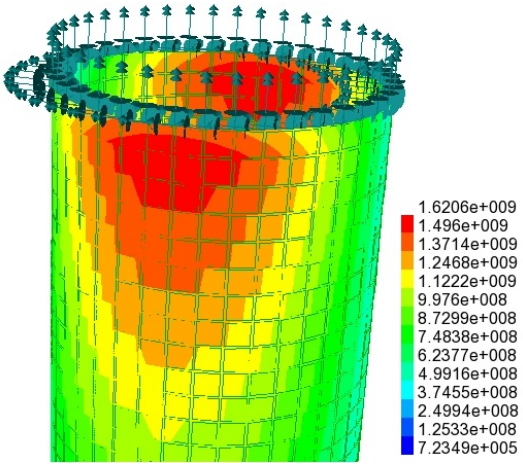

Figure 3.15: *BC1: clamped*

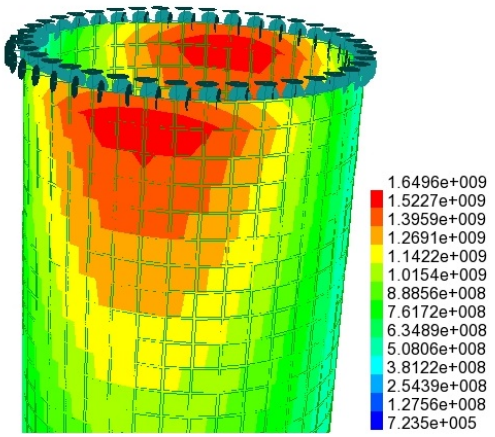

Figure 3.16: *BC2: free rotations*

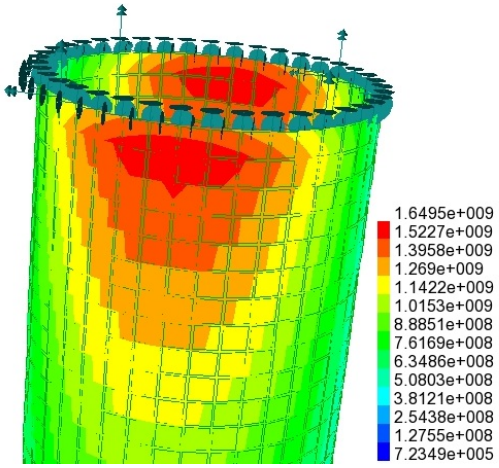

Figure 3.17: *BC3: free rotations plus 4 fixed points*

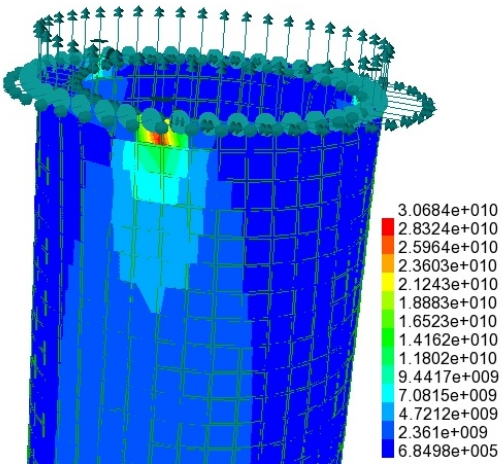

Figure 3.18: *BC4: free translations in -x and -y plus 3 fixed points*

most conservative option, but fairly adequate as well. The stresses close to the boundaries are rather uniform, and decrease fast enough, becoming almost independent of the BC in the region of interest, which is the intersection between the column and the pontoon.

Note: The hot spots close to the BC are not of interest for the purpose of this project because they do not actually appear in reality. The structure is free to move at those points, and therefore, the real stresses will be much smaller.

3.6 Mesh

Both models were meshed in the same way, in order to keep the properties the same as much as possible for further comparisons. GeniE has the capability to create an automatic mesh of the whole model, specifying only the mesh density. A relatively coarse mesh was used to create the two FE models, while that the hot spots resulted from the analysis were further investigated with a refined mesh using the sub-modeling technique.

The mesh size was set to 0.5 m, using only first order elements, i.e. 4-node shell elements and 2-node beam elements. The automatic meshing gave good results; at a closer view the pattern is quite symmetric and uniform for both models, with very few triangular elements.

Model	Number of nodes	Number of elements
1	7121	8882
2	5961	7406

Table 3.1: *Number of nodes and elements in the mesh*

The meshed 3D models are illustrated in the next two figures.

3.7 Stress distribution

There are 4 types of stresses which are relevant for the analyzed structure, as follows:

- σ_{xx} - the stress in the direction of the x-axis;
- σ_{yy} - the stress in the direction of the y-axis;
- τ_{xy} - shear stress in the direction of x/y axes;
- Von Mises stress:

$$\sigma_{VM} = \sqrt{\sigma_{xx}^2 - \sigma_{xx}\sigma_{yy} + \sigma_{yy}^2 + 3\tau_{xy}^2} \tag{3.1}$$

The distribution of the stresses for a 2D element is illustrated in Figure 3.21. Note that τ_{xy} and τ_{yx} are the same in this case.

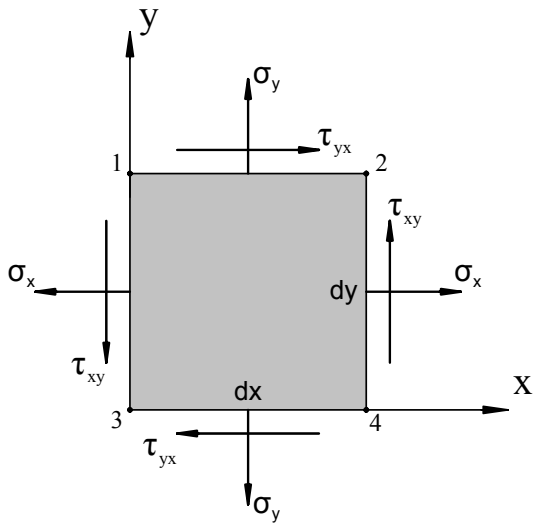

Figure 3.21: *Plane stresses*

Different loads produce different effects in the structure. The way the loads propagate in the structure is of critical importance when designing a structure, especially for such a sensitive region, which is a joint connection. In the following, the load effects and the stress distribution through the structure is explained.

Due to the L-shape of the investigated joint, the load transfer inside the floater needs

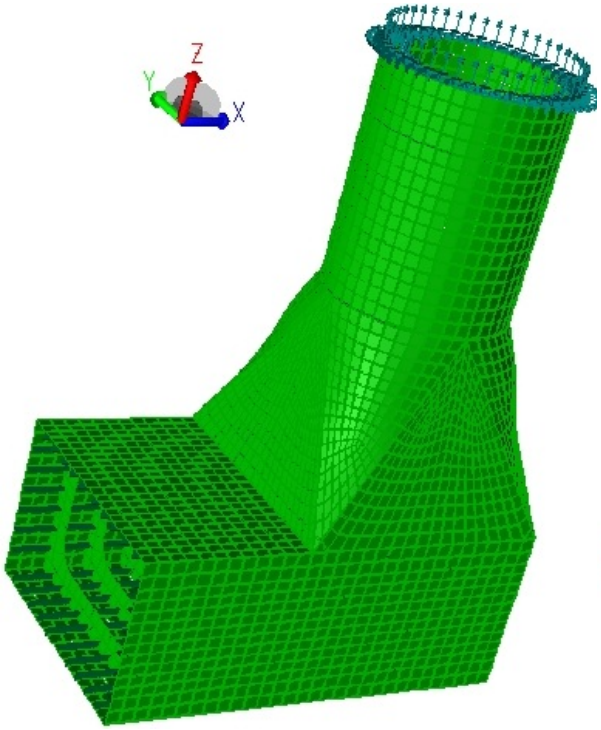

Figure 3.19: *Mesh model 1*

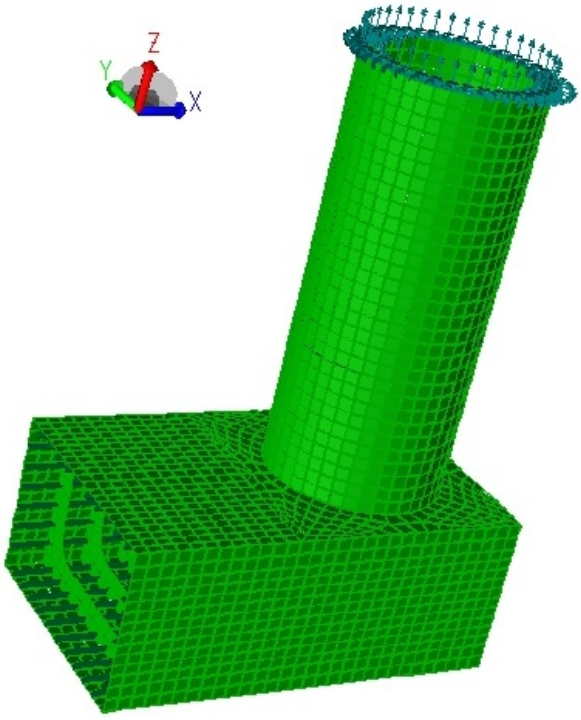

Figure 3.20: *Mesh model 2*

to be made through bulkheads, stiffeners and walls, arranged in a way that can dissipate stresses as uniformly as possible. The column is perpendicular to the pontoon, which means that input loads on the pontoon will induce different effects on the column.

An axial force $\mathbf{F_x}$ applied to the pontoon's section produces mainly σ_{xx} stresses, but this force will become perpendicular to the column, and thus, tangential stresses τ_{xy} will affect it. The lateral force $\mathbf{F_y}$ induces torsion in the column, which will induce shear stresses τ_{xy}, while $\mathbf{F_z}$, acting as a perpendicular force on the pontoon, will become an axial force in the column. Note that due to the complex geometry of the structure, and the input loads, all the principal stresses σ_{xx}, σ_{yy} and τ_{xy} will be present in any point.

The torsion moment $\mathbf{M_x}$ will try to rotate the pontoon around the x-axis, but it will act as a bending moment in the column. Considering a positive bending moment $\mathbf{M_y}$, this will induce tension in the column, while a negative $\mathbf{M_y}$ will produce compression. The bending moment $\mathbf{M_z}$ in the column results in a torsion moment in the column.
One needs to understand these stress patterns on each element of the structure, to be able to improve a geometry and strengthen the critical parts.

In order to calculate the stress at a point in the structure, e.g. the intersection between the column and the pontoon, considering only an axial force and a bending moment, the following analytic formula can be derived:

$$\sigma_{xx} = \frac{N_x}{A} \pm \frac{M_y}{W_y} \tag{3.2}$$

Figure 3.22 illustrates the effects of the moments applied at the pontoon's cut.

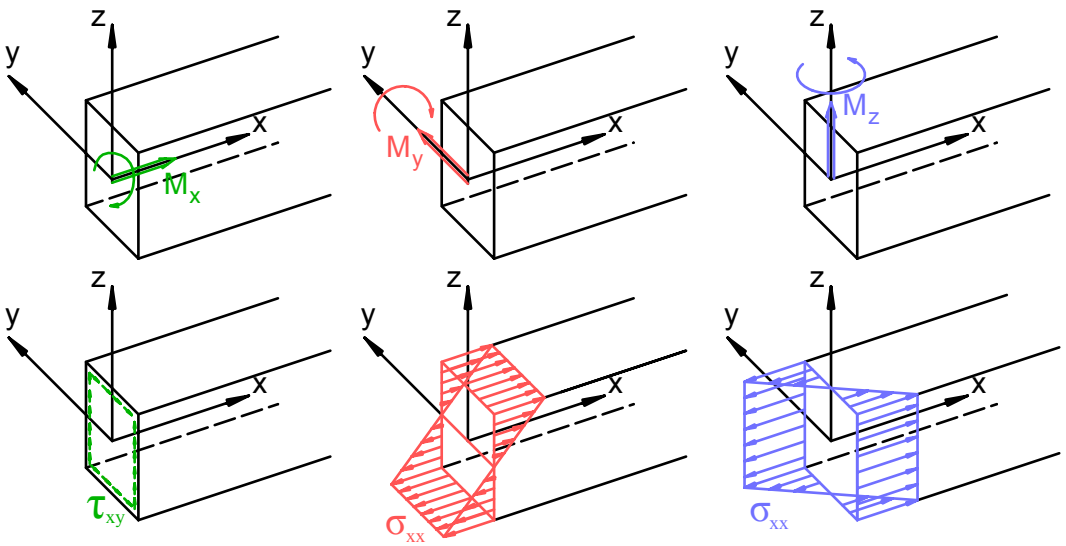

Figure 3.22: *M_x, M_y, M_z and their effects*

3.8 Structural analysis results

A detailed structural analysis was performed in order to identify the stress patterns, locate the hot spots and estimate the stress concentration factors. Six different load cases were created, three forces (F_x, F_y, F_z) and three moments (M_x, M_y, M_z), which were applied at the pontoon's cut. Normalized stresses were used in order to observe the fluctuations in the stress levels. This means that the structure has applied a force/moment that gives an input stress of 100 N/mm^2. In this way, the values in any point are compared to the normalized stress and the intensity of the hot spot can easily be estimated [29].

Model 1

The areas of interest for fatigue analysis in the first model are at the top and at the bottom of the conical element, where it connects with the cylinder and with the pontoon, respectively. The very complex geometry, consisting of curved and plane shell elements, with different angles, connected in a single point, and the irregular coarse mesh, combined with the relatively low stiffness of these areas result in very high stress concentrations. The most intense hot spot is illustrated in Figure 3.23 for the F_x load case.

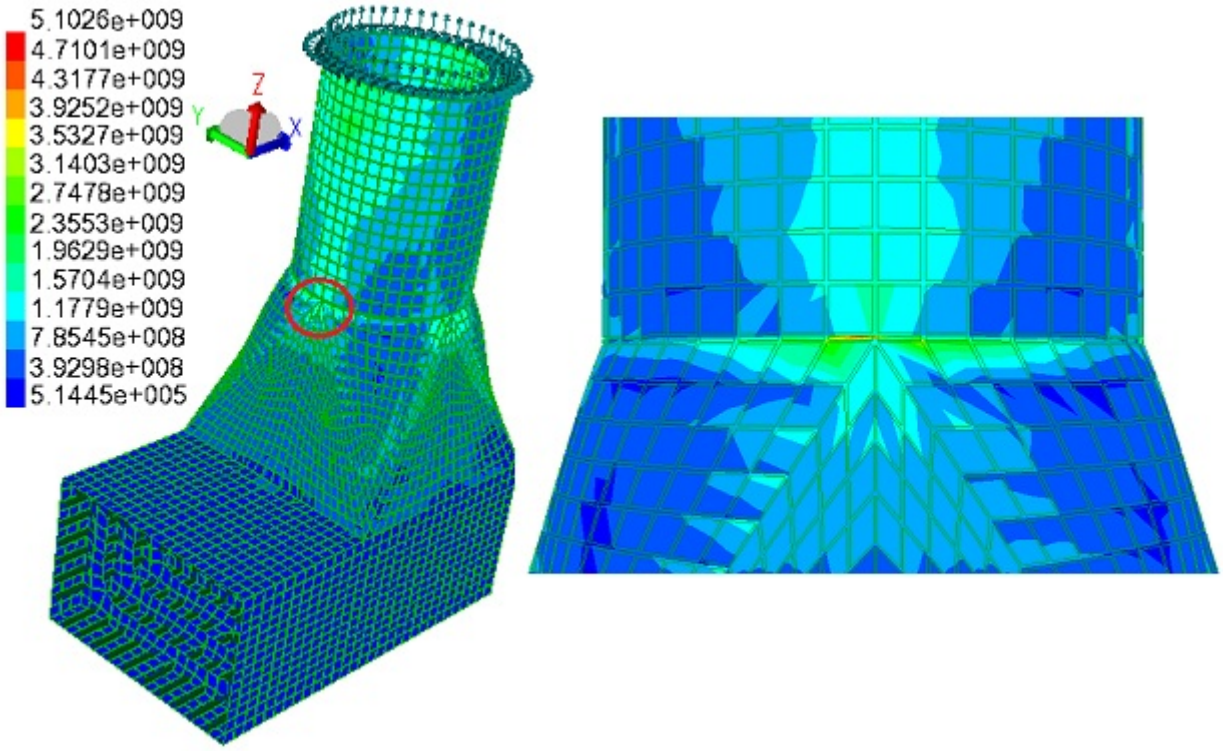

Figure 3.23: *Hot spot in Model 1 - Von Mises stress*

Table 3.2 presents the extreme values of the stresses that occur for each load case. Note that the stress values in the table are dimensionless, representing the ratios between the actual maximum stress and the normalized stress $\sigma_{norm} = 100\ N/mm^2$.

Load case	σ_{xx}	σ_{yy}	τ_{xy}	Von Mises
F_x	36.5	54.5	10.4	51
F_y	69.9	76.3	17.9	70.2
F_z	35.3	76.1	10.3	70.9
M_x	9.1	15.5	2.9	14.1
M_y	11.3	12.2	2.5	10.6
M_z	12.7	14.6	5	13.8

Table 3.2: *Maximum stress values for Model 1*

Note that some of the maximum values occur at the boundary conditions, which represent unrealistic stress concentrations due to the restrains on the degrees of freedom.

Model 2

The regions of interest for fatigue investigation for the second design are located at the intersection between the column and the pontoon and along the vertical bulkheads that go up into the column. Due to the sudden change in the geometry and the number of plates that intersect at the same point, an important hot spot occurs at the base of the column (see Figure 3.24).

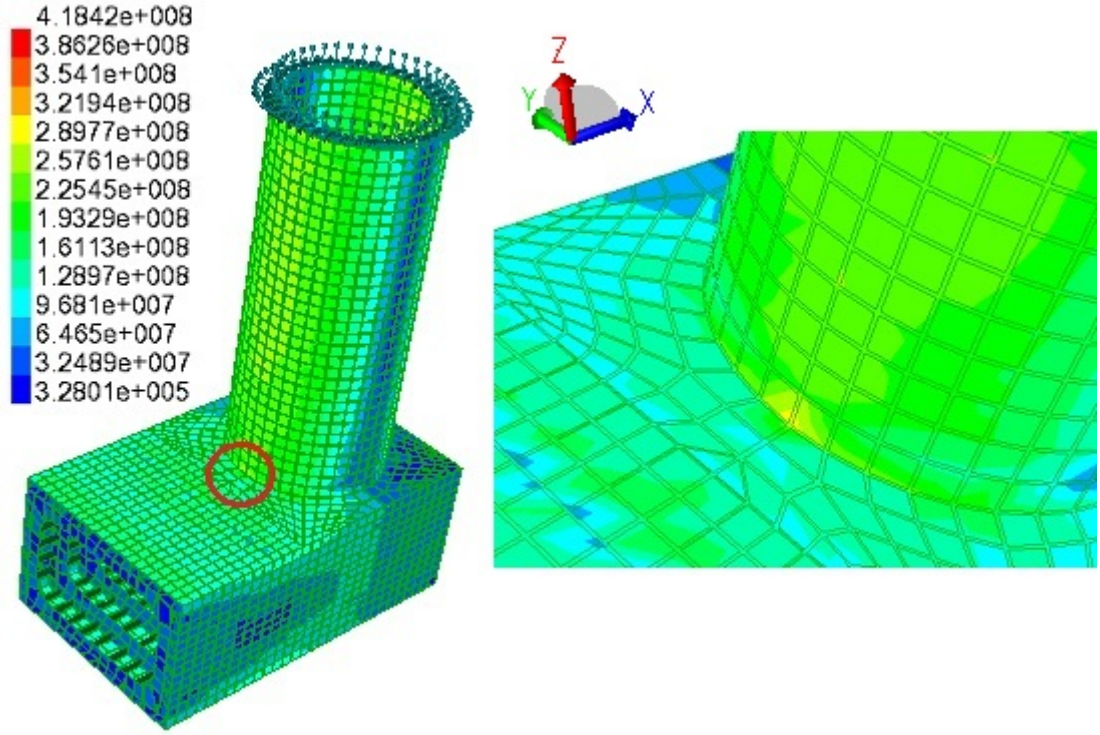

Figure 3.24: *Hot spot 1 in Model 2 - Von Mises stress*

Another two points with stress concentrations are presented in the next two figures. The one illustrated in Figure 3.25 occurs for the load case with axial force F_x and it represents the σ_{xx} stress. It can be explained by the fact that the vertical bulkheads are the structural elements that need to transfer and dissipate the stresses into the column. Therefore, the contact area has accumulated stresses.
The other hot spot, shown in Figure 3.26, at the upper part of the bulkheads, is not important for fatigue because the plate in that region is not welded.

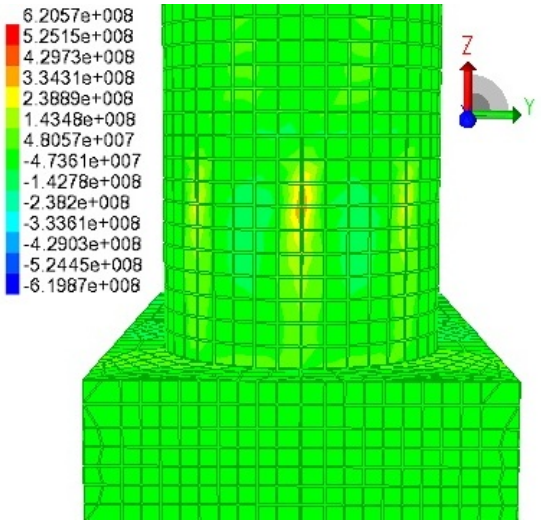

Figure 3.25: *Hot spot 2 in Model 2 - σ_{xx} stress*

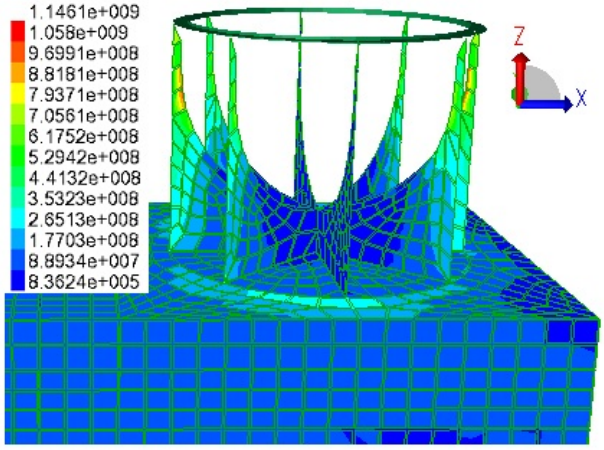

Figure 3.26: *Hot spot 3 in Model 2 - Von Mises stress*

The values of the ratios between the maximum stress and the normalized input stress for the second model are given in Table 3.3.

Load case	σ_{xx}	σ_{yy}	τ_{xy}	Von Mises
F_x	6.2	20.8	2.9	18.5
F_y	7.6	20.9	7.7	20.4
F_z	8.9	12.3	5.4	17.4
M_x	1.9	4.8	1.6	5
M_y	2.3	3.8	1.2	4.2
M_z	2	1.4	1.1	2.8

Table 3.3: *Maximum stress values for Model 2*

Conclusions on the two models

From the preliminary stress analysis in the two models, under different load cases, it can be stated that overall, the second one has a better structural response than the first one. Very intense hot spots occur in the first model due to the complex geometry and different shapes of the plates. The maximum values of the stresses, as shown in tables 3.2 and 3.3, are always higher for the same load case, than for the second model, and it can be up to 10 times higher.

The four corners that connect the column to the pontoon in the first model represent low strength regions, due to the change in geometry and low stiffness, that might be susceptible to fatigue. This does not happen for the second design, even if the transition from the cylindrical column to the rectangular pontoon is made without any smooth surfaces or extra brackets. Moreover, the connection between the cylinder and the conical element in the first model is another sensitive region, with high stress concentrations, up to 70 times larger than the input stress. This is unacceptable for the design and for further

fatigue analysis. Therefore a deeper investigation needs to be carried out. A possible solution to improve the structural response of this model would be to cast the regions of interest, to consider more stiffeners and brackets or to increase the thickness of the plates, or a combination thereof.

For the second model, the stress distribution is more uniform and the maximum values of interest are only up to 7-8 times large than the normalized stress. Further improvement of this structure can still be done, by designing extra brackets, plates or stiffeners, or by creating cut-outs in the existing plates.

It can be concluded that based on the analysis performed, the structural response of the second model is better than the first model, given the stress patterns and the maximum values at the hot spots. The relatively simple and uniform geometry of the second design, compared to the first, is also an important advantage from the manufacturing point of view. Theoretically, the two designs shall have approximately the same performances in terms of stress dissipation and stress concentrations, and this might be achieved if a more detailed analysis were to be performed. For the present thesis though, the results were considered final, and the choice of the better model was made based on the results obtained from the above described analysis. Considering the comparison between the two models, the second model was further analyzed and went through a detailed investigation for fatigue assessment.

It is important to mention that the FEM models might not give very accurate solutions, due to the complex geometries, mesh distribution and application of the loads. The analysis and the comparison were made based on the output that the GeniE software provided in these circumstances.

3.9 Sub-modeling technique

In many cases, global analysis provides insufficient stress information in local areas. The sub-modeling technique is a method that allows a part of the structure to be analyzed in more detail in order to produce more accurate solutions. The Submod software from the SESAM package from DNV is used for this purpose. It is a very efficient tool for extracting global deflections from the global analysis and applying these to a local model for refined analysis, thereby providing detailed stress information in highly stressed areas.

The motivation for such a refined analysis is to achieve more accurate results, or to assess alternative designs of a part of the structure. Provided that the model and results from the global analysis are available, together with a model of the part (the sub-model), Submod will perform a comparison of the two models and determine the position of the sub-model boundaries in the global model. The displacements of the global model at this position are automatically extracted and imposed on the boundary of the sub-model whereupon a standard static analysis of the part may be performed. The FE meshes of the global model and sub-model may be completely different, even using different element types. A node of the sub-model will get its imposed displacement picked up from within an element of the global model. The shape functions of the element theory are employed

to compute the displacements thereby ensuring maximum accuracy.

The standard procedure for sub-modeling is as follows:

1. Create the global model in GeniE and perform a linear analysis using Sestra as solver;
2. Create the local model in GeniE with refined mesh;
3. Set the boundary conditions of the local model as *prescribed*, so they can be transferred from the global model;
4. Run the Submod software through the Sesam Manager tool and get the results file of the local model;
5. Open the results file in Xtract and view the results.

After running the analysis of the global model in GeniE, the results file R1.SIN shall be exported and saved. The local models for this project were created by cutting the global model around the areas of interest, far enough from the hot spots, where the stress distribution is linear. It is crucial that the strength of the two models is not modified, e.g. the geometry remains the same. After creating the local model, the F1.FEM file is exported, and together with the results file from the global model, are uploaded in the Sesam Manager program, which uses the Submod and Sestra tools to output the R2.SIN file. This file can be opened in Xtract, where the results are analyzed in detail. The logical sequence of the sub-modeling technique is illustrated in the figure below.

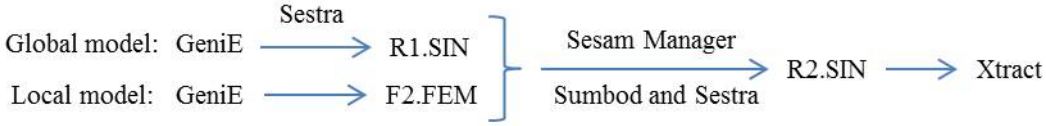

Figure 3.27: *Sub-modeling technique logical sequence*

The hot spot analyzed in this thesis for fatigue assessment is at the intersection between the column and the pontoon, as shown in Figure 3.28.

The mesh in the local model was chosen uniform, with a size of 25x25 mm (t x t), in order to cope with the DNV standard [9] for further analysis and extrapolation of the results. Both first order and second order elements were used, separately, in order to compare the results and observe the differences.

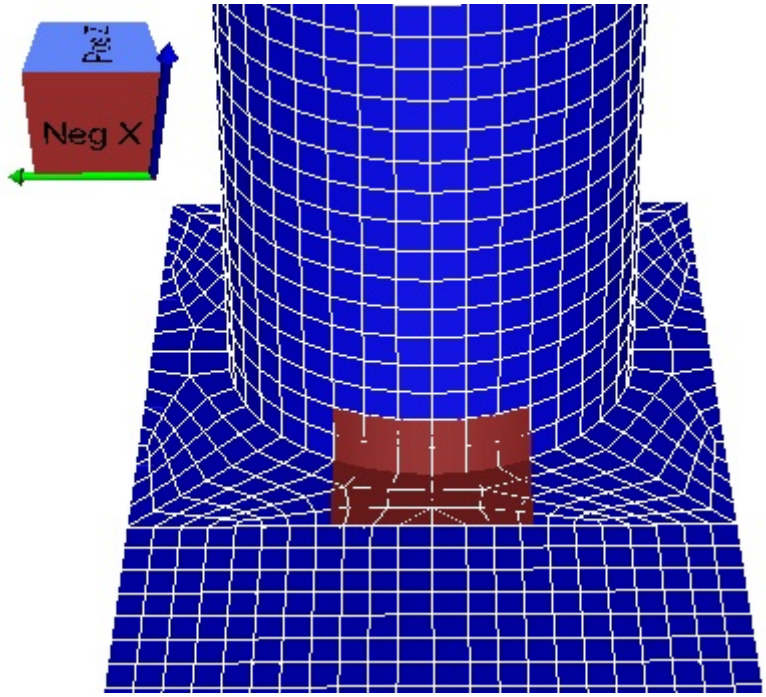

Figure 3.28: *Position of the sub-model in the global model*

Two different views of the sub-model are shown in the figures below, as captured from Xtract.

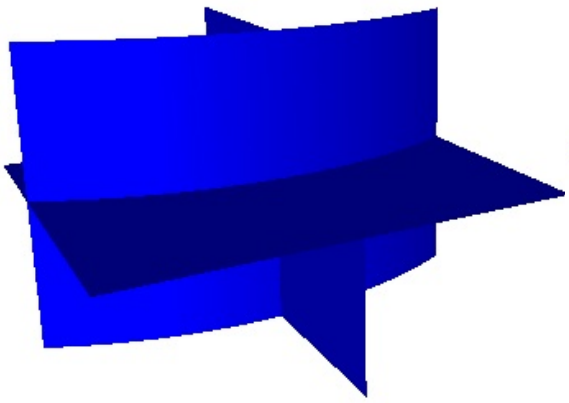

Figure 3.29: *Sub-model view 1*

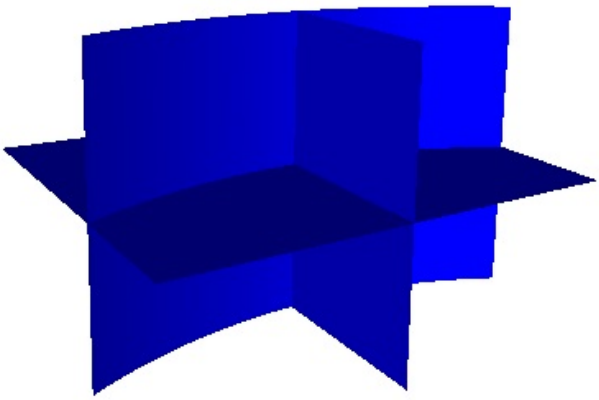

Figure 3.30: *Sub-model view 2*

As a generally valid statement, the stresses increase as the mesh size decreases. In order to show this, the stresses along the curved weld at the intersection between the column and the pontoon were plotted for both the global and the local models. The load case used was the F_x force applied to the pontoon which gives an input stress of 100 N/mm^2. The graph is presented in Figure 3.31.

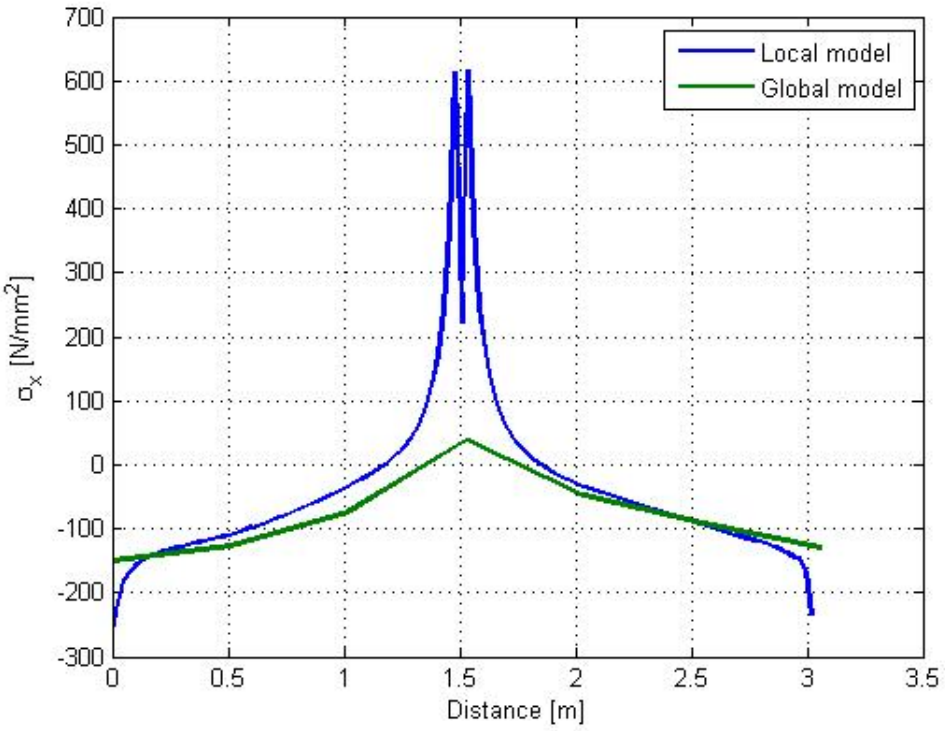

Figure 3.31: *σ_{xx} stress along the weld*

It can be observed that when approaching the hot spot area, the stresses in the local model start to grow exponentially because of the very fine mesh that can accurately capture the transition.

The FEM modeling requires deep understanding of the method and careful attention to all the steps along the process. Due to the complexity of the mathematical modeling, the results may be affected by errors. Some of the sources of errors that might affect the solutions are listed below [30]:

- simplifications in the mathematical model;
- discretization error;
- numerical approximation in the computer;
- poor input data in the software, e.g. geometry, material properties;
- incompatibilities and interactions between different element types;
- error in interpreting the results.

Some minor errors might be included when applying the sub-modeling technique because of the boundary conditions. Locally, close to the boundaries, some very high stress concentrations appear due to the interpolation of the displacements. In general, these values do not affect the stress distribution in the areas of interest and can generally be ignored.

Chapter 4

Hot spot stress derivation

The method used in this thesis for the evaluation of the stress magnitude at the weld is the hot spot stress method. This approach can cope with the complicated FE model and the complex stress patterns which resulted in the structure. The method involves linear extrapolation of the hot spot stresses up to the weld. This chapter presents the extrapolation procedure, an improvement of the structure and the hot spot stress results.

4.1 Loading

The global response of the structure, output for different sea states, give random load time-series at the pontoon's cut, consisting of all six components, i.e. three forces and three moments. In order to comply with this, six unit loads, referred to as *load cases* (LC), were created and applied separately on the structure:

- Axial force F_x (LC1)
- Lateral force F_y (LC2)
- Lateral force F_z (LC3)
- Torsion moment M_x (LC4)
- Bending moment M_y (LC5)
- Bending moment M_z (LC6)

The way the loads were applied in the GeniE software is presented in the next six images, for each load case. All the loads are considered to have positive signs, following the right hand rule.

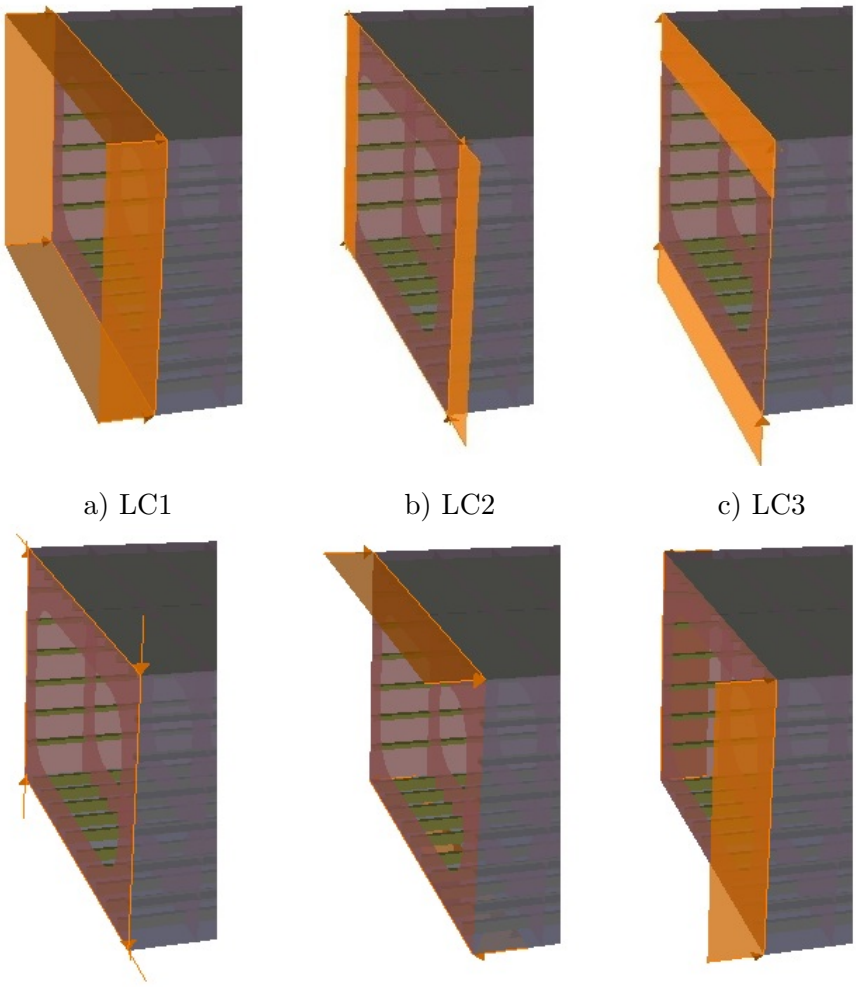

a) LC1 b) LC2 c) LC3

d) LC4 e) LC5 f) LC6

Figure 4.1: *Load cases*

4.2 Critical points for fatigue analysis

The analyzed sub-model has a complex geometry, with three plates intersecting each other. After investigating the stress patterns in the whole column-pontoon connection, the conclusion was that that the highest stresses occur at the intersection of the three plates. The weld between the horizontal plate and the curved plate part of the column, represent the region of concern for fatigue assessment.

Considering the six load cases separately, the stress distribution at the hot spot can be investigated. In the figures below, the σ_{xx} stress patterns for each LC are presented.

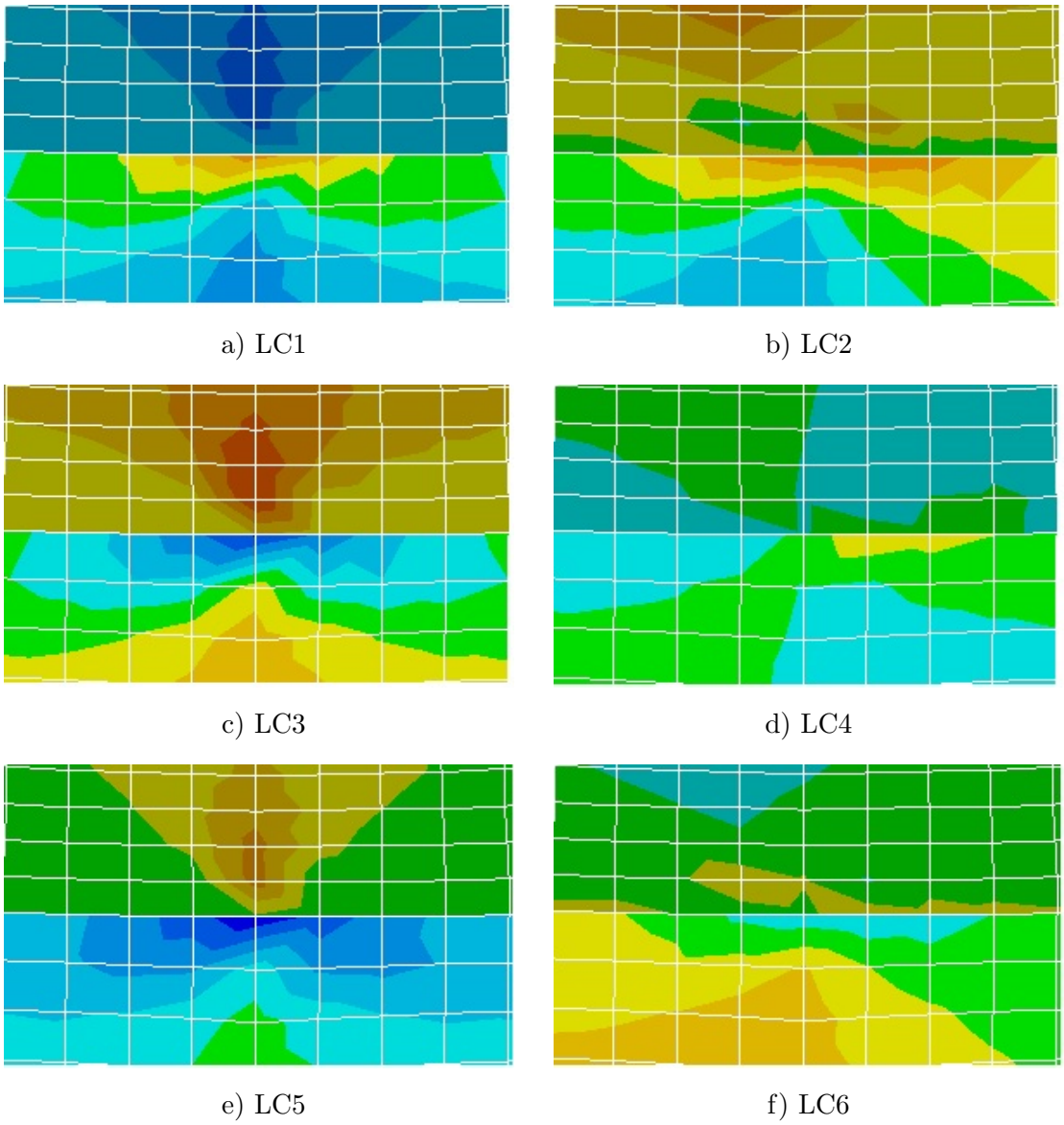

a) LC1 b) LC2

c) LC3 d) LC4

e) LC5 f) LC6

Figure 4.2: *Hot spot area under the six load cases*

The development of stress concentrations are obvious for the axial force, the two lateral forces and the bending moment M_y, while for torsion and bending moment M_z, the patterns are more uniform. Since each of the six load components might have a contribution to the total stress at a certain time step, all of them were further considered.

After analyzing the spread of the hot spot and the stress distribution, five points were chosen for fatigue lifetime prediction. The positions of the points are presented in the figure below. The distance between two neighbor points is one cell size, approximately 25 mm, equal to the plate thickness. Note that P3 is located exactly at the intersection of the three plates that form the joint.

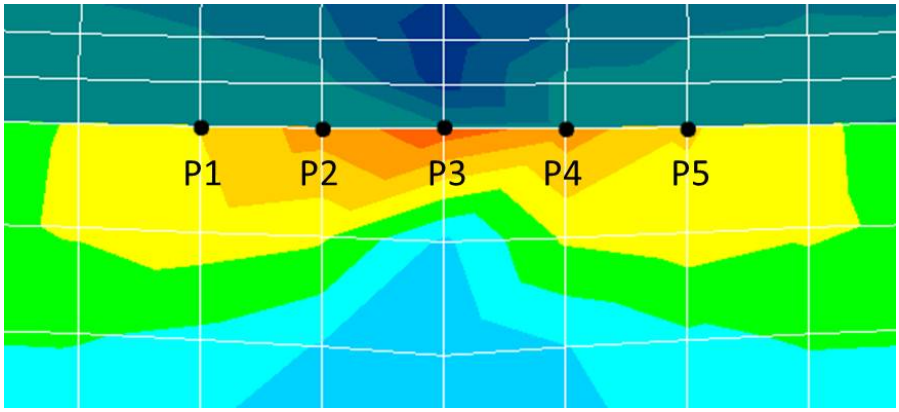

Figure 4.3: *Position of the five points assessed for fatigue*

The magnitude of the stresses at the weld was further calculated using the extrapolation technique presented in the next section.

4.3 Extrapolation procedure

For calculating the hot spot stress at the weld, with or without modeling the weld, the most used method is the extrapolation procedure [9]. A newer method that can provide the stress along the weld is the *Equilibrium Equivalent Structural Stress* method [17], described in section 2.2.8. Although very attractive especially because of its mesh insensitivity, and validated with a large number of experiments, it has the drawback that it requires as input the forces and moments in every node along the weld from the FE analysis. Because of the limitations of the GeniE software that can not provide this information, the application of this procedure becomes impracticable. Therefore, the method that will be followed for deriving the hot spot stress is the extrapolation procedure recommended by DNV [9].

The values of the stresses are read at 0.5 t and 1.5 t away from the weld, also denoted as read-out-points. In order to calculate the ROP values, the Gauss points inside the cells are used, applying linear or higher order extrapolation, depending on the type of mesh elements used. For two neighbor cells, the average value of the stresses are used. After obtaining the stresses at ROPs, linear extrapolation applies, and the stress at a certain node along the weld is calculated, also denoted as the hot spot stress. The notch stress is not taken into account when performing the extrapolation, but it is included in the S-N curve. The figure below illustrates the standard extrapolation procedure.

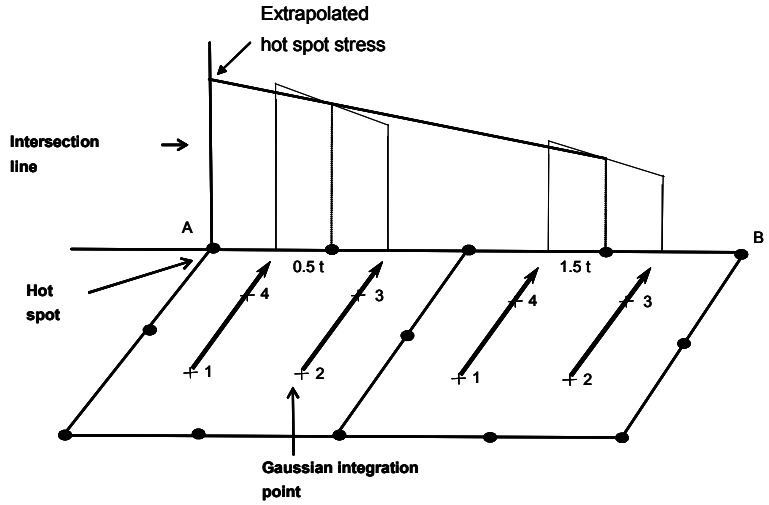

Figure 4.4: *Example of derivation of the hot spot for first order elements [9]*

In this project, the weld was not modeled, therefore the stresses were extrapolated from the read-out-points, situated at 0.5 t and 1.5 t, to the intersection line between the two plates.

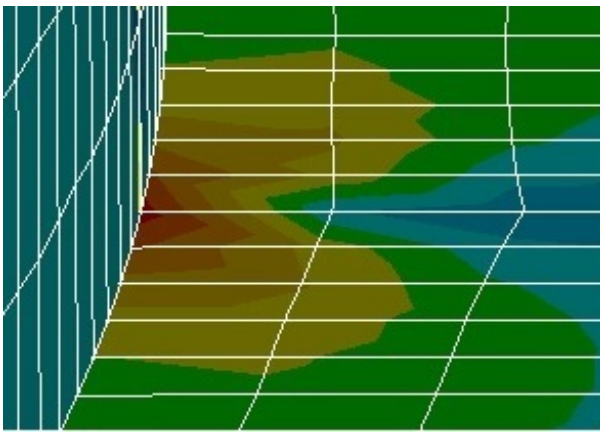

Figure 4.5: *σ_{xx} stress at the hot spot from Xtract*

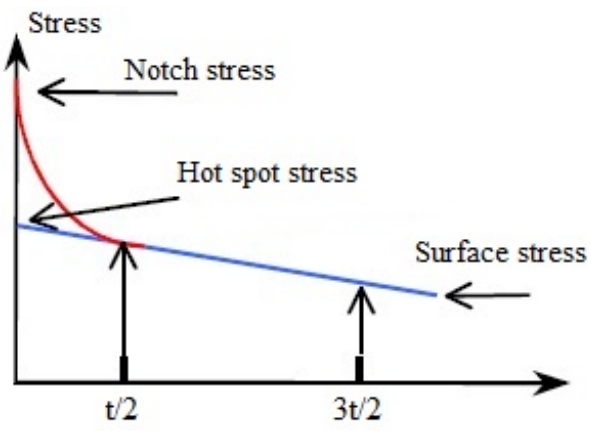

Figure 4.6: *Schematic stress distribution at the hot spot [9]*

4.4 Hot spot stress results

This section presents the stress values at the 5 points investigated, for two different designs of the joint connection. Both 4 nodes and 8 nodes elements were considered and compared. The analyzed weld is parallel to the -y axis, which means that the main damage will be produced by the σ_{xx} stress, which is perpendicular to the weld and it can open a potential crack by repeated cycles. Although it has a more limited impact on the fatigue damage, the tangential stress τ_{xy} is also calculated for further analysis of its influence, while σ_{yy} was disregarded.

The extrapolation of the stresses was performed in an Excel sheet, using first order shape functions for 4-node elements and second order shape functions for 8-node elements.

4.4.1 Design 1

The first geometry analyzed is the sub-model presented in figures 3.29 and 3.30, as it was cut from the global model. The results are presented in the following tables, in N/m^2 and correspond to a 1 kN or 1 kNm applied force or moment, respectively.

Point no.	LC1	LC2	LC3	LC4	LC5	LC6
1	3.11E+03	1.25E+03	-2.74E+04	-3.87E+01	-2.58E+03	-6.62E+01
2	5.22E+04	2.24E+03	-3.16E+04	-4.82E+01	-3.36E+03	-1.23E+02
3	4.88E+03	1.79E+03	-3.18E+04	3.08E+01	-3.40E+03	-1.02E+02
4	5.28E+03	2.45E+03	-3.22E+04	1.19E+02	-3.36E+03	-1.46E+02
5	3.79E+03	2.61E+03	-2.48E+04	9.75E+01	-2.61E+03	-1.47E+02

Table 4.1: *σ_{xx} hot spot stress for 4-node elements - Design 1*

Point no.	LC1	LC2	LC3	LC4	LC5	LC6
1	1.44E+02	-4.70E+03	-1.09E+02	3.40E+02	9.16E+01	2.43E+02
2	4.81E+02	-4.36E+03	-1.50E+03	3.22E+02	-4.66E+01	2.26E+02
3	-1.51E+02	-6.61E+03	6.70E+02	3.48E+02	5.91E+01	3.58E+02
4	-5.86E+02	-5.08E+03	2.00E+03	3.16E+02	9.25E+01	2.67E+02
5	-7.43E+02	-5.47E+03	6.66E+02	3.30E+02	-4.11E+01	2.88E+02

Table 4.2: *τ_{xy} hot spot stress for 4-node elements - Design 1*

Point no.	LC1	LC2	LC3	LC4	LC5	LC6
1	4.40E+03	1.46E+03	-2.80E+04	-2.32E+01	-2.89E+03	-7.80E+01
2	6.03E+03	2.08E+03	-3.62E+04	-1.98E+01	-3.86E+03	-1.15E+02
3	7.29E+03	1.86E+03	-4.40E+04	3.07E+01	-4.69E+03	-1.18E+02
4	6.05E+03	1.51E+03	-3.63E+04	7.68E+01	-3.84E+03	-1.75E+02
5	4.47E+03	1.55E+03	-2.84E+04	7.53E+01	-3.01E+03	-1.77E+02

Table 4.3: *σ_{xx} hot spot stress for 8-node elements - Design 1*

Point no.	LC1	LC2	LC3	LC4	LC5	LC6
1	1.23E+02	-7.26E+03	-1.12E+02	4.39E+02	1.18E+00	4.06E+02
2	2.85E+02	-7.56E+03	-7.56E+02	4.40E+02	1.05E+01	4.13E+02
3	-2.24E+02	-8.09E+03	9.98E+02	4.25E+02	8.94E+02	4.46E+02
4	-6.89E+02	-8.29E+03	2.58E+03	4.33E+02	1.54E+02	4.54E+02
5	-4.86E+02	-8.11E+03	1.82E+03	4.29E+02	7.90E+02	4.44E+02

Table 4.4: *τ_{xy} hot spot stress for 8-node elements - Design 1*

It can be observed that in general, the values for the quadratic elements are up to 40% larger than for the first order elements. The accuracy of second order elements is higher and it can capture more precisely the stress distribution inside of a cell. In order to illustrate these differences, the following two figures were created, for LC1 and LC5, with the values of the five points along the weld.

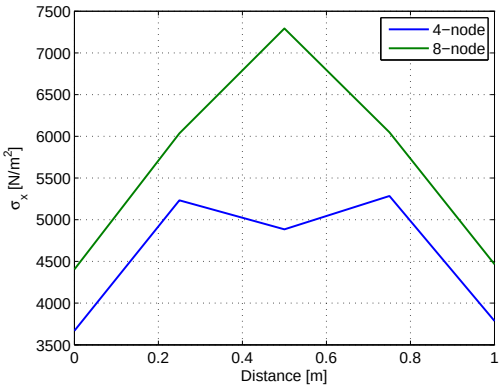

Figure 4.7: *Comparison between first and second order elements for Design 1 - σ_{xx} stress for LC1*

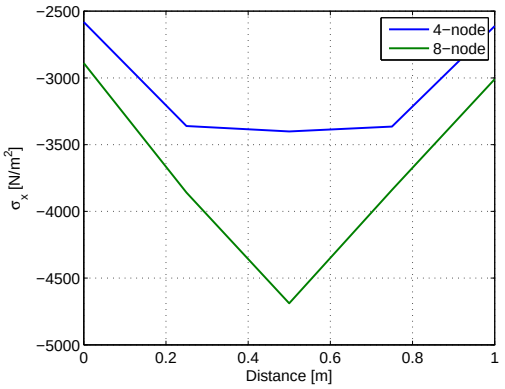

Figure 4.8: *Comparison between first and second order elements for Design 1 - σ_{xx} stress for LC5*

4.4.2 Design 2

The stresses at the weld for the first design were relatively large, which might lead to a very short fatigue lifetime. In order to reduce the stresses, the joint was redesigned, by cutting out a hole in the vertical plate, at the location of the hot spot. This eliminates the effects of the third plate, and the interaction is only between the horizontal plate and the cylindrical part. The stresses are redistributed on the edges at the hole, where large stresses appear. This is not important for fatigue because the vertical plate can be made in one piece, without being affected by welds (see Figure 4.9).

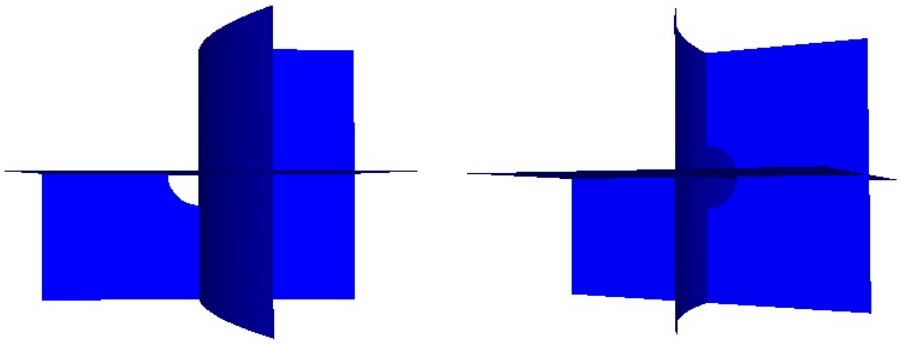

a) View 1 b) View 2

Figure 4.9: *Design 2 of the local model*

The extrapolated hot spot stress values for this design are presented in the tables below.

Point no.	LC1	LC2	LC3	LC4	LC5	LC6
1	1.32E+03	8.02E+02	-1.35E+04	1.54E+01	-1.52E+03	-4.28E+01
2	1.39E+03	8.94E+02	-1.39E+04	1.73E+01	-1.55E+03	4.98E+01
3	1.42E+03	8.93E+02	-1.40E+04	1.91E+01	-1.57E+03	-5.65E+01
4	1.40E+03	1.05E+03	-1.39E+04	2.04E+01	-1.56E+03	-6.20E+01
5	1.36E+03	1.11E+03	-1.37E+04	2.17E+01	-1.53E+03	-6.68E+01

Table 4.5: *σ_{xx} hot spot stress for 4-node elements - Design 2*

Point no.	LC1	LC2	LC3	LC4	LC5	LC6
1	-8.96E+01	-4.90E+03	3.98E+02	3.46E+02	5.16E+01	2.54E+02
2	-6.20E+01	-4.98E+03	3.13E+02	3.45E+02	3.67E+01	2.59E+02
3	-3.57E+01	-5.05E+03	2.34E+02	3.44E+02	2.20E+01	2.63E+02
4	-9.70E+00	-5.12E+03	1.58E+02	3.42E+02	7.47E+00	2.67E+02
5	1.95E+01	-5.18E+03	6.69E+02	3.41E+02	-7.92E+00	2.71E+02

Table 4.6: *τ_{xy} hot spot stress for 4-node elements - Design 2*

Point no.	LC1	LC2	LC3	LC4	LC5	LC6
1	1.80E+03	6.97E+02	-1.52E+04	1.72E+01	-1.72E+03	-3.65E+01
2	2.13E+03	7.50E+02	-1.62E+04	1.66E+01	-1.76E+03	-4.12E+01
3	2.15E+03	8.18E+02	-1.58E+04	1.61E+01	-1.77E+03	-4.69E+01
4	1.88E+03	8.98E+02	-1.57E+04	1.58E+01	-1.76E+03	-5.34E+01
5	1.82E+03	9.92E+02	-1.58E+04	1.56E+01	-1.73E+03	-6.07E+01

Table 4.7: *σ_{xx} hot spot stress for 8-node elements - Design 2*

Point no.	LC1	LC2	LC3	LC4	LC5	LC6
1	-4.98E+02	-7.60E+03	1.12E+03	4.48E+02	1.01E+02	4.14E+02
2	-2.15E+02	-7.67E+03	9.85E+02	4.47E+02	9.42E+01	4.18E+02
3	-1.79E+02	-7.74E+03	8.47E+02	4.46E+02	7.68E+01	4.22E+02
4	-1.33E+02	-7.82E+03	7.06E+02	4.44E+02	5.93E+01	4.29E+02
5	-8.57E+01	-7.88E+03	5.57E+02	4.43E+02	4.14E+01	4.31E+02

Table 4.8: *τ_{xy} hot spot stress for 8-node elements - Design 2*

The hot spot values presented above were combined directly and linearly with the load time-series obtained from the dynamic response analysis in order to obtain the stress time-series.

It is difficult to estimate the intensity of the hot spot looking at the stresses along the weld, obtained from unit loads applied on the column. Therefore, an estimation of the stress concentration factors needs to be done. This is shown in the next section.

4.5 Stress concentration factors

A stress concentration factor (SCF) is defined as the ratio between the hot spot stress and the nominal stress [9].

$$SCF = \frac{\sigma_{hotspot}}{\sigma_{nominal}} \tag{4.1}$$

From an FE analysis it is difficult to calculate the SCF because the nominal stress is hard to be estimated due to the complexity of the geometry. The beam theory is not applicable here and therefore, a solution of compromise that would allow a fair evaluation of the SCF needs to be found. Even if the SCF were not directly used in further calculations, it is important to have an idea about their range. The fatigue lifetime of the structure is very sensitive to the variation of the SCF, as it can be seen in equation (2.8). An increase by a factor of 2 will result in an increase of the stress by a factor of 2^m, where m is the negative inverse slope of the S-N curve.

The nominal stress (σ_{xx}) was considered 1 m away from the weld, in a region unaffected by the hot spot. The SCF were evaluated for the two designs, for each of the six load cases and for both 4-node and 8-node elements.

4.5.1 Design 1

The stress concentration factors for the first design are presented in the following tables:

Point no.	LC1	LC2	LC3	LC4	LC5	LC6
1	3.4	15.3	14.9	8.9	4.2	10.9
2	5.0	49.5	17.4	8.6	5.4	42.7
3	5.2	15.9	41.3	5.8	6.2	10.2
4	4.9	35.5	19.2	27.2	5.5	43.5
5	3.8	54.2	14.7	20.0	4.3	68.6

Table 4.9: *SCFs for Design 1 - 4-node elements*

Point no.	LC1	LC2	LC3	LC4	LC5	LC6
1	4.3	16.9	15.8	5.3	5.7	12
2	5.5	52.3	20.8	3.7	7.2	44.3
3	7.2	8.7	25.5	36.1	9.5	7.9
4	5.5	29.7	21	22.6	7.2	36.5
5	4.3	64	16.3	18.2	5.9	68

Table 4.10: *SCFs for Design 1 - 8-node elements*

Again, for most of the points and load cases, the quadratic elements have higher SCFs. The extremely large values in the tables above occur because the nominal stress is close to zero at 1 m away from the weld due to the way the loads were applied. Some load cases do not induce any axial stress in the structure, but because of the interaction between the structural elements, the hot spot will be affected by σ_{xx} stresses.

4.5.2 Design 2

For the design with a cut-out, the SCFs are listed in the tables below.

Point no.	LC1	LC2	LC3	LC4	LC5	LC6
1	1	9.2	7.3	3.5	2.5	6.4
2	1.1	30.5	7.6	3.1	2.5	27.4
3	1.2	8.2	10.5	3.6	2.9	5.1
4	1.0	14.8	8.3	4.5	2.5	18
5	1.0	21.6	8.1	4.2	2.5	34.3

Table 4.11: *SCFs for Design 2 - 4-node elements*

Point no.	LC1	LC2	LC3	LC4	LC5	LC6
1	1.4	7.6	8.6	3.9	2.8	6.9
2	1.6	18.5	9.3	3.1	2.8	19.1
3	1.8	3.4	9.1	18.4	3.2	3
4	1.4	9.6	9.1	4.5	2.9	16.4
5	1.4	20.4	9.1	3.6	2.8	39.7

Table 4.12: *SCFs for Design 2 - 8-node elements*

4.6 Comparison between the two designs

It can be clearly observed from the tables presenting the extrapolated stresses, that the design with a cut-out has lower values, which means that it can distribute the stresses more efficiently, without large concentrations. To illustrate this, the values along the weld were plotted in the next two graphs, for LC1 and LC5, for 8-node elements.

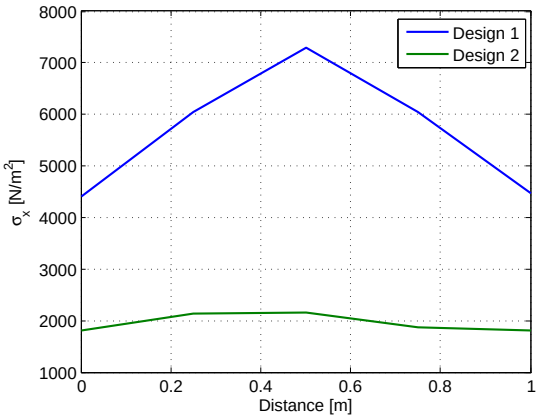

Figure 4.10: *Comparison between the two designs - σ_{xx} stress for LC1*

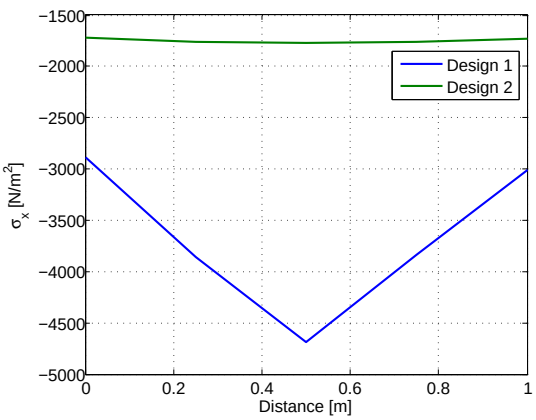

Figure 4.11: *Comparison between the two designs - σ_{xx} stress for LC5*

4.6.1 Histogram presentations

For a better overview, the results are presented below, in histograms.

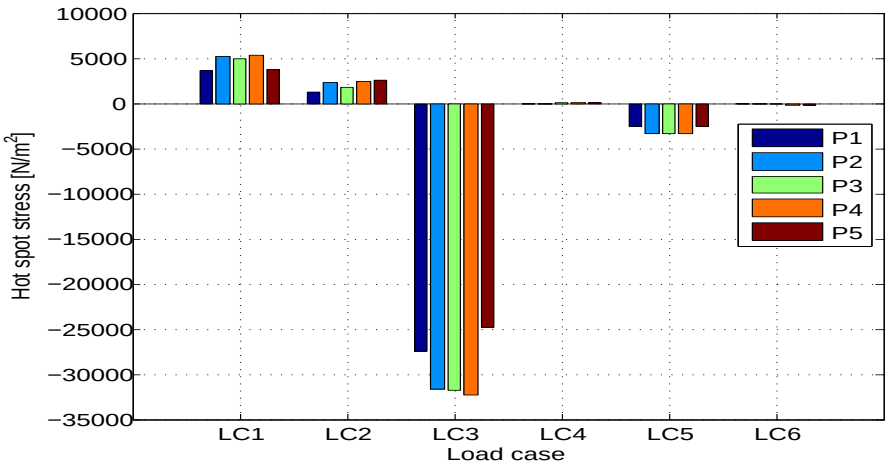

Figure 4.12: *Hot spot stress histogram for Design 1 - 4-node elements*

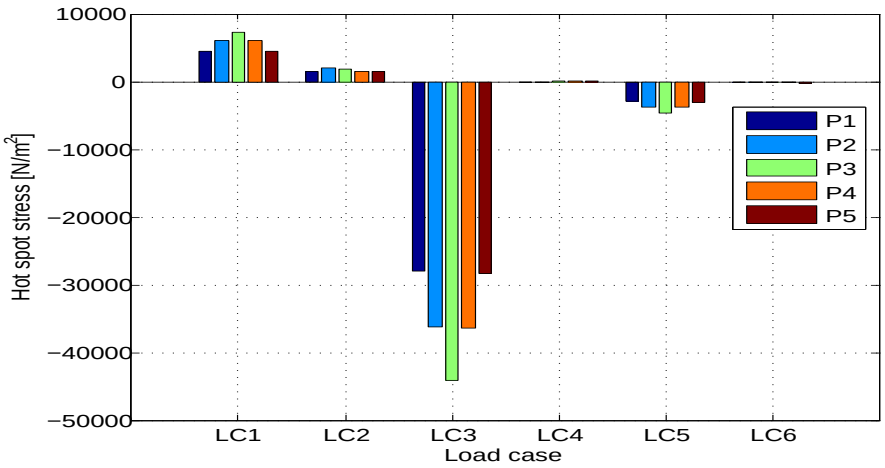

Figure 4.13: *Hot spot stress histogram for Design 1 - 8-node elements*

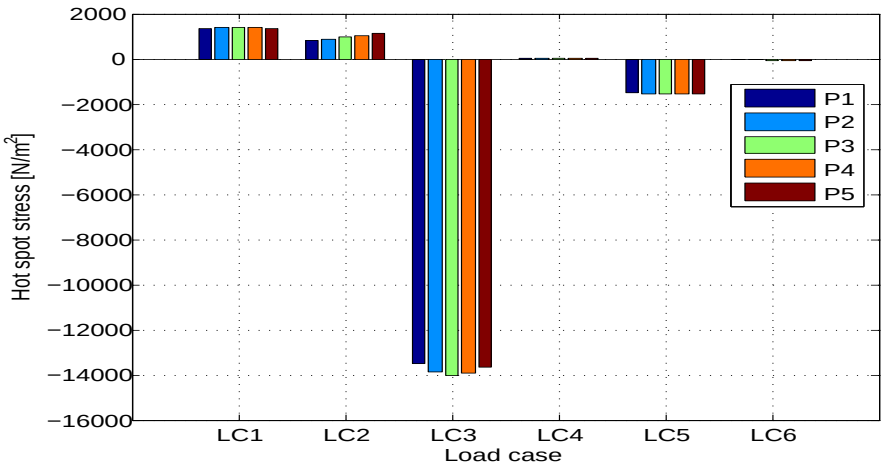

Figure 4.14: *Hot spot stress histogram for Design 2 - 4-node elements*

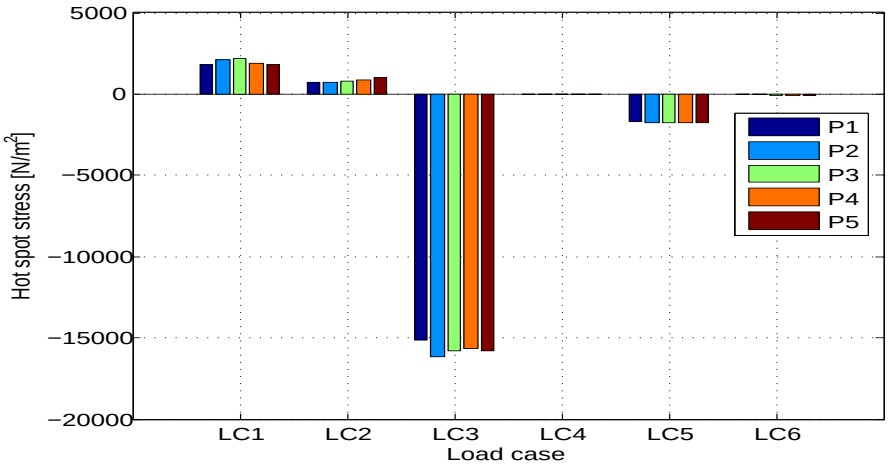

Figure 4.15: *Hot spot stress histogram for Design 2 - 8-node elements*

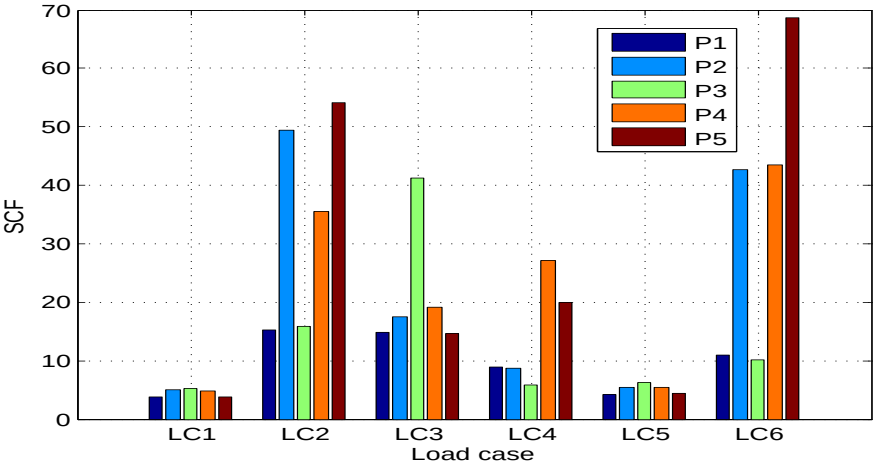

Figure 4.16: *SCF histogram for Design 1 - 4-node elements*

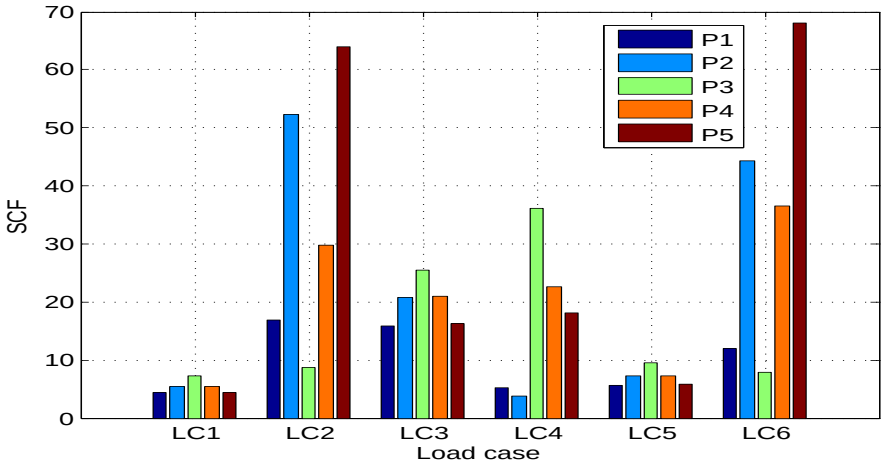

Figure 4.17: *SCF histogram for Design 1 - 8-node elements*

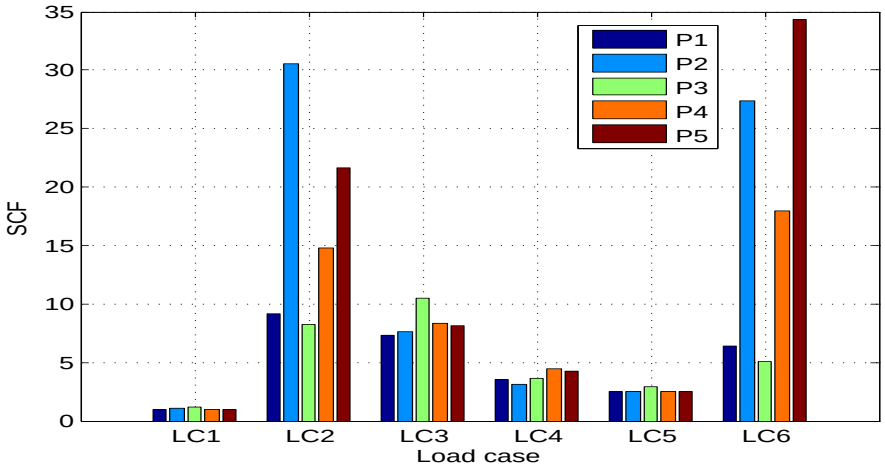

Figure 4.18: *SCF histogram for Design 2 - 4-node elements*

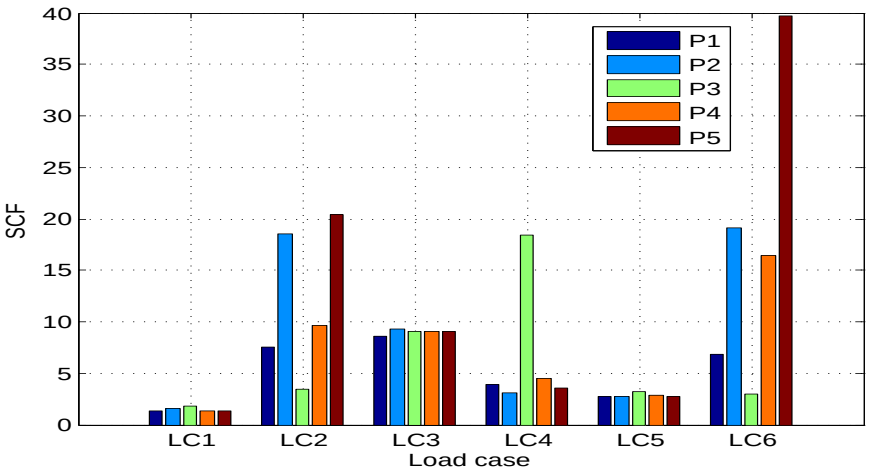

Figure 4.19: *SCF histogram for Design 2 - 8-node elements*

It is important to have in mind that the values of the SCF are not very accurate, due to the way the nominal stress was chosen. More importantly for fatigue in this project are the hot spot stresses, which were directly used to obtain the stress time-series. It can be concluded from the comparisons, that the second design, with the hole in the vertical plate has lower stresses, which will lead to a longer fatigue lifetime. Therefore, this design will be further analyzed to predict the fatigue damage.

Chapter 5

Uni-axial fatigue calculation

This chapter presents the uni-axial fatigue calculations procedure and results for the 5 fatigue points investigated, under different wind and wave directions.

5.1 Stress time-series

The stress time-series that were used for fatigue calculations were obtained by linearly combining the load time-series from the global response analysis with the hot spot stress derived in the previous chapter. This was performed by summing up the single stress components from each of the six load cases. For one point, the following formulas were applied:

$$\sigma_{total} = \sum_{i=1}^{k} F_i \cdot \sigma_{hss_i} \tag{5.1}$$

$$\tau_{total} = \sum_{i=1}^{k} F_i \cdot \tau_{hss_i} \tag{5.2}$$

where,

σ_{total}, τ_{total}	the total normal and shear stresses respectively, obtained by superposition of the stress components
F_i	load component (force or moment), with the dimension of $[kN]$ or $[kNm]$
σ_{hss_i}, τ_{hss_i}	derived hot spot stress for each of the six load components

To have an idea about the magnitude of the forces and moments comprised in the sea states, the mean values and standard deviations are presented in Appedix B for each sea states and for each of the 4 sea headings.

5.2 Design S-N curve

Using the DNV standard [9] , the right S-N curve for the analyzed joint was chosen. The hot spot is located below the sea level and it is consider to have cathodic protection. For this case, and also because the hot spot stresses were derived from an FEM model, the D-curve was used.

S-N curve	m_1	$log\bar{a}_1$	m_2	$log\bar{a}_2$	Fatigue limit	Thickness exponent
D	3	11.764	5	15.606	52.63	0.2

Table 5.1: *D curve*

The 2D plot of the D-curve is illustrated in the next figure.

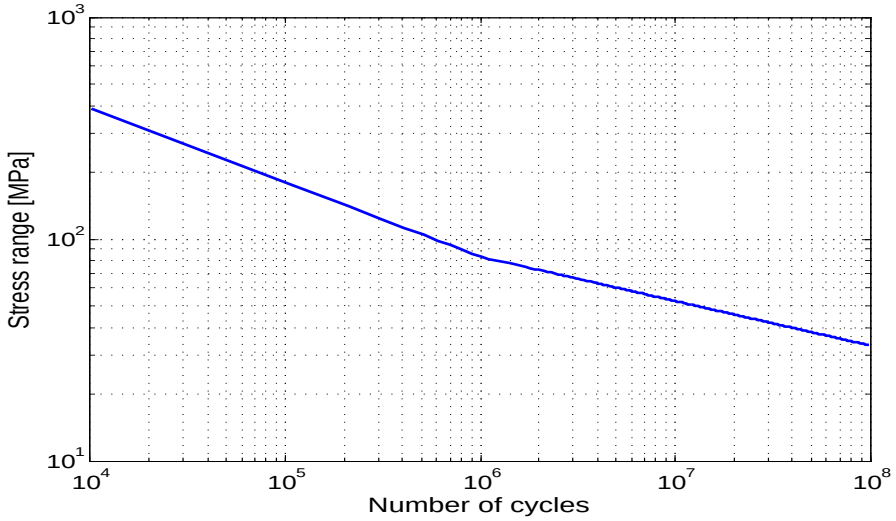

Figure 5.1: *D-curve*

5.3 Design fatigue factor

The design fatigue factor (DFF) is a safety factor dependent on consequence of failure, accessibility for inspection, inspection method, maintenance philosophy, etc. This design factor is to be applied in order to reduce the probability for fatigue failures [7].

> "DFFs shall be applied to the design fatigue life. The calculated fatigue life shall be longer than the design fatigue life times the DFF. The design requirements may alternatively be expressed as the cumulative damage ratio for the number of load cycles of the defined design fatigue life multiplied with the DFF shall be less or equal to 1 [11]."

Based on the considerations presented above, DNV and NORSOK standards classify the DFF as follows:

Classification of structural components based on damage consequence	Not accessible for inspection and repair or in the splash zone	Accessible for inspection, maintenance and repair, and where inspections or maintenance is planned	
		Below splash zone	Above splash zone or internal
Substantial consequences	10	3	2
Without substantial consequences	3	2	1

Table 5.2: *Design fatigue factors [12]*

DFF	*Structural element*
1	Internal structure, accessible and not welded directly to the submerged part.
1	External structure, accessible for regular inspection and repair in dry and clean conditions.
2	Internal structure, accessible and welded directly to the submerged part.
2	External structure not accessible for inspection and repair in dry and clean conditions.
3	Non-accessible areas, areas not planned to be accessible for inspection and repair during operation.

Table 5.3: *Design fatigue factors [11]*

The analyzed joint connection is submerged, part of the external structure, and accessible for inspection, maintenance and repair, underwater. Considering these features and the above two tables, the design fatigue factor was chosen as **DFF=2**.

The common design fatigue life for an offshore wind turbine is 20 years, which is also the desired life span for the current structure. Applying the design fatigue factor, the fatigue requirement yields:

$$L_d \cdot DFF \leq Lc \tag{5.3}$$

where L_d is the design fatigue life, and L_c is the calculated fatigue life. This leads to the conclusion that the calculated fatigue life should exceed 40 years in order to meet the standards' requirements.

5.4 Sea states

In order to perform a proper fatigue calculation, one needs to consider a large number of real sea states that are relevant for a certain location. Many time-domain dynamic response analyses considering different directions for wind and wave, combined with the corresponding wave height and peak period, and the probability of occurrence shall be analyzed. This would require a lot of input data, computer processing, statistical evaluations and time resources.

For the present thesis, a very detailed analysis with a lot of data and computation is not realistic because of the limited amount of time. Instead, the long-term fatigue assessment was performed using short-term sea states characterized by significant wave height,

peak period, mean wind speed and probability of occurrence. A total number of 13 short-term sea states, each with 10 random seeds were run. The duration of each sea state is one hour, and the damage is calculated as the average of the 10 realizations, corresponding to a certain sea state, in order to improve the statistical accuracy. Four cases, with different sea state headings were considered, as show in Figure 5.2. Note that the wind and waves are always aligned.

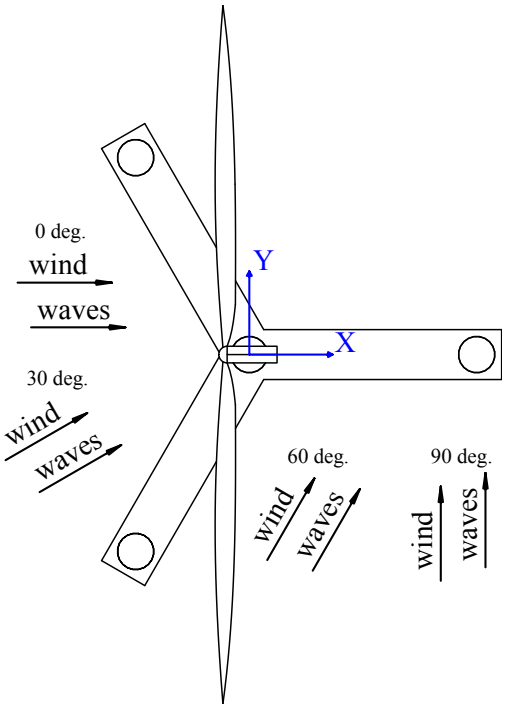

Figure 5.2: *Directions of the incoming wind and wave*

The characteristics of the 13 sea states are presented in the table below [31].

Analysis case number	Mean wind speed [m/s]	Turbulence intensity [%]	Significant wave height [m]	Peak spectral period [s]	Power production
1	4.9	23	1	7.8	Yes
2	8	17	2	8.5	Yes
3	11	15	3	9.4	Yes
4	13.8	14	4	10.2	Yes
5	16.5	13	5	10.7	Yes
6	18.9	12.6	6	11.1	Yes
7	21.3	12	7	11.5	Yes
8	23.4	11.9	8	12.1	Yes
9	25.4	11.7	9	12.6	Yes
10	27.1	11.5	10	13.1	No
11	28.8	11.3	11	13.7	No
12	30	11.2	12	14	No
13	31.3	11.1	13	14.4	No

Table 5.4: *Short term sea states*

The cut-in wind speed for the NREL 5MW wind turbine is 3 m/s, the rated speed is 11.4 m/s, and the cut-out speed is 25 m/s, above which, the turbine is parked for safety reasons.

Probability of occurrence for the sea states

By applying the probabilities corresponding to each short term sea state, the damage can be calculated, and by expanding the calculations to a long-term approximation, the fatigue life time of the joint can be estimated.

The total fatigue damage was calculated as the sum of the individual damages from all the short-term sea states, multiplied by the corresponding probability of occurrence.

$$D_{tot} = \sum_{i=1}^{13} D_i \cdot p_i \tag{5.4}$$

where,

D_{tot} total fatigue damage from all the sea states in one hour period
D_i fatigue damage from an individual short term sea state
p_i probability of occurrence corresponding to a certain sea state

The probability of occurrence for the individual short term sea states are given in the table below.

Sea state	Probability
1	0.2062
2	0.3040
3	0.2207
4	0.1313
5	0.0751
6	0.0353
7	0.0163
8	0.0070
9	0.0027
10	0.0010
11	0.0002
12	0.00008
13	0.00012
$\sum$	1

Table 5.5: *Sea states probabilities*

The global structural response was obtained for each of the 13 short term sea states. The output used for the present thesis represents the 6 load time-series (3 forces and 3 moments), for each sea state, which result at the pontoon's cut and is used as input for the fatigue analysis.

5.5 Uni-axial fatigue

For estimating the uni-axial fatigue lifetime, only one stress component is considered in the calculations. The total fatigue damage is calculated per sea state, applying the probability of occurrence, and summing up the damage for each sea state. One sea state gives only one damage, calculated as the average of all the different seeds corresponding to it. A flowchart illustrating the steps in the fatigue calculation is presented in Figure 5.3.

The procedure shown above calculates the fatigue lifetime for one of the five investigated points, considering either first or second order mesh elements, in the following steps:

1. The Gauss points from Xtract are processed in 'ROP 8n d2.xlsx' file, where the stresses are extrapolated to the weld.
2. The files 'hss8d2_sx.asc' and 'hss8d2_tau.asc' contain the hot spot stresses for σ and τ, respectively.
3. The Matlab function file 'fatdam.m' calculates the fatigue damage for one set of load time-series, and uses the 'cc2damTM.m' file which was modified by the author to be in accordance with the D-curve.
4. 'fatigue_calc.m' runs all the sea states from the ascii files and outputs the lifetime estimation for a certain point.

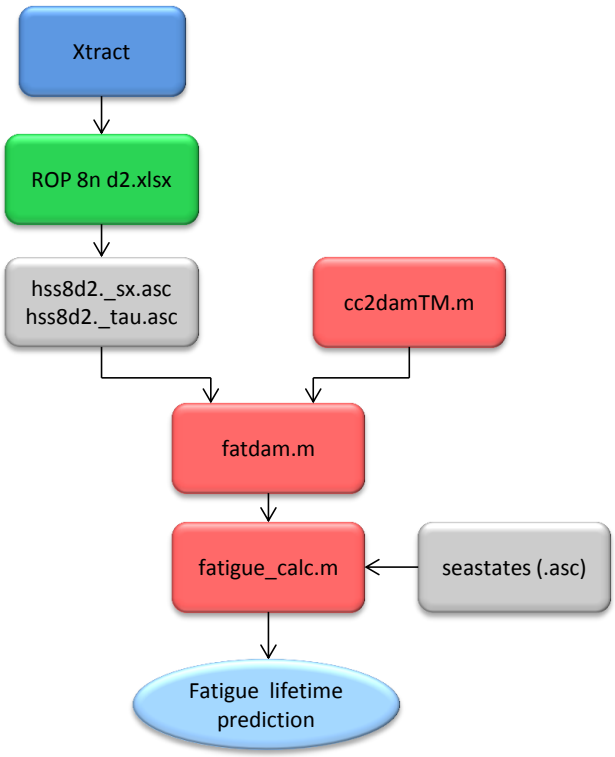

Figure 5.3: *Flowchart describing the fatigue calculation procedure*

5.6 Validation of the Matlab code with analytic solution

In order to validate the solution given by the code, a comparison was made with an analytic solution, found by hand calculations. The Matlab file 'test_fatigue' contains the full calculation for a short sinusoidal stress time-series and outputs the expected fatigue life span. The variables used in the file are:

- $\omega = 2 \cdot \frac{\pi}{15}$
- $t = 0.2 \cdot \omega \cdot i$, where i runs from 1 to 900
- the time-series is defined as: $cos(t) \cdot 50$

Graphically, the stress variation appear as in Figure 5.4.

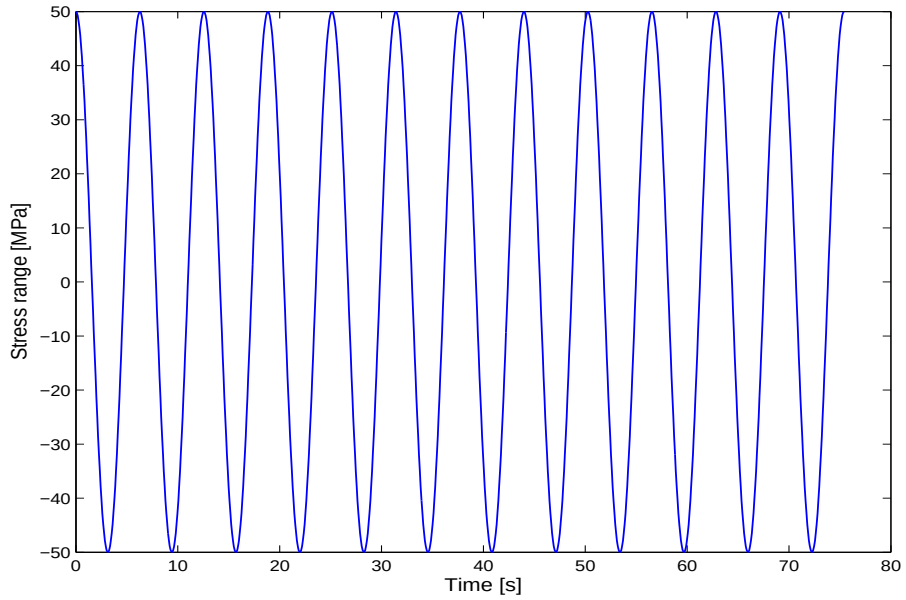

Figure 5.4: *Stress time-series for testing the code*

For the graph above, Matlab calculates a lifetime of the theoretical joint of 42.29 days.

Solution by hand calculation

The number of cycles and their ranges are easy to observe from the above plot, and together with the D-curve, the lifetime estimation can be performed.

There are 12 cycles of 50 MPa amplitude, or 100 MPa range. In the S-N curve, the stress ranges are considered, together with the full cycles. The value of 100 MPa, corresponding to the stress range, is before the knee point and therefore, it corresponds to the negative inverse slope of the S-N curve, $m_1 = 3$, and $log\bar{a}_1 = 11.764$.
The total number of cycles to failure for the constant amplitude of 100 MPa can be calculated as:

$$N = 10^{(log\bar{a}_1 - m_1 \cdot log\Delta\sigma)} = 10^{(11.764 - 3 \cdot 2)} = 5.808 \cdot 10^5 \text{ cycles}$$

Then the damage can be calculated as:

$$D = \frac{n}{N} = \frac{12}{5.808 \cdot 10^5} = 2.066 \cdot 10^{-5}$$

The length of the time-series in seconds is:

$$T_{ts} = 0.2 \cdot \frac{2 \cdot \pi}{15} \cdot 900 = 75.40s$$

Finally, the total lifetime in days can be approximated with the formula:

$$T_{days} = \frac{1}{D} \cdot T_{ts} \cdot \frac{1}{3600} \cdot \frac{1}{24} = \frac{1}{2.066 \cdot 10^{-5}} \cdot 75.40 \cdot \frac{1}{3600} \cdot \frac{1}{24} = \underline{42.24 \quad days}$$

It can be observed that the two methods, from Matlab and from hand calculation, give the same result. Therefore, the same algorithm will be further used to calculate the fatigue damage of the joint connection, using real sea states.

5.7 Results

The results in this section are presented and compared, for each of the four cases with different sea headings and for each of the 5 analyzed points, considering separately the effects of σ_{xx} and τ_{xy}.

When considering only the effect of shear stress, the stress time-series are multiplied by $\sqrt{\beta}$, which is a material constant. The physical meaning of this factor can be expressed as the ratio between the normal stress-based fatigue tests, and shear stress based tests, within a life range of interest, derived from fatigue experiments [25].

$$\sqrt{\beta} = \frac{\Delta\sigma_s(N)}{\Delta\tau_s(N)} \tag{5.5}$$

For steel welds, the usual value of β ranges between 2 and 4. For the present thesis, the value considered is 3, the same value that is also recommended in [25]. The implementation of this factor in the fatigue calculations results in a decreases of the life span prediction by a factor of $(\sqrt{\beta})^5$.

Damage by sea state

An analysis of the fatigue damage produced by each sea state was carried out in order to identify the most damaging sea states and the corresponding environmental conditions. The figures below show the damage produced by each sea state in one hour, for 0 and 30 degrees sea headings. Only the normal stress was considered, corresponding to fatigue point P3, and using 8-node elements.

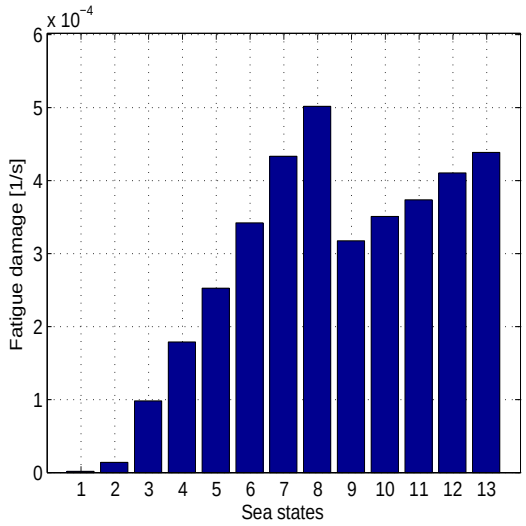

a) Full contribution of the sea state

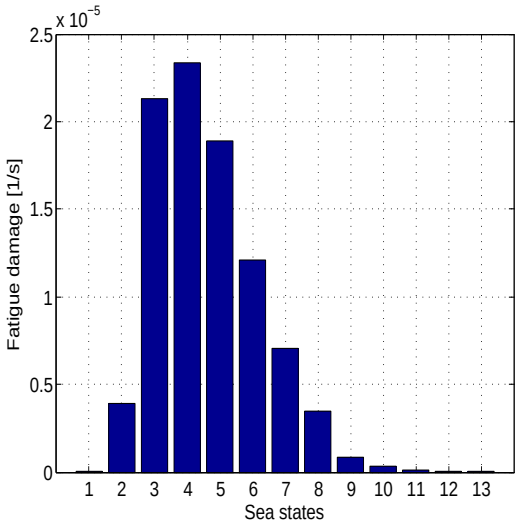

b) Damage x Probability

Figure 5.5: *Damage per sea state in one hour for 0 degrees heading*

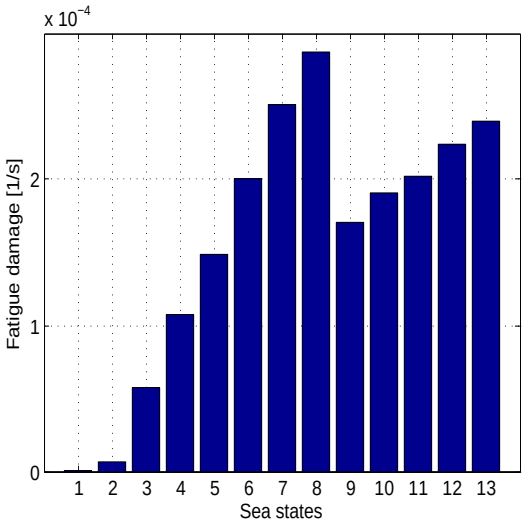

a) Full contribution of the sea state

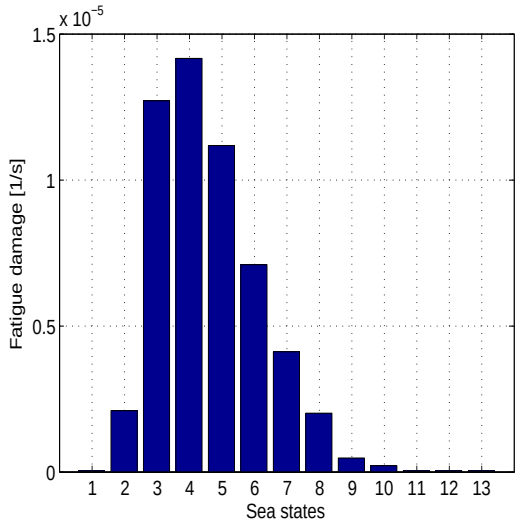

b) Damage x Probability

Figure 5.6: *Damage per sea state in one hour for 30 degrees heading*

The two plots above on the left hand side show the damage for each sea state as if they would be applied for one hour on the structure. The other two figures show the real contribution of each sea state in a one hour period using the probability function. For both 0 and 30 degrees wind and wave directions, the most damaging sea state is number 4, corresponding to a mean wind speed of 13.8 m/s, and a significant wave height of 4 m, followed by sea states number 3 and 5. Those are rather calm to average sea states (Figure 5.5a and 5.6a), but because of their high probability of occurrence, the effect is

major. The damage produced by sea states 3, 4 and 5 together, contribute to the total damage with as much as 70%.

Fatigue lifetime prediction

The lifetime estimation in years for each of the 5 analyzed points, considering all the four sea headings is presented in the next tables, considering normal and shear stress separately.

Stress	Sea heading	P1	P2	P3	P4	P5
σ_{xx}	0 deg	1.99E+00	1.85E+00	1.80E+00	1.84E+00	1.94E+01
	30 deg	3.52E+00	3.26E+00	3.16E+00	3.22E+00	3.40E+00
	60 deg	6.96E+01	6.18E+01	5.90E+01	6.06E+01	6.50E+01
	90 deg	1.68E+03	1.54E+03	1.49E+03	1.62E+03	1.62E+03
τ_{xy}	0 deg	4.54E+05	8.84E+05	1.51E+06	2.02E+06	2.06E+06
	30 deg	4.54E+04	3.62E+03	2.90E+03	2.34E+03	1.87E+02
	60 deg	2.34E+02	2.16E+02	2.00E+02	1.87E+02	1.73E+02
	90 deg	6.10E+02	6.16E+02	6.22E+02	6.28E+02	8.98E+02

Table 5.6: *Lifetime prediction using 4-node elements*

Stress	Sea heading	P1	P2	P3	P4	P5
σ_{xx}	0 deg	1.35E+00	1.28E+00	1.24E+00	1.23E+00	1.31E+00
	30 deg	2.28E+00	2.18E+00	2.12E+00	2.10E+00	2.24E+00
	60 deg	3.62E+01	3.46E+01	3.20E+01	3.20E+01	3.64E+01
	90 deg	9.80E+02	9.80E+02	8.20E+02	8.16E+02	9.92E+02
τ_{xy}	0 deg	6.60E+04	4.78E+04	8.56E+04	1.53E+05	2.62E+05
	30 deg	1.31E+03	1.44E+03	1.17E+03	9.74E+02	7.88E+02
	60 deg	5.36E+01	5.46E+01	5.10E+01	4.80E+01	4.44E+01
	90 deg	1.46E+02	1.46E+02	1.52E+02	1.52E+02	1.52E+02

Table 5.7: *Lifetime prediction using 8-node elements*

The lifetime fatigue prediction when considering 4-node elements is always higher than in the case of 8-node elements. The latter option is therefore more conservative and shall be used for design.

The expected life span of the weld is given by the lowest value of the 5 fatigue points. The most damaging wind and wave alignment is the degrees, when the sea state is parallel to the pontoon. The minimum life expectation is found for fatigue point 4, 1.23 years. On the other hand, the minimum fatigue life calculated considering only the shear stress, for the 0 degrees sea heading is 47 800 years, which means that τ_{xy} has very limited effect for this situation.
As the angle between the sea state direction and the pontoon increases, the normal stress decreases in intensity, while the shear stress becomes more and more important. For 60 degrees, the lifetime prediction for the two principal stresses fall in the same ranges, 32

years when considering normal stresses, and 44.4 years corresponding to the shear stress. This means that for this case, the magnitudes of σ_{xx} and τ_{xy} are comparable, because of the balanced contributions of forces and moments time-series under 60 degrees wind and wave direction.
When the sea is perpendicular to the pontoon, the shear stresses overtake the normal stresses in importance, and the fatigue lifetime is up to 6 times longer for σ than for τ. This is because, theoretically, there is no axial force and no bending moment M_y induced in the pontoon, while the dominating load components are those which induce shear stress, F_y and M_x.

For a better view, the results presenting the lifetime estimation for all the analyzed cases, for 8-node elements are presented in the histograms below.

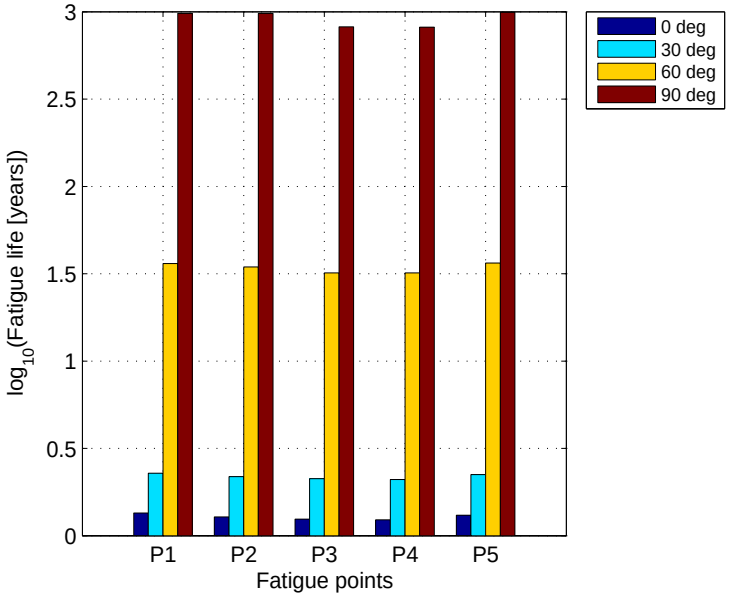

Figure 5.7: *Lifetime prediction for uni-axial fatigue considering normal stress*

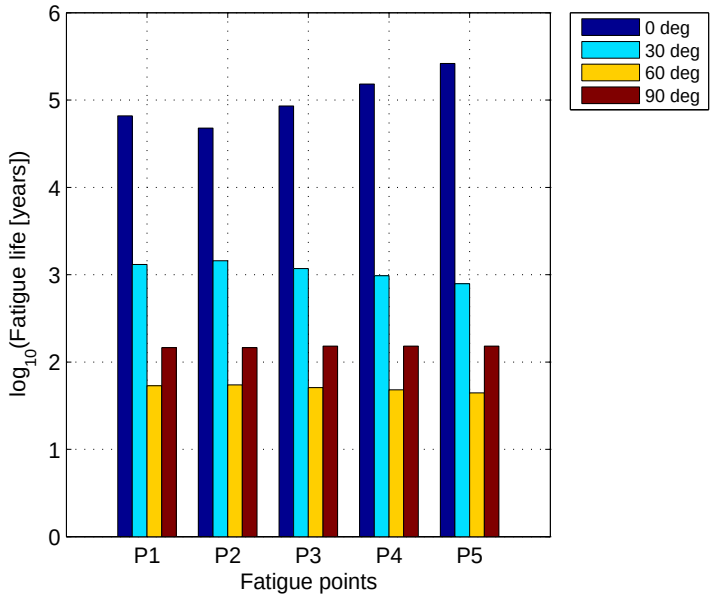

Figure 5.8: *Lifetime prediction for uni-axial fatigue considering shear stress*

For the current offshore wind turbine, the calculated fatigue life span needs to be at least 40 years, higher than the fatigue lifetime obtained for 0, 30 and 60 degrees when considering only normal stress. In reality, a combination of different misaligned wind and waves condition occur over a long period of time. Thus, for a proper fatigue calculation, the probability of occurrence for every direction shall be taken into account. In the current thesis though, the estimations were made for each case individually, without combining the probabilities afterwards.

Even though the joint connection was redesign in order to lower the SCF, as shown in Chapter 4 (Design 2), it still needs further improvement to meet the requirements of such a structure, with regards to fatigue life. The design process shall go in a loop, until the calculated fatigue lifetime for the most critical fatigue point and load condition is higher than 40 years.

Chapter 6

Multi-axial fatigue approach

The previous chapter presented the fatigue calculation procedure and results, considering only one stress component at a time, together with the S-N curve, rainflow counting algorithm and the Miner's rule, following the standard procedure used for common uniaxial fatigue problems. This can be considered a simplified model, because it ignores the interaction between σ and τ. The fatigue life span shall be shorter when this interaction is considered, therefore, a closer look needs to be taken on this aspect.

In this chapter, a method for calculating the fatigue lifetime of the investigated structure, considering multi-axial effects is presented. Also, the impact of combined normal and shear stresses is assessed, for each of the four directions of the considered sea states.

In the literature there are many methods to cope with the multi-axial effects in steel structures, as it was shown in Chapter 2. Even though, a reliable solution for out-of-phase and variable amplitude loading problem is not straight forward to achieve, a lot of resources are still being invested to research this problem. In the last few years, some new innovative methods were developed and tested, which seem to provide reliable results for complex problems. Two of these methods are explained here to show their capability to deal with the multi-axial problem for the particular case of the investigated structure. The *Equilibrium Equivalent Structural Stress Method* for calculating the stress at the weld, and the *Path Dependent Maximum Range Method*, for counting the variable amplitude normal and shear stress ranges are used together as one method to describe the steps to be taken in solving the proposed problem.

6.1 Structural stress calculation

This section presents the procedure for calculating the stress at the weld, using the *Equilibrium Equivalent Structural Stress Method* developed by P. Dong and adopted in ASME, API and BV [23], [22]. The method was tested [27], and it proved to give accurate results for a great variety of different joint types, load conditions and weld types. The stress concentration effects are consistently captured, regardless of the mesh size. This is an important advantage because it does not require a very fine mesh, as the classical extrapolation methods require. Hence, it reduces significantly the computation time.

The assumptions and the physics behind the method were explained in Chapter 2 and hence in the following, the step-by-step implementation of the procedure is presented. Note that the method is not implemented numerically in this thesis, because of the limitations of the FEM software GeniE, which can not provide the forces and moments at the nodes of the mesh cells.

The flowchart below show the steps that are to be taken for calculating the structural stress along the weld.

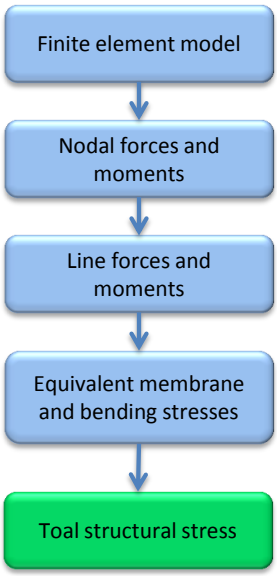

Figure 6.1: *Structural stress calculation flowchart*

The first step is to transform the global coordinate system x-y-z to local coordinate system x'-y'-z', so the local x'-axis is along the weld and the y'-axis is perpendicular, as shown in Figure 6.2.

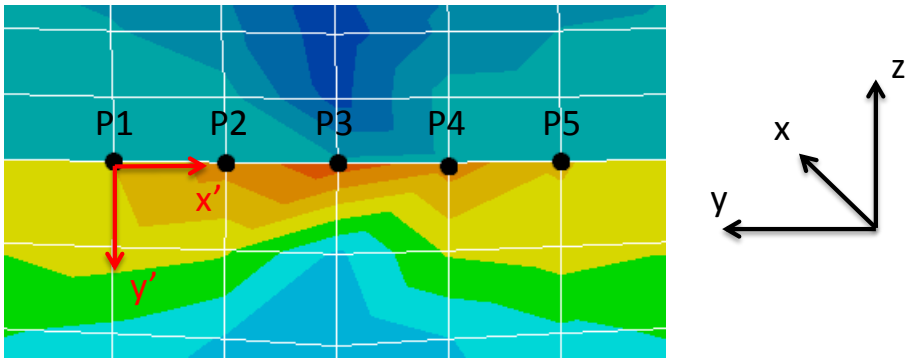

Figure 6.2: *Transformation of the coordinate system for the analyzed weld*

Next, the nodal forces and moments of interest are extracted from the FE model, i.e. the forces and moments along the -x' and -y' axes, for each of the 5 fatigue points.

$$\begin{pmatrix} F_1 \\ F_2 \\ F_3 \\ F_4 \\ F_5 \end{pmatrix} = \begin{bmatrix} \frac{l_1+l_0}{3} & \frac{l_1}{6} & 0 & 0 & 0 \\ \frac{l_1}{6} & \frac{l_1+l_2}{3} & \frac{l_2}{6} & 0 & 0 \\ 0 & \frac{l_2}{6} & \frac{l_2+l_3}{3} & \frac{l_3}{6} & 0 \\ 0 & 0 & \frac{l_3}{6} & \frac{l_3+l_4}{3} & \frac{l_4}{6} \\ 0 & 0 & 0 & \frac{l_4}{6} & \frac{l_4+l_5}{3} \end{bmatrix} \cdot \begin{pmatrix} f_1 \\ f_2 \\ f_3 \\ f_4 \\ f_5 \end{pmatrix} \tag{6.1}$$

where f_1,...,f_5 are the line forces corresponding to each point, and F_1,...,F_5 are nodal forces in the local coordinate system at the nodal points 1 to 5. l_i represents the i^{th} element's edge length projected onto the weld toe. For simplicity, the weld in this case can be considered a straight line due to the large radius of the column.

From equation (6.1), the line forces along the local y' axis are calculated, and are used further to compute the membrane component in the structural stress. In order to obtain the line moment m'_x along the weld, equation (6.1) is used again, replacing the nodal forces along the y'-direction with balanced nodal moments M_1,...,M_5, with respect to the local x'-axis.

The structural stress is then calculated combining the membrane part and the bending part, for both normal and shear stresses.

$$\sigma_s = \sigma_m + \sigma_b = \frac{f_{y'}}{t} - \frac{6m_{x'}}{t^2} \tag{6.2}$$

$$\tau_s = \tau_m + \tau_b = \frac{f_{x'}}{t} - \frac{6m_{y'}}{t^2} \tag{6.3}$$

$$\tau_z = \frac{f_{z'}}{t} \tag{6.4}$$

The transverse shear stress component (τ_z) is only represented by membrane part, which is consistent with structural mechanics theory. In general, for engineering applications, the transverse shear structural stress component is negligible. In this paper, only σ_s and τ_s are considered, the problem being simplified to a 2D multi-axial fatigue problem.

The procedure described so far shall be applied for each of the 6 unit loads, as described in Chapter 4. Consequently, there will be one normal structural stress component and one shear structural stress component for each of the 6 load cases.
As the load time-series from the global dynamic response analysis are combined with the structural stress using equations (5.1) and (5.2), the total stress time-series for normal and shear stresses are computed and ready to be used in a counting algorithm to output the combined stress ranges.

6.2 Stress range calculation

For calculating and counting the combined stress ranges, a new method was proposed in recent years, the *Path-Dependent Maximum Range Method (PDMR)*. The features of the method are presented in Chapter 2, while here the step-by-step implementation is described, to cope with the current structure.

Although there are articles written by the developers to describe the method ([25],[38],[39], [24]), the method is still under development to be implemented in commercial software, and the algorithm is currently not available. Because the PDMR code is fairly complex, and the validation would be very tedious, it was not possible to develop a reliable Matlab code to calculate the multi-axial fatigue life. In the following flowchart, the PDMR procedure is explained.

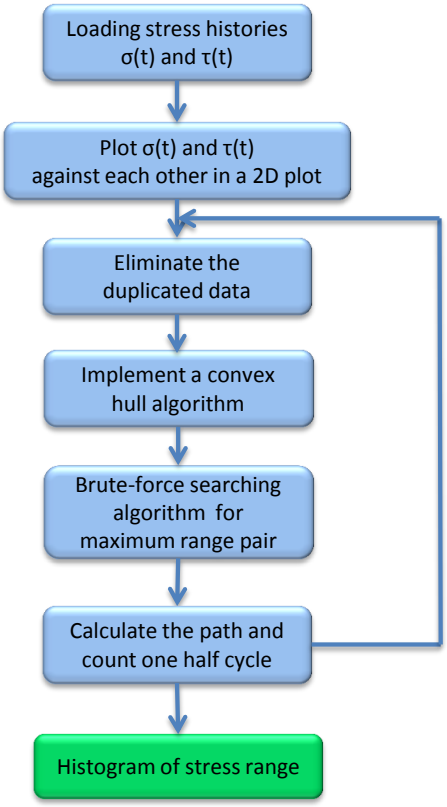

Figure 6.3: *PDMR counting procedure*

To exemplify the method with current data, the next two graphs were plotted using sea state number 5, corresponding to the 30 degrees wind and wave heading. These graphs give an idea about the importance of each of the two stress components, considering their magnitudes.

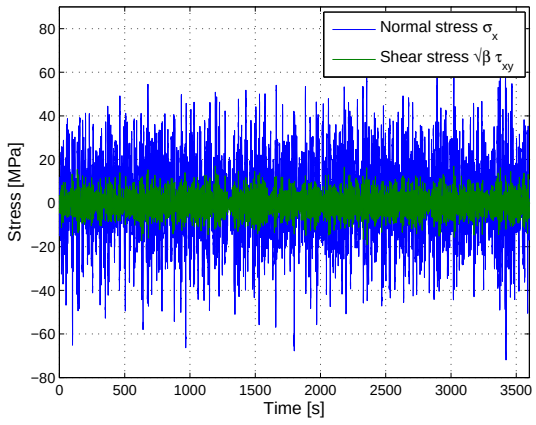

Figure 6.4: *Load time history*

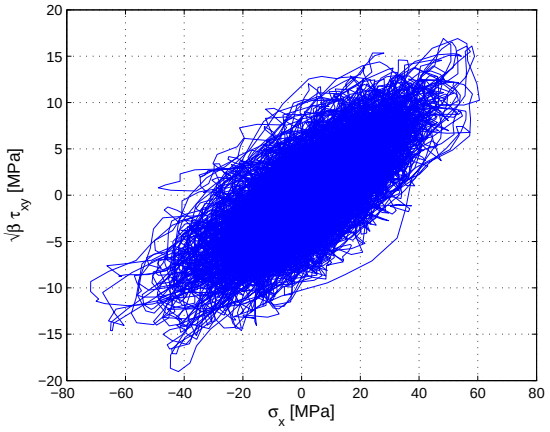

Figure 6.5: *Loading path*

It can be observed from the plots above, that the normal stress ranges are on average about 4 times larger than the shear stress ranges. The dominating stress in this case is

clearly σ_{xx}, which would also contribute the most to the fatigue damage.

The next step in the calculation procedure is to apply the convex hull algorithm, using the plot in Figure 6.5. The scope is to identify the points situated on an exterior contour, which enclose all the other points, a procedure that will improve the computation time for the maximum stress range searching. In order to find the maximum stress range, a classical *brute force algorithm* could also be used. Even though it is simple to implement, it has the drawback that the computational time increases with $O(n^2)$, becoming very slow and impracticable for large data. There are a few algorithms to calculate the convex hull, e.g. Andrew's monotone chain, Graham scan or Merge sort. A straight forward way to implement a convex hull algorithm in Matlab is to use the *convhull* function offered by the software. This function applied on the plot in Figure 6.5 outputs the next graph.

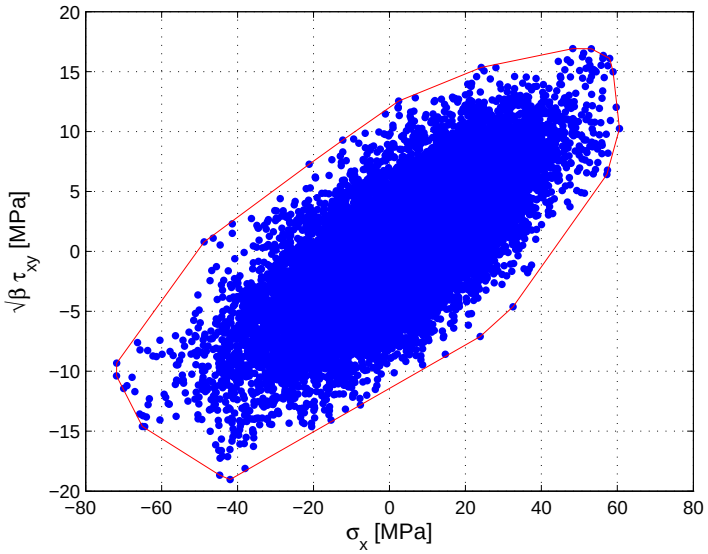

Figure 6.6: *Convex hull for the given loading path*

After the convex hull is found, the maximum distance between every two points on the external contour shall be calculated, using a brute-force algorithm. In order to speed up the searching procedure, a *Rotating Caliper* algorithm can also be applied to find the antipodal pairs of the convex hull [24]. Once the maximum distance is found, the corresponding reference range and effective range need to be output and half a cycle counted. This step is illustrated below, using an example given in [25].

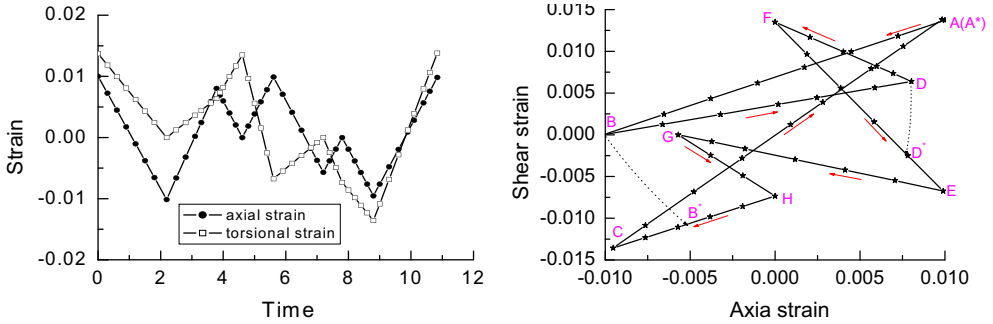

Figure 6.7: *Multi-axial loading example [25]*

Note that in the example from Figure 6.7, the load history is given in the strain space, while in the present thesis, stresses are used. To be consistent with the stress space used in this paper, the method is explained below as if stresses were used, and not strains. The PDRM method can be used for both strain and stress ranges, in 2D and 3D space.
A step-by-step illustration is shown in the graphs below, to illustrate the PDMR counting algorithm.

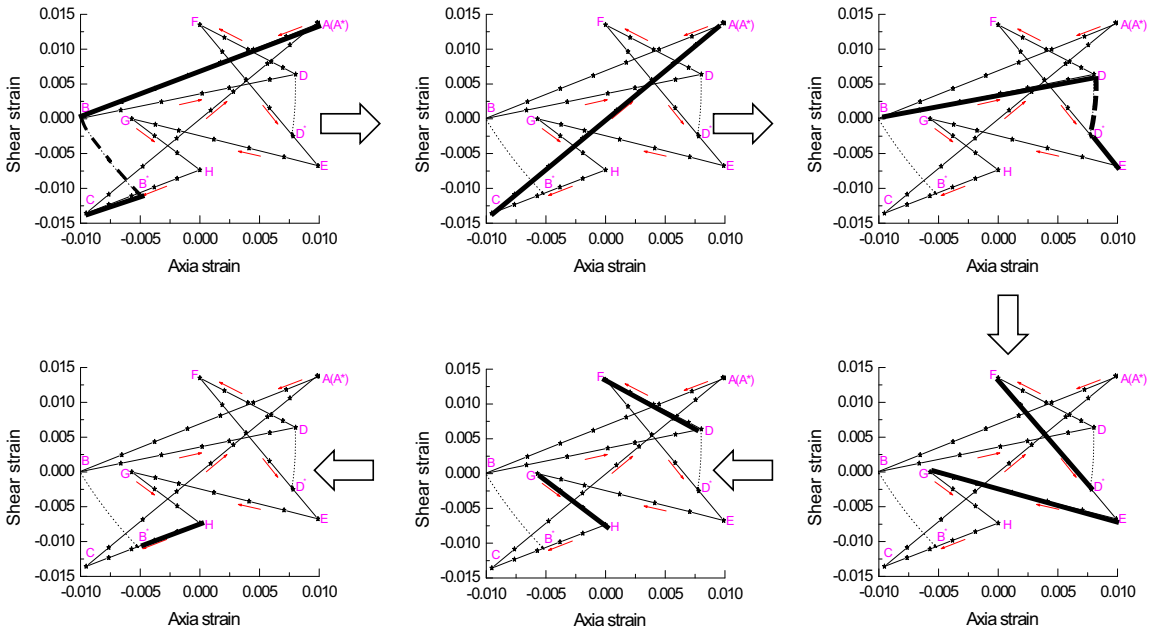

Figure 6.8: *A step-by-step illustration of the PDMR procedure for Fig. 6.7. [25]*

To describe the PDMR algorithm for the load history presented in Figure 6.7, the procedure is described in steps, as follows [25]:

1. Search the maximum possible distance within the entire history path over time, i.e. $t_1 \leq t \leq t_n$, which is found for the example in Figure 6.8 as the distance between point A and point C, denoted also as the *reference stress* $\Delta\sigma_e$.

2. Starting from point A, the path towards point C is followed while maintaining a monotonic increase in distance until point B is reached. A further increase in time

would result in a decrease in distance. Point B is then identified as a local maximum or a turning point. To maintain a monotonic increase in distance in continued search, point B* (a projected turning point) is obtained by the intersection between the load path and an arc with a radius of length A-B, centered on A. The search for maximum distance measured from point A is continued until all data points from B* to C are fully counted since there are no additional turning points.

3. The load paths traversed in the process of identifying the maximum distance $\Delta\sigma_e$ consist of three load path segments, i.e. AB, BB* and B*C. Note that BB* is a virtual load path. Both the reference stress range $\Delta\sigma_e$ and the length of the three path segments AB, BB* and B*C together completely define one half cycle in the PDMR method.

4. Document the reference stress range $\Delta\sigma_e$ as the distance between A and C and path length ΔS_e for the half cycle identified at step 3 by summing the path segment lengths, i.e. ΔS_e = AB + BB* + B*C.

5. Repeat steps 1-4 by identifying reference effective stress range and the corresponding path length for the rest of the loading paths, until all paths have been counted and counted only once.

6. Document reference effective stress ranges (or distances), effective stress ranges (path lengths), and the corresponding number of cycles.

The results from the PDMR cycle counting for the loading path presented in Fig. 6.7 are summarized in Table 6.1.

Cycle counted	Range	Path length
0.5	A - C	AB+BB*+B*C
0.5	C - C	CA
0.5	B - E	BD+DD*+D*E
0.5	F - D*	FD*
0.5	D - F	DF
0.5	E - G	EG
0.5	G - H	GH
0.5	H - B	HB*

Table 6.1: *PDMR cycle counting results for Fig. 5.7*

The maximum distance between two points (the reference stress range), can be calculated analytically using the following formula:

$$\Delta\sigma_e = \sqrt{(x_A - x_C)^2 + \beta(y_A - y_C)^2} \tag{6.5}$$

For the calculation of the path length described before, for a given reference stress range

$\Delta\sigma_e$, the following formula is used:

$$\Delta S_e = \int dS_e = \int \sqrt{(d\sigma)^2 + \beta(d\tau)^2} \tag{6.6}$$

which is equivalent to:

$$\Delta S_e = \sum_{i=1}^{k} \sqrt{(x_{i+1} - x_i)^2 + \beta(y_{i+1} - y_i)^2} \tag{6.7}$$

Once all the stress ranges and the number of cycles are extracted using the previously described method, the fatigue damage can be calculated using a proper S-N curve and Miner's rule.

6.3 Fatigue life calculation

The standard fatigue life prediction for uni-axial conditions is straight forward, using the design S-N curves recommended by the specialized standards in the industry, together with the Miner's rule of accumulated damage. The classical S-N curves are customized for different types of structures, loading modes and material properties. A newly developed method to assess the fatigue life is the Master S-N curve [20], which is one single curve that can accommodate a large variety of joints under different conditions. In general, the procedure used for calculating the stress at the weld toe dictates the type of S-N curve to be used for fatigue life prediction.

> "The master S-N curve based on mode-I cracking has been successfully developed for Battelle structural stress method based on a two-stage crack growth model. Further research should provide a similar two-stage crack growth model for mode-III cracking. In this way, a single in-plane shear master S-N curve can be developed for assessing a large number of joint configurations, loading modes, and plate thicknesses. Then, a unified PDMR treatment of multi-axial fatigue based on normal and in-plane shear Master S-N curve can be developed [39]."

The last paragraph summarizes the current and future state of the development of S-N curves for assessing multi-axial fatigue. At the present moment, there is no reliable solution for calculating the fatigue life using the stress ranges obtained with the PDMR method.

In order to be consistent with the procedure used earlier for the uni-axial fatigue life prediction, the same S-N curve (D-curve) shall be used for the multi-axial problem. Having the stress ranges and the number of cycles, the procedure is the same, the accumulated fatigue damage is calculated using the Miner's rule with D=1 [25], and the damage fatigue factor equals to 2.

6.4 Testing procedure for multi-axial fatigue procedure

So far, the results obtained using the PDMR method were compared with other existing methods from the literature and it proved to give good results [25]. In order to become a reliable solution to be used in the industry, sustained research still needs to be carried out in order to be validated and accepted as a viable method in the industry. A mandatory step in this process is to prepare fatigue testing experiments and compare them with the numerical solutions obtained through calculations. This might be a tedious process, given the complexity of the input data, which should be processed by a sophisticated computer system, implemented in a fatigue testing machine.

The figure below represents a possible test set-up for such an experiment, proposed by the author.

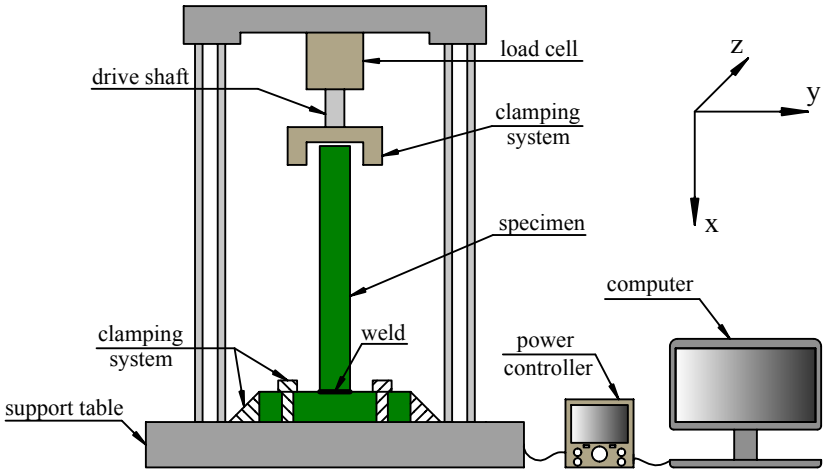

Figure 6.9: *Multi-axial fatigue test set-up*

In order to perform a multi-axial experiment, the actuator inside the load cell has to have at least 2 degrees of freedom, in order to induce significant normal and shear stresses at the same time. The following tests shall be possible to be carried out with the machine presented in Fig 6.9:

- Combined axial force F_x and torsion moment M_x
- Combined axial force F_x and bending moment M_y
- Combined axial force F_x and lateral force M_y
- Uni-axial fatigue tests for each of the load cases separately

The specimen used could be a T-type rectangular section or tubular section pipe, or a single straight pipe welded in the middle. The clamping system shall be designed to also accommodate joints made from simple plates.

For multi-axial fatigue tests, some simple algorithms can output a variable amplitude

combined loads which can produce stress ranges for normal and shear stress at the same time, as shown in Fig. 6.10. The code used to produce the graph below can be found in the Matlab file 'test_random'.

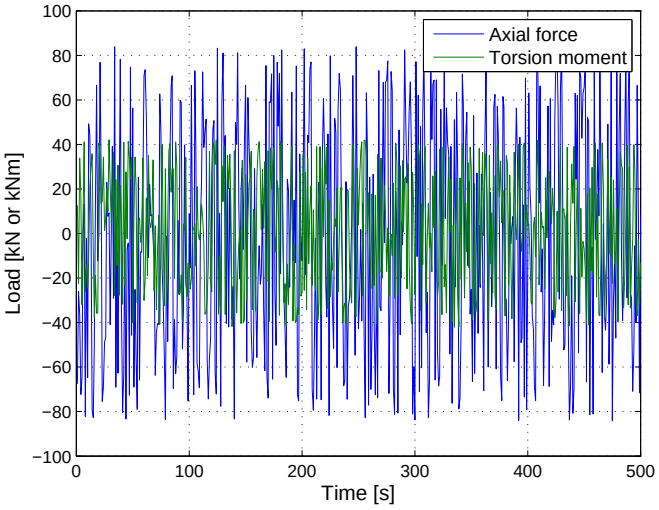

Figure 6.10: *Multi-axial load time-series test input*

Once the algorithm is implemented in the computer system of the testing machine, and the load cell can cope with the given input so it generates combined motions imposed on the specimen, the experiment can be performed. After the fatigue failure of the joint occurs, the test stops, and the input load history is analyzed. Assuming linear material behavior, the structural stress at the weld toe shall be calculated in an FEM software, applying one unit load for axial and torsion moment and following the procedure described earlier in this chapter. The stress time-series for normal and shear stresses can then be found by combining the structural stress with the load time-series. At this point the PDMR procedure is ready to be used in order to compute the combined stress ranges and number of cycles for the load history. Further, by applying a documented S-N curve and an accumulated fatigue damage rule, the fatigue lifetime of the joint can be estimated and compared with the real fatigue life obtained through the experiment.

It is obvious that a large number of tests shall be run in order to obtain reliable results and validate the method. Sensitivity studies shall also be perform with different S-N curves, accumulated fatigue damage coefficients, and correction factors in order to correlate the results obtained from experiments with the calculated output.

6.5 Considerations on multi-axial effects

In the present thesis, a fatigue lifetime calculation was performed only for uni-axial fatigue, considering normal and shear stress separately. In reality, the fatigue damage would accumulate faster if the two stresses combined were considered, reducing the fatigue life of the structure. An assessment of the influence of multi-axial fatigue is presented in the

following.

The magnitude of σ and τ in the stress history is dependent on the load components comprised in the analyzed sea state. The wind and wave headings relative to the global x-axis of the pontoon determine the dominating forces and moments acting on the joint, which decide the magnitude of the two principal stress components.

The axial force F_x, the lateral force F_z and the bending moment M_y produce mainly normal stresses at the joint connection, while the lateral force F_y, the torsion moment M_x and the bending moment M_z produce shear stress, as the dominating stress component. The four sea state headings used in this thesis (0 deg., 30 deg., 60 deg. and 90 deg.) induce different stress states at the hot spot locations. To illustrate this, for each of the four cases, the loading path $\sigma - \tau$ is presented in the graphs below.

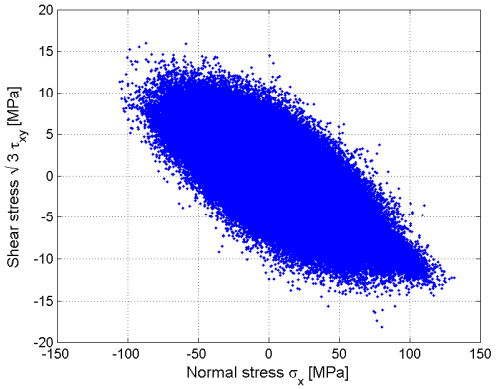

Figure 6.11: *Load path for 0 deg. sea heading*

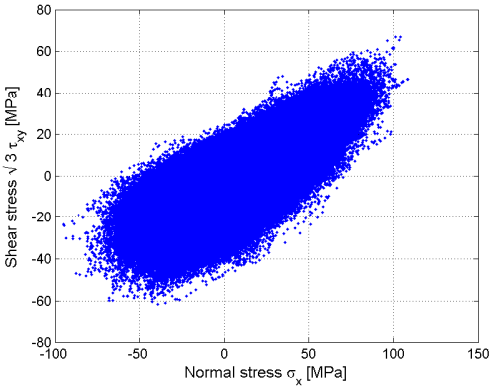

Figure 6.12: *Load path for 30 deg. sea heading*

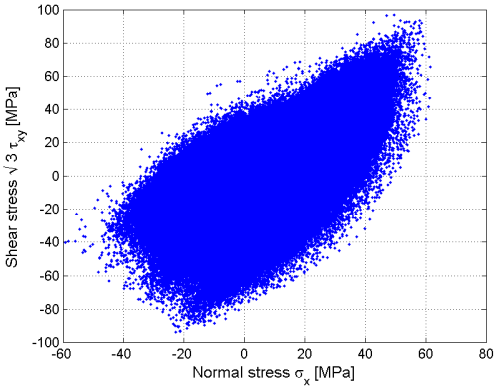

Figure 6.13: *Load path for 60 deg. sea heading*

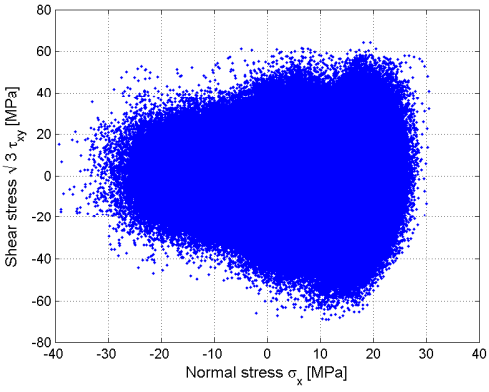

Figure 6.14: *Load path for 90 deg. sea heading*

It can be observed that as the wind and wave heading angle increases, the shear stress component amplifies, i.e. multi-axial effects become more significant. For the 0 degrees angle, when the wind and waves are parallel to the pontoon, the dominating load com-

ponents induced at the pontoon's cut is the axial force F_x, lateral force F_z and bending moment M_y. The other three components have lower magnitudes, therefore the resulting stresses at the weld are σ dominated. In this case, the shear stress takes values between -18 to 17 MPa, while the normal stress, from -110 to 130 MPa, as shown in Figure 6.11. Hence, the multi-axial effects are not very significant, yet a fatigue calculation combining the two stress components may result in a small reduction of the structure's lifetime due to shear stresses.

For a 30 degree sea heading, the ratio between shear stress ranges and normal stress ranges increases, because the importance of lateral force F_y and torsion moment M_x becomes higher. Consequently, the σ values range from -90 to 110 Mpa, while the τ values are situated between -60 to almost 70. Considering these results, it can be stated that the multi-axial effects become significant, and a thorough assessment of the combined normal and shear stresses shall be performed.

The influence of the wind and wave direction becomes even more clear in Figure 6.13, for a 60 degree sea heading, where the values of the shear stress exceed those of the normal stress. Now, the torsion moment and lateral load components comprised in the sea states seem to overtake in importance the axial force and bending moment. Even if on the graph the shear stress seems to be the dominant one, the calculated fatigue lifetime given by shear stress alone is still longer than for normal stress, which means that σ is still dominating by the means of number of cycles with larger amplitude. For this case, the multi-axial effects may have dramatic effects on the structure's fatigue life, and it shall be further investigated for a complete fatigue assessment.

Looking at Figure 6.14, the case with the wind and waves perpendicular to the pontoon, it can be observed that the stress ranges decrease for both τ and σ, while the ratio between them continue to increase, as there is less normal stress induced by the sea states. Theoretically, for this particular case, there should be no axial force F_x and bending moment M_y induced, while the lateral force F_y and torsion moment M_x, both producing shear at the hot spot, shall be at their maximum. The multi-axial effects in this case are also obvious and can not be neglected.

From the four graphs above it can be seen that the variation of the two stress components is completely random in time, still it follows some patterns for different load angles. For the 0 degree sea state heading, most of the points occur for negative values of shear stress and positive values of normal stress, or the other way around. For the 30 and 60 degrees instead, most of the stress values that occur at a certain time instance have the same sign, as the elongated loading path suggests. In the last case, the values are the most spread and do not seem to follow any pattern.

Using common sense, it can be predicted that a side joint will most probably experience sea states coming parallel on the pontoon. While one connection will experience this kind of sea heading, the other two will experience waves coming from the 300 degree direction, at the same time, as the turbine's yaw system will allow it to turn to face the wind. It is difficult to estimate the reduction in fatigue life due to combined normal and shear stresses for direction. In order to have a more clear idea about this, a more

detailed analysis considering probabilistic methods for each sea state heading should be considered, and a final load path shall be assessed.

Chapter 7

Conclusions and future work

7.1 Conclusions

A side column-pontoon connection in the 5-MW-CeSoS novel semi-submersible floating offshore wind turbine [31] was analyzed for fatigue assessment. Two different geometries were proposed and compared in order to choose the best option for further investigation. The winning design was optimized and the most important hot spot went through a detailed stress analysis for the calculation of the stresses along the weld. The extrapolation procedure recommended by DNV [9], together with the hot spot stress method was applied for this purpose. The stress concentration factors were also estimated and compared for two designs of the hot spot location and for two different mesh elements. Along the weld, 5 fatigue points were chosen and their fatigue lifetime was estimated.

The uni-axial fatigue approach was used to output the fatigue lifetime of the joint, considering separately the normal and the shear stresses. The D-curve, together with the rainflow counting algorithm and the Miner's accumulated fatigue damage rule were used to compute the fatigue lifetime. The 13 sea states used for this assessment, each with 10 random seeds, were considered to come from 4 different directions relatively to the pontoon (0, 30, 60 and 90 degrees). Thus, the accumulated damage and the lifetime prediction for the four cases were calculated and compared.

A proper calculation of the multi-axial fatigue damage and life estimation was difficult to perform due to the complex algorithm that needed to be developed and the limited amount of time available. Instead, a new innovative approach for this problem was presented and described step-by-step. The *Equilibrium Equivalent Structural Stress* together with the counting method *Path-Dependent Maximum Range* represent an exciting solution for dealing with stochastic variable amplitude multi-axial loading conditions. Since the method is relatively new, it was not validated through experiments yet. Therefore, a possible laboratory testing procedure was also proposed. The importance of the multi-axial effects on the analyzed structure for each of the 4 sea headings was finally evaluated.

7.1.1 Geometry design

The first model proposed for the column-pontoon connection is characterized by a conical elements which connects the column with the pontoon, assuring a smooth transition from a cylinder section to a rectangular section.
The second model was based on the idea that the column needs to go all the way through the pontoon, and has to be connected to it through vertical internal bulkheads. For this model, a strong connection cage is created, and the configuration allows the cylinder to be manufactured in one piece.
After a linear static analysis in GeniE, it was concluded that the second model has a better structural response than the first one, and it was chosen to be further investigated for fatigue assessment. Even if the choice was made based on the stress variations at the hot spot locations, a more thorough analysis of the first structure, with design optimization, might have revealed that it can be improved to be competitive with the second design.

7.1.2 Hot spot stresses and SCFs

Two different designs were proposed to calculate the stresses at the weld and the stress concentration factors. The first one is the unmodified geometry found in the sub-model, while the second one includes a cut-out in the vertical bulkhead in order to reduce the stresses at the hot spot location. The stresses were extrapolated for both first order and second order mesh elements and it was demonstrated that the 8-node elements generally give up to 40% higher stresses, as they can capture more accurately the rapid variation of the stresses at the weld. Also, for the second design, the decrease in the stress magnitude was obvious, because the stresses are redistributed around the hole.
In order to estimate the SCFs, the nominal stress was considered 1 m away from the weld for each of the 5 fatigue points. The SCFs values followed the same rule, higher values for quadratic elements and lower values for the second design. The fatigue calculations were therefore performed considering the results obtained for the second design.

7.1.3 Fatigue life

The fatigue life was calculated considering only one stress component at a time, and using the hot spot stresses together with the load time series from the global dynamic response analysis. A full long-term uni-axial fatigue analysis was approximated using 13 one-hour sea states, with 10 random seeds each, and considering 4 different incoming directions of aligned wind and wave. The damage from each sea state was multiplied with the probability of occurrence, and the contributions were summed up to get the total fatigue damage. The largest contribution to fatigue damage, about 70% comes from 3 sea states, with corresponding wind speeds between 11 and 16.5 m/s.

The sea states headings have a great impact on the fatigue lifetime of the joint, because of the contribution of each load component (force or moment) to the sea state. For 0 degrees heading, i.e. the wind and waves are aligned with the x-axis of the pontoon, the fatigue life is just 1.23 years when considering only the normal stress, while the calculation gives a lifetime of almost 50 thousand years when the shear stress is considered. This is also

the most damaging case for uni-axial fatigue. As the angle of the wind and waves relative to the x-axis is increased, the shear stress becomes more and more important, overtaking in magnitude the values of the normal stress, for 90 degree heading. In this case, the lifetime prediction is 816 and 146 years, for σ and τ, respectively. It was observed that the most vulnerable fatigue point changes for each case. Therefore, it can not be stated which of the 5 points is the most critical.

7.1.4 Multi-axial fatigue

An approach for estimating the fatigue lifetime considering multi-axial effects was proposed and described in this thesis. The approach is based on the EESS and PDMR method, recently developed by researchers ([17], [25]), and it is one of the few reliable approaches for evaluation of out-of-phase variable amplitude loading.

The impact of multi-axial effect was also evaluated in this thesis. It was shown that as the sea heading creates a larger angle with the pontoon (from 0 to 90 degrees), the importance of the shear stress relative to the normal stress becomes more significant. When the heading angle is 0 or 30 degree, the normal stress component is clearly dominant, mainly because of the dominant axial force F_x and bending moment M_y induced in these circumstances. For 60 degrees sea heading, the two stress components have almost the same contribution to fatigue, while for the perpendicular direction, the shear stress becomes the dominant component.

7.2 Future work

- **Optimize the structure.** The hot spot stresses along the weld are directly linked to the fatigue lifetime. Therefore, a reduction in magnitude of these stresses would result in an improvement regarding the expected life. For this, a closer look needs to be taken to the geometry of the joint connection, and some methods of redesign and improvement of the design shall be applied. Variation of the plate thickness around the hot spot, pre-casting the region of interest or considering extra elements such as brackets, beams and bulkheads would help to reduce the stresses and hence increase the fatigue lifetime.

- **Improve statistical uncertainties.** A more accurate long-term fatigue analysis would require longer sea states with more seeds, deeper study to identify the main parameters (W, H_s and T_p), and probability functions for the directions of the sea states. An ideal fatigue assessment would be based on a full-term analysis, in which the sea states are simulated for a period of e.g. 20 years.

- **Multi-axial fatigue life estimation.** The most challenging step in performing this analysis using the approach proposed in this thesis is to implement the PDMR algorithm. Also, the FE analysis shall be carried out using software that can provide the forces and moments in the nodes of the mesh elements. A long term fatigue analysis needs to be performed, and the resulting fatigue lifetime shall be compared with those from the uni-axial calculations. In this way, a valuable comparison can

be made between the two approaches, and the impact of multi-axial effects can be evaluated properly.

References

[1] http://www.keytometals.com/.

[2] http://en.wikipedia.org/wiki/Fracture_mechanics.

[3] http://www.pro-emfatic.com/.

[4] http://http://www.ewea.org/.

[5] *Erocode 3, Design of steel structures - Part 1-1: General rules and rules for buildings (ENV 1993-1-1)*. 1992.

[6] *SFS 2379.1992 Welding. Load capacity of welded joints in fatigue loaded steel structures*. Finnish Standards Association, Helsinki, 1992.

[7] Norsok Standard N-005, Condition Monitoring of Loadbearing Structures. Norwegian Technology Standards Institution, December 1997.

[8] Recommended Practice DNV-RP-C103 Column-Stabilised Units. Det Norske Veritas AS, October 2010.

[9] Recommended Practice DNV-RP-C203 Fatigue Design of Offshore Steel Structures. Det Norske Veritas AS, April 2010.

[10] Recommended Practice DNV-RP-C205 Environmental Conditions and Environmental Loads. Det Norske Veritas AS, October 2010.

[11] Offshore Standard DNV-OS-C101 Design of Offshore Steel Structures, General (LRFD Method). Det Norske Veritas AS, April 2011.

[12] Norsok Standard N-005, Integrity of Offshore Structures. Norwegian Technology Standards Institution, September 2012.

[13] Offshore Standard DNV-OS-C103 Structural Design of Column Stabilised Units (LRFD Method). Det Norske Veritas AS, October 2012.

[14] A. Almar-Næss, H. Anderson, T. Moan, and S. Berge. *Fatigue Handbook*. Tapir Publishers, NTNU, Trondheim, 1985.

[15] Mika Bäckström. *Multiaxial fatigue life assessment of welds based on nominal and hot spot stresses*. PhD thesis, Lappeenranta University of Technology, Lappeenranta, Finland, August 2003.

[16] S. Berge. *Fatigue and Fracture Design of Marine Structures II, Fracture Design of Welded Structures*. Institutt for Marin Teknikk, Trondheim, Sptember 2004.

[17] P. Dong. A structural stress definition and numerical implementation for fatigue analysis of welded joints. *International Journal of Fatigue*, pages 865–876, June 2001.

[18] P. Dong. A robust structural stress method for fatigue analysis of ship structures. Center for Welded Structures Research, Battelle, June 2003.

[19] P. Dong and J.K. Hong. The master s-n curve approach to fatigue evaluation of offshore and marine structures. Center for Welded Structures Research, Battelle, June 2004.

[20] P. Dong and J.K. Hong. The master s-n curve approach to fatigue evaluation of offshore and marine structures. Battelle, Center for Welded Structures Research, June 2004.

[21] P. Dong and J.K. Hong. A robust structural stress parameter for evaluation of multiaxial fatigue of weldments. *Journal of ASTM International*, 3(7), June 2006.

[22] P. Dong, J.K. Hong, D.A. Osage, D. Dewees, and M. Prager. The Master S-N Curve Method for Fatigue Evaluation of Welded Components, WRC Bulletin, No. 474 , Welding Research Council, New York, August 2002.

[23] P. Dong, J.K. Hong, D.A. Osage, and M. Prager. The Master S-N Curve Method: An implementation for fatigue evaluation of welded components in the ASME B&PV Code, Section VIII, Division 2 and API 579-1 ASME FFS-1,WRC Bulletin No 523, 2007.

[24] P. Dong, Z. Wei, and T. P. Forte. A rapid convex hull algorithm for implementing path-dependent multi-axial fatigue. Proceedings of the ASME 2010 Pressure Vessels & Piping Division / K-PVP Conference, July 2010.

[25] P. Dong, Z. Wei, and J.K. Hong. A path-dependent cycle counting method for variable-amplitude multi-axial loading. *International Journal of Fatiguel*, 32:720–734, 2010.

[26] J. Gustafsson and J. Saarinen. Multi-axial fatigue in welded details. Master's thesis, Chalmers University of Technology, 2007.

[27] H. Kyuba and P. Dong. Equilibrium-equivalent structural stress approach to fatigue analysis of a rectangular hollow section joint. *International Journal of Fatigue*, pages 85–94, June 2005.

[28] Chenyu Luan. Dynamic response analysis of a semi-sumbersible floating wind turbine. Master's thesis, Norwegian University of Science and Technology, Trondheim, Norway, June 2011.

[29] T. I. Marin. *Pre-Project Thesis in Marine Technology, Design and Stress Analysis of the Column-Pontoon Connection in a Semi-Submersible Floating Wind Turbine.* Norwegian University of Science and Technology, December 2013.

[30] T. Moan. *Finite Element Modelling and Analysis of Marine Structures.* Institutt for Marin Teknikk, Trondheim, NTNU, 2003.

[31] T. Moan, Z. Gao, and C. Luan. Conceptual designs of a 5-MW and a 10-MW semi-submersible wind turbine with emphasis on the design procedure. *Journal of Offshore Mechanics and Arctic Engineeringl*, 2014.

[32] E. Niemi. *Analysis of variable amplitude fatigue using equivalent constant amplitude stress range.* Technical Research Centre of Finland, Espoo, 1996.

[33] Darrell F. Socie and Gary B. Marquis. *Multiaxial Fatigue.* Society of Automotive Engineers, 2000.

[34] Det Norske Veritas. Sesam User Manual, GeniE Vol. 1-6.

[35] Det Norske Veritas. Sesam User Manual, Sestra - Superlements Structural Analysis, February 2013.

[36] Det Norske Veritas. Sesam User Manual, Xtract - Postprocessor for Presentation, Animation and Reporting of Results, February 2013.

[37] WAFO group. a Matlab Toolbox for Analysis of Random Waves and Loads. http://www.maths.lth.se/, March 2011. Lund University, Centre for Mathematical Sciences.

[38] P. Dong Z. Wei. A rapid path-length searching procedure for multi-axial fatigue cycle counting. In *Fatigue & Fracture of Engineering Materials & Structures*, pages 556–571. Blackwell Publishing Ltd., October 2011.

[39] P. Dong Z. Wei, J.K. Hong, and T.P. Forte. Multi-axial cycle counting and fatigue life assessment based on nominal and battelle structural stresses. July 2010.

Appendix A

Joint design

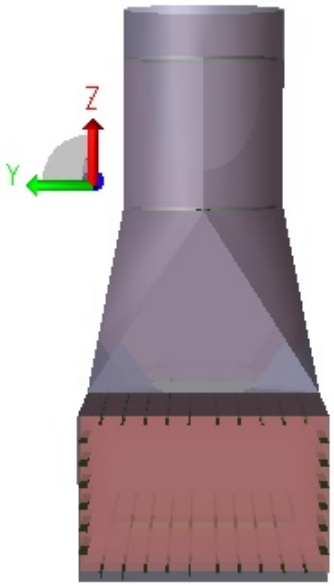

Figure A.1: *Model 1 - view 1*

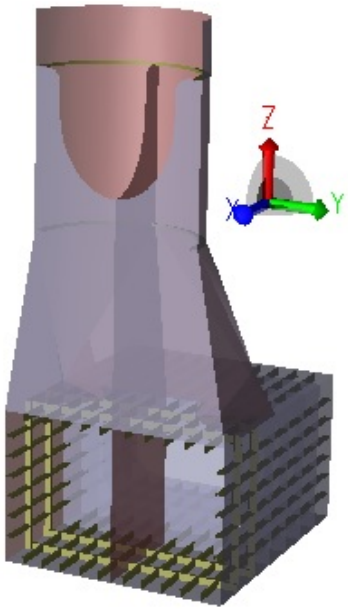

Figure A.2: *Model 1 - view 2*

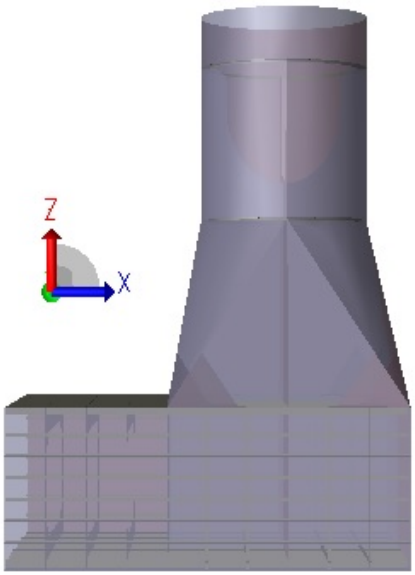

Figure A.3: *Model 1 - view 3*

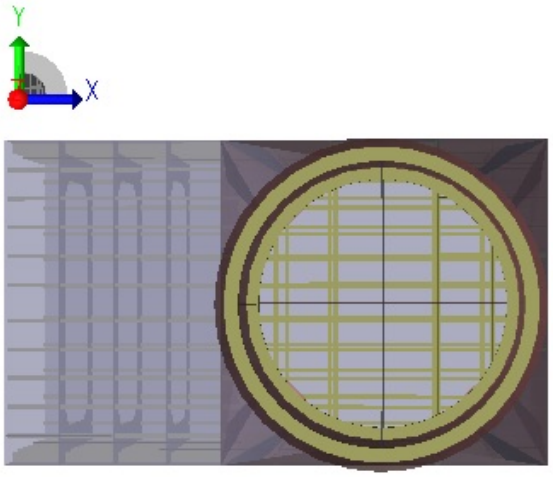

Figure A.4: *Model 1 - view 4*

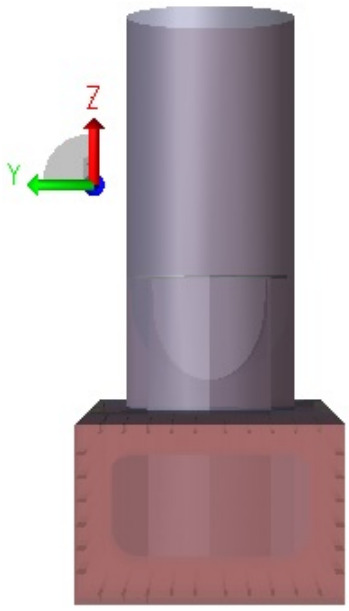

Figure A.5: *Model 2 - view 1*

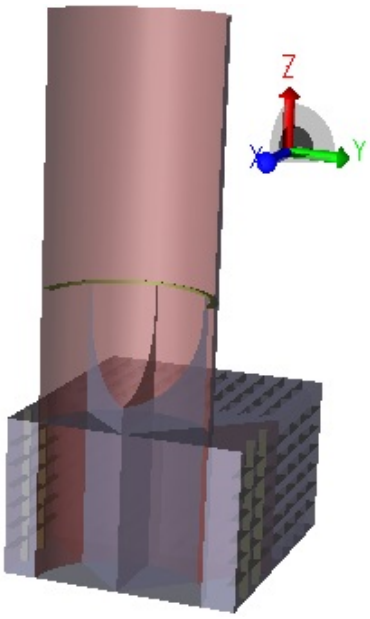

Figure A.6: *Model 2 - view 2*

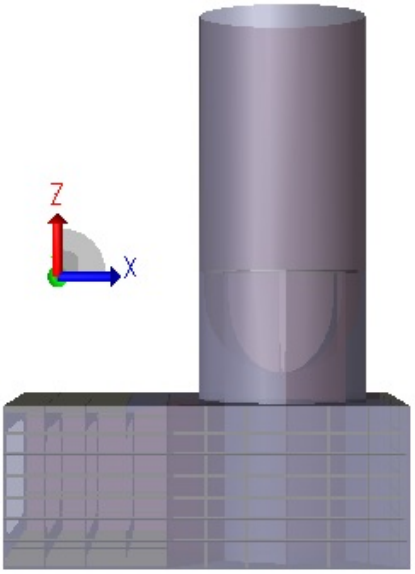

Figure A.7: *Model 2 - view 3*

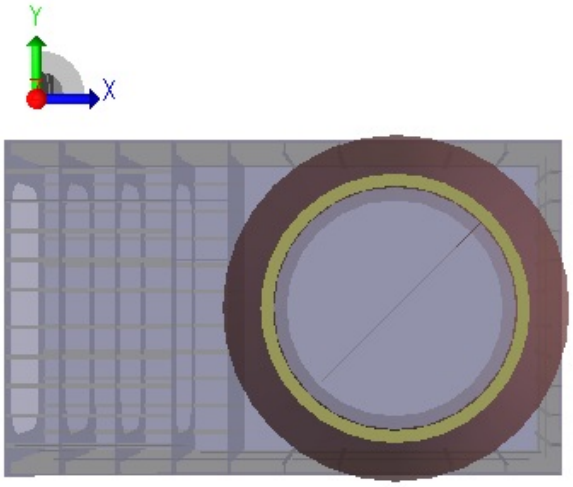

Figure A.8: *Model 2 - view 4*

Appendix B

Mean values and standard deviation of the load time series

Sea state	F_x [kN]	F_y [kN]	F_z [kN]	M_x [kNm]	M_y [kNm]	M_z [kNm]
1	-1.31E+03	-2.20E+00	-1.91E+03	5.58E+01	8.61E+03	-2.27E+01
2	-1.08E+03	-9.61E+00	-2.51E+03	2.44E+02	1.91E+04	-1.00E+02
3	-7.97E+02	-2.19E+01	-3.14E+03	5.49E+02	3.16E+04	-2.34E+02
4	-9.31E+02	-2.58E+01	-2.84E+03	6.44E+02	2.57E+04	-2.74E+02
5	-1.05E+03	-2.74E+01	-2.58E+03	6.68E+02	2.05E+04	-2.91E+02
6	-1.11E+03	-2.93E+01	-2.45E+03	6.97E+02	1.80E+04	3.15E+02
7	-1.14E+03	-3.17E+01	-2.36E+03	7.32E+02	1.64E+04	-3.43E+02
8	-1.16E+03	-3.39E+01	-2.31E+03	7.70E+02	1.55E+04	-3.69E+02
9	-1.44E+03	2.68E+00	-1.50E+03	-6.14E+01	1.97E+03	2.83E+01
10	-1.43E+03	3.13E+00	-1.51E+03	-7.18E+01	2.10E+03	3.30E+01
11	-1.43E+03	3.63E+00	-1.52E+03	-8.39E+02	2.23E+03	3.82E+01
12	-1.43E+03	4.03E+00	-1.53E+03	-9.33E+01	2.31E+03	4.22E+01
13	-1.42E+03	4.49E+00	-1.54E+03	-1.04E+02	2.42E+03	4.67E+01

Table B.1: *Mean values of forces and moments for the 0 degrees sea heading*

Sea state	F_x [kN]	F_y [kN]	F_z [kN]	M_x [kNm]	M_y [kNm]	M_z [kNm]
1	-1.30E+03	-2.25E+00	-1.91E+03	5.65E+01	8.61E+03	-2.31E+01
2	-1.08E+03	-9.82E+00	-2.51E+03	2.47E+02	1.91E+04	-1.02E+02
3	-7.96E+02	-2.22E+01	-3.14E+03	5.53E+02	3.16E+04	-2.36E+02
4	-9.30E+02	-2.63E+01	-2.84E+03	6.50E+02	2.58E+04	-2.76E+02
5	-1.05E+03	-2.79E+01	-2.58E+03	6.77E+02	2.05E+04	-2.94E+02
6	-1.10E+03	-2.98E+01	-2.45E+03	7.09E+02	1.80E+04	-3.16E+02
7	-1.14E+03	-3.22E+01	-2.36E+03	7.50E+02	1.64E+04	-3.44E+02
8	-1.16E+03	-3.43E+01	-2.31E+03	7.99E+02	1.55E+04	-3.66E+02
9	-1.43E+03	2.03E+00	-1.50E+03	1.52E+01	2.03E+03	2.72E+01
10	-1.43E+03	2.86E+00	-1.51E+03	2.29E+01	2.17E+03	3.91E+01
11	-1.42E+03	3.23E+00	-1.52E+03	3.74E+01	2.31E+03	4.84E+01
12	-1.42E+03	3.62E+00	-1.53E+03	5.86E+01	2.41E+03	5.78E+01
13	-1.41E+03	4.13E+00	-1.54E+03	7.95E+01	2.53E+03	6.98E+01

Table B.2: *Mean values of forces and moments for the 30 degrees sea heading*

Sea state	F_x [kN]	F_y [kN]	F_z [kN]	M_x [kNm]	M_y [kNm]	M_z [kNm]
1	-1.31E+03	-2.19E+00	-1.91E+03	5.54E+01	8.61E+03	-2.24E+01
2	-1.08E+03	-9.65E+00	-2.51E+03	2.43E+02	1.91E+04	-9.96E+01
3	-7.97E+02	-2.20E+01	-3.14E+03	5.47E+02	3.16E+04	-2.32E+02
4	-9.32E+02	-2.60E+01	-2.84E+03	6.44E+02	2.57E+04	-2.71E+02
5	-1.05E+03	-2.78E+01	-2.58E+03	6.77E+02	2.05E+04	-2.90E+02
6	-1.11E+03	-2.98E+01	-2.45E+03	7.12E+02	1.80E+04	-3.13E+02
7	-1.14E+03	-3.24E+01	-2.36E+03	7.62E+02	1.64E+04	-3.42E+02
8	-1.16E+03	-3.48E+01	-2.31E+03	8.19E+02	1.51E+04	-3.68E+02
9	-1.44E+03	1.03E+00	-1.50E+03	3.98E+01	1.99E+03	2.03E+01
10	-1.44E+03	1.62E+00	-1.51E+03	5.29E+01	2.13E+03	2.75E+01
11	-1.43E+03	1.66E+00	-1.52E+03	7.66E+01	2.28E+03	2.96E+01
12	-1.43E+03	1.68E+00	-1.52E+03	1.04E+02	2.39E+03	3.17E+01
13	-1.42E+03	2.01E+00	-1.53E+03	1.31E+01	2.51E+03	3.74E+01

Table B.3: *Mean values of forces and moments for the 60 degrees sea heading*

Sea state	F_x [kN]	F_y [kN]	F_z [kN]	M_x [kNm]	M_y [kNm]	M_z [kNm]
1	-1.30E+03	-2.21E+00	-1.91E+03	5.59E+01	8.61E+03	-2.29E+01
2	-1.08E+03	-9.68E+00	-2.51E+03	2.44E+02	1.91E+04	-1.01E+02
3	-7.79E+02	-2.21E+01	-3.14E+03	5.51E+02	3.16E+04	-2.36E+02
4	-9.32E+02	-2.61E+01	-2.84E+03	6.43E+02	2.57E+04	-2.77E+02
5	-1.05E+03	-2.78E+01	-2.58E+03	6.69E+02	2.05E+04	-2.97E+02
6	-1.11E+03	-2.98E+01	-2.45E+03	6.94E+02	1.80E+04	-3.22E+02
7	-1.14E+03	-3.23E+01	-2.36E+03	7.37E+02	1.64E+04	-3.54E+02
8	-1.17E+03	-3.46E+01	-2.31E+03	7.75E+02	1.55E+04	-3.82E+02
9	-1.44E+03	4.18E-01	-1.49E+03	-6.89E+00	2.02E+03	3.27E+00
10	-1.44E+03	7.26E-01	-1.50E+03	-1.01E+01	2.17E+03	5.62E+00
11	-1.44E+03	1.04E+00	-1.51E+03	-6.96E+00	2.32E+03	7.19E+00
12	-1.43E+03	1.34E+00	-1.52E+03	-6.41E+00	2.43E+03	8.97E+00
13	-1.43E+03	1.59E+00	-1.53E+03	-8.32E-01	2.55E+03	1.05E+01

Table B.4: *Mean values of forces and moments for the 90 degrees sea heading*

Sea state	F_x [kN]	F_y [kN]	F_z [kN]	M_x [kNm]	M_y [kNm]	M_z [kNm]
1	1.75E+02	7.61E+00	1.32E+02	1.12E+02	3.48E+03	8.60E+01
2	3.64E+02	1.87E+01	2.63E+02	3.62E+02	7.38E+03	1.92E+02
3	5.39E+02	4.09E+01	3.38E+02	9.78E+02	1.09E+04	4.15E+02
4	6.95E+02	4.12E+01	4.17E+02	9.79E+02	1.30E+04	4.15E+02
5	8.31E+02	4.74E+01	3.22E+02	1.13E+03	1.31E+04	4.73E+02
6	9.61E+02	5.28E+01	2.85E+02	1.26E+03	1.40E+04	5.29E+02
7	1.07E+03	5.89E+01	2.80E+02	1.40E+03	1.50E+04	5.91E+02
8	1.15E+03	6.41E+01	2.87E+02	1.53E+03	1.56E+04	6.47E+02
9	1.21E+03	1.57E+01	2.04E+02	3.96E+02	1.41E+04	1.48E+02
10	1.26E+03	1.75E+01	2.37E+02	4.40E+02	1.45E+04	1.67E+01
11	1.29E+03	1.94E+01	2.77E+02	4.85E+02	1.48E+04	1.86E+02
12	1.34E+03	2.07E+01	3.16E+02	5.18E+02	1.53E+04	2.02E+02
13	1.36E+03	2.24E+01	3.60E+02	5.56E+02	1.46E+04	2.18E+02

Table B.5: *Standard deviation for forces and moments for the 0 degrees sea heading*

Sea state	F_x [kN]	F_y [kN]	F_z [kN]	M_x [kNm]	M_y [kNm]	M_z [kNm]
1	1.56E+02	6.50E+01	1.33E+02	1.30E+03	3.25E+03	6.67E+02
2	3.15E+02	1.32E+02	2.64E+02	2.68E+03	6.84E+03	1.40E+03
3	4.51E+02	2.01E+02	3.37E+02	4.22E+03	9.90E+03	2.21E+03
4	5.68E+02	2.61E+02	4.16E+02	5.01E+03	1.18E+04	2.83E+03
5	6.64E+02	3.20E+02	3.20E+02	5.73E+03	1.13E+04	3.43E+03
6	7.57E+02	3.77E+02	2.82E+02	6.43E+03	1.18E+04	4.02E+03
7	8.37E+02	4.29E+02	2.76E+02	7.07E+03	1.24E+04	4.56E+03
8	8.94E+02	4.73E+02	2.82E+02	7.54E+03	1.28E+04	5.01E+03
9	9.37E+02	4.98E+02	2.08E+02	6.70E+03	1.14E+04	4.78E+03
10	9.72E+02	5.29E+02	2.38E+02	7.04E+03	1.17E+04	5.08E+03
11	9.93E+02	5.52E+02	2.37E+02	7.29E+03	1.20E+04	5.29E+03
12	1.03E+03	5.82E+02	3.09E+02	7.63E+03	1.23E+04	5.57E+03
13	1.05E+03	6.06E+02	3.49E+02	7.89E+03	1.27E+04	5.80E+03

Table B.6: *Standard deviation for forces and moments for the 30 degrees sea heading*

Sea state	F_x [kN]	F_y [kN]	F_z [kN]	M_x [kNm]	M_y [kNm]	M_z [kNm]
1	4.50E+01	1.12E+02	1.32E+02	2.37E+03	2.42E+03	1.18E+03
2	1.55E+02	2.18E+02	2.62E+02	4.82E+03	5.21E+03	2.38E+03
3	2.05E+02	3.14E+02	3.31E+02	7.30E+03	7.36E+03	3.53E+03
4	2.43E+02	3.90E+02	4.08E+02	8.53E+03	8.72E+03	4.33E+03
5	2.45E+02	4.62E+02	3.06E+02	9.54E+03	6.85E+03	5.07E+03
6	2.64E+02	5.27E+02	2.62E+02	1.05E+04	6.27E+03	5.73E+03
7	2.86E+02	5.84E+02	2.50E+02	1.13E+04	6.23E+03	6.31E+03
8	3.03E+02	6.25E+02	2.50E+02	1.18E+04	6.32E+03	6.73E+03
9	3.12E+02	6.63E+02	1.79E+02	1.08E+04	4.89E+03	6.62E+03
10	3.27E+02	6.96E+02	2.05E+02	1.12E+04	5.20E+03	6.93E+03
11	3.38E+02	7.21E+02	2.34E+02	1.15E+04	5.53E+03	7.16E+03
12	3.54E+02	7.53E+02	2.63E+02	1.20E+04	5.91E+03	7.48E+03
13	3.66E+02	7.79E+02	2.94E+02	1.23E+04	6.33E+03	7.72E+03

Table B.7: *Standard deviation for forces and moments for the 60 degrees sea heading*

Sea state	F_x [kN]	F_y [kN]	F_z [kN]	M_x [kNm]	M_y [kNm]	M_z [kNm]
1	5.07E+01	5.99E+01	1.31E+02	2.70E+03	2.16E+03	7.17E+02
2	1.14E+02	1.11E+02	2.59E+02	4.52E+03	4.75E+03	1.37E+03
3	1.44E+02	1.51E+02	3.25E+02	6.65E+03	6.67E+03	1.92E+03
4	1.61E+02	1.78E+02	4.04E+02	7.73E+03	7.98E+03	2.28E+03
5	1.17E+02	2.03E+02	2.98E+02	8.60E+03	5.61E+03	2.61E+03
6	1.03E+02	2.26E+02	2.48E+02	9.43E+03	4.54E+03	2.90E+03
7	1.04E+02	2.43E+02	2.31E+02	1.01E+04	4.18E+03	3.13E+03
8	1.09E+02	2.53E+02	2.28E+02	1.05E+04	4.11E+03	3.28E+03
9	7.28E+01	2.71E+02	1.39E+02	9.70E+03	2.35E+03	3.24E+03
10	7.99E+01	2.80E+02	1.60E+02	1.00E+04	2.67E+03	3.36E+03
11	8.63E+01	2.86E+02	1.82E+02	1.02E+04	2.93E+03	3.43E+03
12	9.41E+01	2.95E+02	2.03E+02	1.06E+04	3.20E+03	3.54E+03
13	1.01E+02	3.02E+02	2.25E+02	1.08E+04	3.48E+03	3.63E+03

Table B.8: *Standard deviation for forces and moments for the 90 degrees sea heading*